SEMMELWEIS EGYETEM

DOKTORI ISKOLA

Ph.D. értekezések

2434.

JAKAB GÉZA

A gyógyszerészeti tudományok korszerű kutatási irányai

című program

Programvezető: Dr. Antal István, egyetemi tanár

Témavezető: Dr. Antal István, egyetemi tanár

Development and Formulation of Baicalin-loaded Drug Delivery Systems

PhD Thesis

Dr. Géza Jakab

Doctoral School of Pharmaceutical Sciences

Semmelweis University

Supervisor: István Antal, D.Sc.

Official reviewers:

Angéla Jedlovszky-Hajdú, Ph.D.

Ildikó Bácskay, D.Sc.

Head of the Complex Examination Committee:

Romána Zelkó, D.Sc.

Members of the Complex Examination Committee:

Éva Szökő, D.Sc.

Miklós Vecsernyés, D.Sc.

Budapest, 2020

Table of contents

List of abbreviations

ABC	ATP-binding Cassette
ADMET	Absorption-Distribution-Metabolism-Excretion-Toxicity
AFM	Atomic Force Microscopy
ANOVA	Analysis of Variance
API	Active Pharmaceutical Ingredient
BBB	Blood Brain Barrier
BCRP	Breast Cancer Resistance Protein
BCS	Biopharmaceutical Classification System
BRM	Biorelevant Media
BSNEDDS	Baicalin-loaded Self-nanoemulsifying Drug Delivery System
CD	Cyclodextrin
CYP 450	Cytochrome P450 Enzymes
DDS	Drug Delivery System
DLS	Dynamic Light Scattering
DSC	Differential Scanning Calorimetry
EC	European Commission
EMA	European Medicines Agency
FaSSGF	Fasted State Simulated Gastric Fluid
FaSSIF	Fasted State Simulated Intestinal Fluid
FDA	Food and Drug Administration
FeSSIF	Fed State Simulated Intestinal Fluid
GAL	GalenIQ™ 800

GIT	Gastro-intestinal Tract
GRAS	Generally Regarded as Safe
HLB	Hydrophilic-Lipophilic Balance
HME	Hot-melt Extrusion
HPMC	Hydroxypropyl Methylcellulose
HP-β-CD	2-hydroxypropyl-β-CD
HRE	Heat Reflux Extraction
ICH	International Conference on Harmonization
JPC	Japan Pharmaceutical Codex
LBDD	Lipid-based Drug Delivery
LD	Laser Diffraction
LFCS	Lipid Formulation Classification System
MCC	Microcrystalline Cellulose
MRP	Multidrug Resistance-associated Protein
MWI	Microwave Irradiation
NCE	New Chemical Entity
NIBS	None-Invasive-Back-Scattering
NMR	Nuclear Magnetic Resonance
OATP1B1	Organic Anion-transporting Polypeptide 1B1
PDI	Polydispersity Index
Ph. Eur.	European Pharmacopoeia
PVP	Polyvinylpyrrolidone
RAMEB-CD	Random Methylated β-CD

ROESY	Rotating Frame Nuclear Overhauser Effect Spectroscopy
SBE-β-CD	Sulfobutylether-β-CD
SEDDS	Self-emulsifying Drug Delivery System
SEM	Scanning Electron Microscopy
SFE	Supercritical Fluid Extraction
SMEDDS	Self-microemulsifying Drug Delivery System
SNEDDS	Self-nanoemulsifying Drug Delivery System
UAE	Ultrasound-assisted Extraction
USP	United States Pharmacopoeia

1. Introduction

One of the most tremendous challenges faced by pharmaceutical scientists is poor solubility and/or permeability and the concomitant low bioavailability of new chemical entities (NCE). Researchers often find promising candidates during drug screening; however, if the molecule exhibits unsuitable physico-chemical properties, the chance of delivering the adequate dose to the site of action is diminished. In the last years a negative tendency has appeared in the drug discovery pipeline: approx. 70% of NCEs demonstrate low solubility and high permeability, therefore belongs to Biopharmaceutical Classification System (BCS) II. Conversely, about only 30% of drugs previously brought to the market resides to BCS II (1). This challenging shift is also expressed in case of BCS IV (low solubility and low permeability) compounds: there is an increase of 3-4 times in favour of NCEs compared to marketed drugs *(Fig.1.)* (2). Baicalin -the subject of this PhD Thesis- is a bioactive phytopharmacon and can be classified as Class IV (3). In the scientific literature numerous approaches came up to improve the low bioavailability of different active pharmaceutical ingredients (APIs). With no claim of being exhaustive I would like to notice some of them: cyclodextrin complexation (4), solid dispersions (5), liposomes (6), lipid-based formulations (7), self-emulsifying systems (8). In the following sections a detailed explanation can be found related to lipid-based formulations focused on self-emulsifying systems and cyclodextrin complexes.

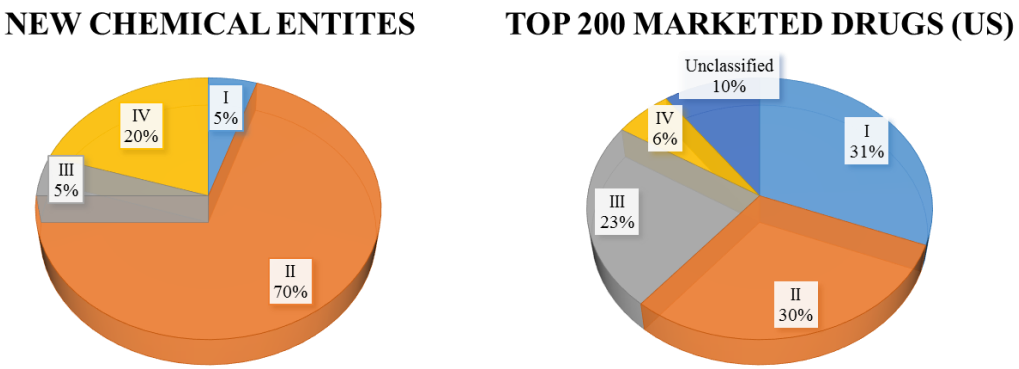

Figure 1. Trending in Biopharmaceutical Classification System (BCS)
(http://www.samedanltd.com/magazine/11/issue/158/article/3039; 01/10/2019)

(BCS I – high solubility and permeability, BCS II – low solubility, high permeability, BCS III – high solubility, low permeability, BCS IV- high solubility and permeability of drug substance)

In the last decade the pharmacological and formulation aspects of phytopharmacons captured the attention of scientist worldwide. This is largely a result of the higher tendency among the general population to use complementary and alternative medicine and live a health-conscious lifestyle. The motivation behind the topic selection was the renaissance of natural products and the challenging physico-chemical and biological properties of baicalin.

1.1.Scutellaria baicalensis Georgi (Baical skullcap)

Scutellaria baicalensis G. (*S. baicalensis G.*) is one of the fundamental herbs in traditional Chinese herbal medicine known as Huang Qin (*mandarin: 黄芩*) (9). It is indigenous to several East Asian countries (Mongolia, China, Korea) and the Russian Federation and has been cultivated in many European countries *(Fig.2.)* (10). Baical skullcap is a species of flowering plant in the family *Lamiaceae*. The root is officially listed in the Chinese Pharmacopoeia and was assumed in European Pharmacopoeia (Ph. Eur.) 9th Edition in 2018 (11). The major components in the dried root of the herb are baicalin (D-Glucuronic acid-5,6-dihydroxyflavone) and its aglycone, baicalein (5,6,7-trihydroxyflavone) (12). As minor component wogonin (5,7-dihydroxy-8-methoxyflavone) and wogonoside (5,7-Dihydroxy 8-methoxyflavone 7-glucuronide) can be extracted from the dried root. Heat reflux extraction (HRE), ultrasound-assisted extraction (UAE), and supercritical fluid extraction (SFE) are common extraction methods to isolate and purify baicalin (13).

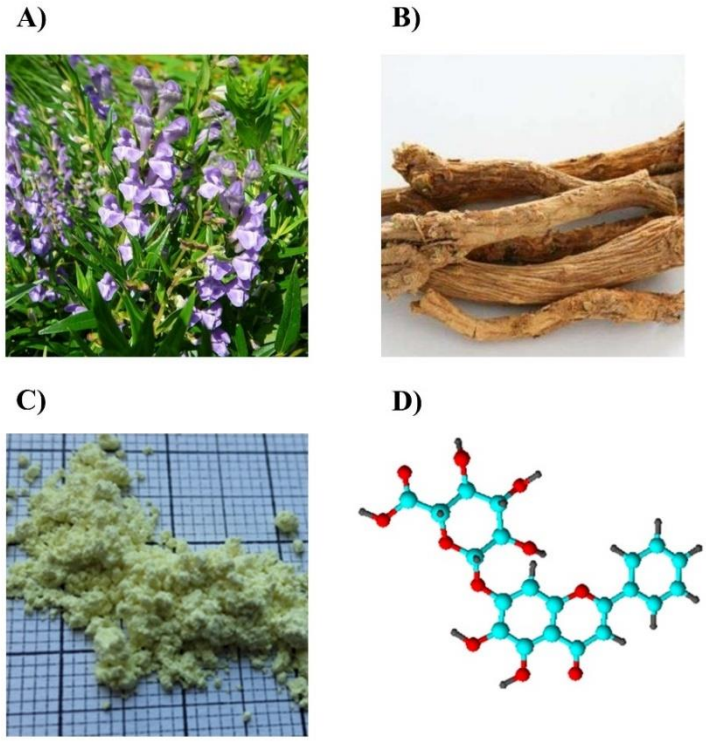

Figure 2. The medical plant of *Scutellaria baicalensis* (A) and its dried root (B). Extracted and purified powder of baicalin (C). 3D structure of baicalin (D). *(https://en.wikipedia.org/wiki/Scutellaria_baicalensis; 01/10/2019) C and D are self-made*

*1.2.*Baicalin

1.2.1. General notes

Baicalin is a flavone glycoside extracted from the root of *Scutellaria baicalensis*. In traditional Chinese medicine it had been used for the treatment of diarrhoea, dysentery, haemorrhaging, insomnia, inflammation and different respiratory infections (10). Nowadays baicalin extracts are easily accessible over-the-counter herbal remedies, purchasable online and in numerous stores in liquid, bulk powder, capsule or tablet dosage form. Recommended daily dosage of powder is 60-500 mg. Baicalin enjoys fairly high popularity in ointments, lipsticks and skin care preparations. As a flavonoid derivate, its anti-oxidant and anti-aging property can contribute to the skin's overall quality and appearance. Food industry utilizes baicalin as a nutritional adjuvant for improving production performance and nourishing feed intake in farm animals (14).

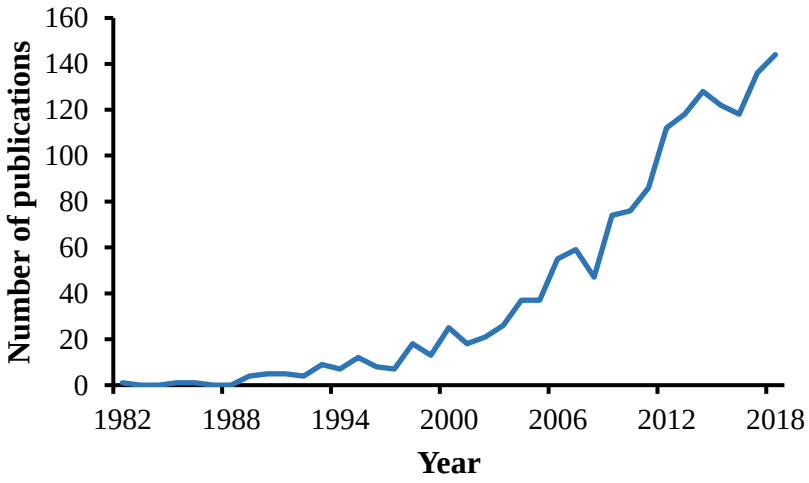

Figure 3. Growing interest in baicalin as a bioactive phytopharmacon 1982-2019
Source: PubMed, keyword: baicalin [all]

Baicalin is easily extractable and it has a wide range of therapeutical and pharmacological effects *(see detailed in section: 1.2.4.)*, which have brought it into focus as a safe and natural phytopharmacon. A PubMed search with the key word Baicalin [all] returns approx. 1700 articles from '80s to date with 50% of them published in the last five years *(Fig.3.)*. Since 2000 the interest in the subject has been increasing gradually. On the one hand, in the US and Europe baicalin-loaded formulations have no marketing authorization

as of December 2019. On the other hand, in 2005 the State Food and Drug Administration of China approved baicalin (approval No. H20158009) for the adjuvant therapy of hepatitis (1500 mg/day, 2 times 3 capsules).

1.2.2. Physicochemical Profiling

The most important physicochemical properties influencing the pharmacokinetic behavior of drugs and biomolecules are the acid-base properties, lipophilicity, permeability and solubility (15). Physicochemical profiling is an integral part of preformulation studies, which lays down foundation for transforming a new drug entity into a pharmaceutical dosage form in such a way that it can be administered in a right way, in right amount, and on the right target (16). Possessing these kinds of information, the optimization of an active molecular entity is also possible.

The acid-base character determines the ionization state of a molecule in solution having a particular pH. Consequently, all pharmacokinetic properties, namely absorption, distribution, metabolism, excretion and toxicity (ADMET) are influenced by the ionization state under varying pH conditions (17). Molecular structure of baicalin can be derived from its aglycone, baicalein by linking a glucuronic acid to the aglycone via a glycosidic bond in position 7 *(Fig.4.)*. It has three acidic functional groups, namely one carboxyl *(ring: D)* and two phenolic hydroxyl groups *(ring: A)*.

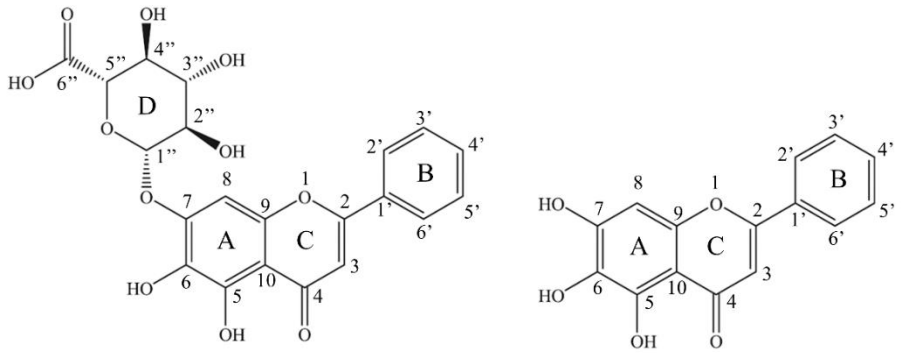

Figure 4. Chemical structure of Baicalin and Baicalein *(self-made)*

Proton transfer processes can be regarded either from the point of view of dissociation or association. Because of the acidic nature of baicalin, these processes will be characterized by acid dissociation constants (K_a). The determination of pK_a value is important in understanding the in vivo behaviour of a drug, which influences not only its solubility and dissolution, but also the membrane-penetration capacity (18). The acid-base properties of baicalin have been investigated before, resulting in pK_a values of 5.05, 7.6 and 10.1 (19). However, internal Nuclear Magnetic Resonance (NMR) investigations showed the molecule rapidly decomposes above pH 9, making the reported values in alkaline solutions highly dubious.

The determination of the octanol/water partition coefficient (log *P*) is essential during preformulation studies, which is in close correlation with membrane-penetration capability and is the most frequently determined lipophilicity descriptor (20). There have been attempts in characterizing the lipophilicity of baicalin ((log *P*=1.27 (pH=7)), but the applied methods and study design can induce doubts (19). It is not exactly clear what the authors meant by this, probably they calculated the log *P* of baicalin from log *D* measured at pH 7. Therefore, the data provided is to be considered as indicative only. However, if we accept with restrictions the above-mentioned value, the lipophilicity of baicalin must be considered as low. Calculation of log P value provides data regarded to passive diffusion through biological membranes, but it does not describe properly the carrier-mediated active transport mechanisms. The Caco-2 monolayer is isolated from human colorectal adenocarcinoma and widely used across the pharmaceutical industry as an *in vitro* model of the human intestinal barrier to predict the active and passive absorption mechanisms of orally administered drugs (21). The permeability potential of baicalin was evaluated by Caco-2 assay (P_{app} 9.2×10^{-8} cm/s), which revealed low permeability (22). The low lipophilicity and permeability value of baicalin presumes low absorption from the gastro-intestinal tract (GIT).

Aqueous solubility is a fundamental attribute of an active substance and its examination is a mandatory step during the drug discovery process. To achieve adequate plasma drug levels and clinical response, dissolution of the active ingredient in physiological environment is a leading precondition. New drug molecules as well as phytopharmacons tend to have larger molecular weights, resulting often in decreased solubility and dissolution, which may lead to limited absorption and poor pharmacokinetics. Like pK_a

and log *P* values of baicalin, its aqueous solubility is also marked by discrepancies in the scientific literature; 0.18 mg/ml, 0.08 mg/ml and 0.052 mg/ml can be found (23–25). Furthermore, the factors affecting solubility (e.g. temperature, pH, ionic strength, surface tension) were not investigated yet in a comprehensive study. It can be seen from the chemical structure that both the glucuronide and the flavone part forms intramolecular H-bonds, which can be partly responsible for the poor water solubility and high melting point (26). If an oral drug is under development, particularly one with low solubility, biorelevant measurements are extremely useful because through simple *in vitro* tests they can predict how it's likely to dissolve *in vivo* in the GIT. Over the past 15–20 years, biorelevant media simulating conditions in the stomach and small intestine before and after meals have been developed (27). Simulated intestinal fluid in fasted state (FaSSIF) and in fed state (FeSSIF) along with fasted state gastric fluid (FaSSGF) have been suggested first by Dressman et al (28). In addition, the application of these media can be used to predict food effects (29). In case of baicalin these kind of physiologically relevant solubility data have not been published yet.

The chemical stability of baicalin was evaluated in buffered aqueous solutions at different pH (2.0, 3.0, 4.5, 6.8, 7.4 and 9.0) and temperatures (4, 25 and 40 °C). Acidic environment and low temperature were protective factors for the long term stability of this compound (30).

1.2.3. Biopharmaceutical properties

Several studies described the pharmacokinetics of baicalin according to the ADME concept. The absorption mechanism was evaluated in rats by Liu et al. and found that baicalin was moderately absorbed in the stomach but poorly in the small intestine and colon (31). More research pointed out that baicalin undergoes extensive hydrolysis by intestinal β-glucuronidase or intestinal microbiome to form its aglycone, baicalein *(Fig.5.)*.

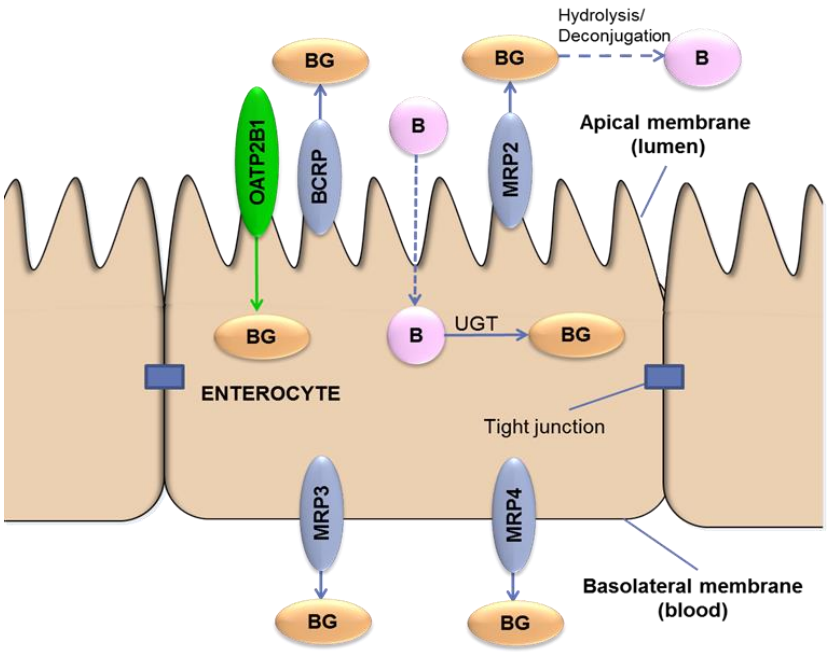

Figure 5. Role of transporters in transport of baicalin in enterocytes (Interaction of baicalin with transporters, Bernadett Kalaposné Kovács, Semmelweis University, 2016)

Since the aglycone is absorbed much more better compared to baicalin, this cleavage reaction has a potent role in the absorption process (32, 33). Baicalin is substrate of uptake transporter organic anion-transporting polypeptide 1B1 (OATP1B1) (33). In the intestinal enterocyte baicalein is transformed to baicalin, and effluxed to the blood mainly by multidrug resistance associated protein 3 (MRP3) and MRP4, located on the basolateral side of the cell (33). Accordingly, after administration of a single ascending dose of baicalein (100-2800 mg) chewable tablets to healthy subjects, the C_{max} values of

baicalin were about ten-fold higher than C_{max} values of baicalein (34). Part of baicalin is pumped back to the intestinal lumen by apically located MRP2 and breast cancer resistance protein (BCRP) (35).

In the distribution mechanisms of baicalin the high plasma protein-binding capacity (86-92%) plays a prominent role (36). Wei et al. revealed the tissue distribution of baicalin after intravenous administration of liposomal and injectable formulations to rabbits. Liposomal drug delivery indicated a significantly increased lung accumulation compared to injectable solution (37). Baicalin penetrates moderately through the blood-brain-barrier (BBB) (38).

Validated method was applied to analyse and screen the *in vivo* metabolism of baicalin in rats. No less than 32 metabolites were identified in the rat plasma and urine. The results demonstrated that the rat liver and kidney are the most important organs for the distribution of baicalin metabolites. Methylation, hydrolysis, hydroxylation, methoxylation, glucuronide conjugation, sulphate conjugation, and their composite reactions were all identified (39).

Baicalin is primarily excreted in bile in the form of glucuronides and undergoes a prominent enterohepatic recycling through different ABC transporters (33, 40). As an alternative excretion pathway, the fraction of baicalin excreted in urine appears to be negligible compared to the biliary route (41).

1.2.4. Pharmacological effects

Baicalin has numerous pharmacological activities demonstrated by *in vitro* and *in vivo* studies among others anti-inflammatoric, anti-allergic, anti-depressant, anti-microbial, anti-oxidant as well as anti-psoriatic effects (42–47). Ding et al. showed that baicalin relaxes vascular smooth muscle and lowers blood pressure in spontaneously hypertensive rats by regulating K_{ATP} channels and the intracellular Ca^{2+} level (48). It was revealed that long-term baicalin administration ameliorates metabolic disorders and hepatic steatosis in rats given a high-fat diet (49). Baicalin might serve in the future as a novel compound in the treatment of the most common neurodegenerative diseases in elderly patients, the Parkinson's (50). The preliminary results suggest that the mechanism of action is a decreased iron accumulation in the substantia nigra. Wang et al. investigated the

hyperglycaemia-induced cardiovascular malformation of embryos in mice. The cardiovascular abnormality can be attenuated by baicalin administration. This compound is a promising candidate for women suffering from gestational diabetes mellitus (51). Cancer is one of the leading causes of death worldwide and is very likely to overtake heart diseases, which has traditionally topped the list as the leading cause of death in higher income countries. Scientific projects reveal an ever-increasing number of evidence that baicalin exhibits its antitumor function in a wide range of cancers such as breast cancer, colon cancer, gallbladder carcinoma, haematological malignancies, hepatic cancer, lung cancer, prostate cancer (52–57). The chemical modification of the baicalin aglycone pointed out promising development in preclinical studies (58). Therefore, the chemical and pharmacological optimization and the production of semisynthetic derivates could be an interesting research direction in the future. It is important to note that extensive clinical studies are needed for the confirmation of the above mentioned *in vitro* and *in vivo* results.

1.2.5. Baicalin-drug interactions

Several studies have been carried out on the effects of baicalin and co-administered drugs. Remarkable baicalin-drug interactions can be observed, when both compounds share the same cytochrome P450 (CYP) enzyme or exhibiting high plasma protein binding. The relevant preclinical and clinical research findings and the mechanism of herb-drug interactions are summarized in *Table I.*

Two clinical trials can be found in the literature regarding baicalin-drug interactions. Liu et al. executed the first clinical study to investigate the effect of baicalin on cyclosporine A pharmacokinetics in humans (n=16) (59). The applied dosage was 500 and 200 mg in case of baicalin and cyclosporine A, respectively. The combination was well-tolerated and the pharmacokinetic behaviour of cyclosporine A was not changed to a clinically relevant extent. The reported adverse events were mild and the data didn’t lay down evidence that baicalin co-administration with cyclosporine A would cause an additional risk. Fan et al. analysed the pharmacokinetics of rosuvastatin, an antihyperlipidemic drug co-administered with baicalin. In the study 18 healthy adults were enrolled, possessing various organic anion-transporting polypeptide 1B1 (OATP1B1) haplotypes (60). OATP1B1 is considered the main uptake mechanism for rosuvastatin into the liver (61).

The volunteers received placebo or 50 mg baicalin 3 times a day for 14 days than on the 15th day, all subjects were given a single oral dose of 20 mg rosuvastatin. It was revealed that baicalin reduces systemic plasma exposure of rosuvastatin in an OATP1B1 haplotype–dependent manner. Baicalin treatment was well-tolerated in the administered dose and can be considered as safe.

Table I. Interactions between baicalin and prescribed drugs

Co-administered drug	**Pharmacokinetic parameter**	**Mechanism of herb-drug interaction**	**Ref.**
Caffeine	CYP1A, CYP2B ↓	Conc. of baicalin was not enough to inhibit CYP enzymes	(62)
Chlorzoxazone	C_{max}↓, $t_{1/2}$↑, V↑, CL Ø AUC Ø	Competition for plasma protein binding and CYP2E1 inhibition	(63)
Cyclosporine A	Ø	No relevant interaction	(59)
Dextromethorphan	C_{max}↑, $t_{1/2}$ Ø, V↓, CL↓, AUC↑	Competition for plasma protein binding and CYP3A inhibition	(64)
Midazolam	C_{max}↑, $t_{1/2}$↑, V↓, CL↓, AUC↑,	CYP3A inhibition	(65)
Nifedipine	C_{max}↓, V↑, CL↑, AUC↓	Competition for plasma protein binding and CYP3A inhibition	(66)
Phenacetin	C_{max}↓, $t_{1/2}$↑, V↑, CL↓, AUC↑	Competition for plasma protein binding and CYP1A2 inhibition	(67)
Rosuvastatin	$t_{1/2}$↓, CL↑, AUC↓	OATP1B1 induction	(60)
Theophylline	C_{max}↓, $t_{1/2}$↑, V↑, CL AUC depends on regime	Competition for plasma protein binding and CYP1A2 inhibition	(68, 69)

Abbreviations: $C_{max:}$ peak plasma concentration, $t_{1/2}$: terminal half-life, V: apparent volume, CL: clearance, AUC: area under the curve, OATP1B1: organic anion-transporting polypeptide B1, ↑: increase, ↓: decrease, Ø: no change

1.2.6. Bioavailability enhancement

Baicalin has diversified pharmacological effects, however its low solubility and permeability along with the concomitant poor bioavailability precludes sufficient oral administration. It was pointed out that the absolute bioavailability of baicalin is 2.2 ± 0.2% in rats (40). In order to overcome the physico-chemical and pharmacokinetic limitations of baicalin, the development of novel drug delivery systems (DDS) and formulations has attracted an increasing attention in the pharmaceutical field. Summary of innovative formulations are listed in *Table II*.

Table II. Innovative methods for the solubility and bioavailability enhancement of baicalin

Drug Delivery System	**AUC ↑ (fold)**	**Excipients used**	**Ref.**
Liposome	2.81	Tween 80, Phospholipon 90H, citric acid	(70)
Surfactant-free nanosuspension	2.01	Co-processed nanocrystalline cellulose-carboxymethyl starch	(71)
PEGylated lipid nanoparticles	7.2	Glycerol monostearate, oleic acid, polyethylene glycol monostearate	(72)
Nanoemulsion	7.0	Soy-lecithin, Tween® 80, PEG 400, Isopropyl myristate, Distilled water	(73)
Solid self(nano)-emulsifying system	-	Peceol™, Kolliphor® EL, Transcutol® P, Microcrystalline Cellulose, Isomalt	(74)
Cyclodextrin complex	-	α-, β-, γ-, HP-β-, SBE-β-, RAMEB-CD	(3)
Solid dispersion	3.38, 1.83	Polyvinyl-pyrrolidone, Mesoporous carbon nanopowder	(75, 76)
Mixed micelle system	1.54	Pluronic P123, Sodium taurocholate	(77)
Thermosensitive hydrogel	3.3	Chitosan, Glycerophosphate, PEG 6000, Hydroxypropyl methyl cellulose	(78)

1.3. Lipid-based formulations

Lipid-based drug delivery (LBDD) have gained much importance in the recent years due to their ability to improve the solubility and bioavailability of drugs with poor water solubility. Lipid formulations generally consist of a drug dissolved in a blend of two or more excipients, which may be triglyceride oils, partial glycerides, surfactants and/or co-surfactants. The absorption of drug from these formulations depend on numerous factors, e.g. particle size, degree of emulsification, rate of dispersion and precipitation of drug upon dispersion (79). These systems increase absorption from the gastrointestinal tract by accelerating the dissolution process (rate-limiting liberation step is excluded), facilitating the formation of solubilized phases by reduction of particle size to the molecular level, changing drug uptake, efflux and disposition by altering enterocyte-based transport, and enhancing drug transport to the systemic circulation *via* intestinal lymphatic system (7). Pouton et al. introduced the Lipid Formulation Classification System (LFCS) in 2000 *(Tbl. III.)*. The foundation of LFCS rests on the principle of the polarity of the blend and differentiates 4 types. Preparations which comprise drug dissolved in triglycerides or mixed glycerides, require digestion in GIT are classified as Type I. Adding water insoluble surfactants to the oily phase may improve the solvent capacity of the formulation. Self-emulsifying systems are classified as Type II, which emulsifies into crude oil in water emulsion in aqueous solutions under gentle agitation. There is a threshold in surfactant content at approx. 25% (w/w); passing this value the progress of emulsification is compromised by viscous liquid crystalline gels. Preparations which include water-soluble components are classified as Type III formulations, and have been referred as self-microemulsifying systems (droplet size <200 nm), due to the optical clarity which can be achieved with relatively high hydrophilic emulgent and co-solvent content.

Table III. The Lipid Formulation Classification System

Excipient	Type I	Type II	Type III/A	Type III/B	Type IV
Oil	100	40–80	40–80	<20	–
Hydrophobic surface-active agent (HLB <12)	–	20–60	–	–	0–20
Hydrophilic surface-active agent (HLB >12)	–	–	20–40	20–50	30–80
Hydrophilic co-solvent	–	–	0–40	20–50	0–50

Co-administration of emulgents and co-emulgents induces significant higher solubilisation capacity *in vivo* compared to co-emulgent free preparations (80). Type III systems can be split into Type III/A and Type III/B depending on the oil: hydrophilic content ratio. One of the first Type III products on the market was Sandimmune Neoral®, a supergeneric reformulation of immunosuppressant cyclosporine A (81). Some years later, Pouton and his research group integrated in the classification system a new oily phase free category (Type IV), which disperses to form a micellar solution and remains relevant in case of highly hydrophobic compounds (82). However, the high surfactant and co-solvent content should not be forgotten, because it may be poorly tolerated in chronic use. The choice of formulation requires detailed analysis and depends on several factors: dose, type and molecular weight of drug, stability of drug in various excipients, significance of emulsified droplet size, risk of precipitation due to high surfactant content, solubilisation capacity, digestion by intestinal enzymes (7). *Table IV* indicates some commercially available FDA approved drugs of each lipid-based classes.

Table IV. FDA approved products formulated by lipid-based systems

API/ trade name	**BCS**	**LFCS**	**Indication**	**Excipients**
Topotecan/ Hycamtin®	1	I	Ovarian-, lung cancer	Vegetable oil Glyceryl monostearate
Enzalutamide/ Xtandi®	2	I	Prostate cancer	Caprylocaproyl polyoxyglycerides
Nintedanib/ Ofev®	4	II	Pulmonary fibrosis	Medium chain tryglicerides Lecithin
Calcifediol/ Rayaldee™	2/4	II	Hyperpara-thyroidism	Paraffin, mineral oil, squalene Mixed emulsifiers (HLB <7)
Fenofibrate/ Lipofen®	2	III	High plasma lipid levels	Corn oil glycerides, Kolliphor® RH 40, Ethanol, glycerol, propylene glycol
Ritonavir-lopinavir/ Kaltera®	4	III	HIV	Oleic acid Kolliphor® EL Propylene glycol
Bexarotene/ Targretin®	4	IV	T-cell lymphoma	Polysorbate 20 PEG 400
Tipranavir/ Aptivus®	4	IV	HIV	Vitamin E TPGS, PEG 400 Propylene glycol, water

*1.4.*Self-emulsifying Drug Delivery Systems

Self-emulsifying Drug Delivery Systems (SEDDS) are isotropic mixtures (preconcentrates) of drugs, natural/synthetic oils, hydrophilic/lyophilic emulgents and optionally hydrophilic co-emulgents. Following their oral intake and dilution in gastric juice, the gentle agitation of GIT creates a fine oil in water (o/w) type emulsion *(Fig.6.)*. SEDDS present the drug in a dissolved form, excluding the rate-limiting dissolution step. The onset of action is rapid but it can be sustained by application of polymers. Effective solubilisation is a key attribute of emulsified systems in order to avoid precipitation of drug in GIT. Important aspect the small droplet size in case of micro-, and nanoemulsions provide a large interfacial area for drug absorption. Further advantages of SEDDS are high drug loading capacity, ease of manufacture and scale-up, protection of sensitive drugs and decreased food effects (83). A distinction is made between SEDDS, Self-Nanoemulsifying Drug Delivery Systems (SNEDDS) and Self-Microemulsifying Drug Delivery Systems (SMEDDS) on the basis of emulsified droplet size, thermodynamic stability of droplets and preconcentrate composition.

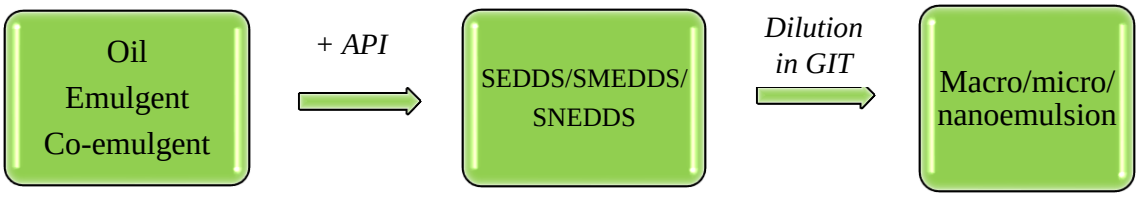

Figure 6. Composition and conception of Self-emulsifying Drug Delivery Systems *(self-made)*

1.4.1. Microemulsions and nanoemulsions: similarities and differences

After dilution in the GIT, SMEDDS or SNEDDS form the corresponsive microemulsions and nanoemulsions. Because of their biopharmaceutical and therapeutical advantages, these are the two most common types of colloidal dispersions (84). Furthermore, they exhibit better stability against aggregation and sedimentation along with the potential for industrial scaling-up (85). These superior properties materialize in colloidal systems possessing a droplet size <200 nm in diameter (86). It is usually easy task to define a macroemulsion (e.g. droplet size, composition, optical properties), but how to distinguish between microemulsions and nanoemulsions? Currently, there is a considerable confusion about the precise use of these terms. The reason is for the misconception that

there are many structural similarities between these two kinds of colloidal dispersion, but there are also basic differences (87).

The terminology commonly used to refer micro-, and nanoemulsions is misleading. Micro is a unit prefix denoting a factor of 10^{-6}, nano means 10^{-9}. At first glance one could believe that there is a three order of magnitude disparity in size between them, which is far from the truth. In practice the opposite is usually the case: the particles in a microemulsion are smaller than those in a nanoemulsion. The answer for this discrepancy lies within the development of colloidal chemistry. The first scientific article using the term "microemulsion" was published in 1961, whereas first article related to "nanoemulsion" appeared in 1996. The term "microemulsion" spread among researchers well before the introduction of term "nanoemulsion", and before they were clearly defined or distinguished from one another (87).

The most meaningful difference between the systems in question is the thermodynamic standpoint: microemulsion forms spontaneously as a thermodynamically stable dispersion, contrary to nanoemulsion which requires minimal energy input (88). The free energy of a microemulsion (droplets in water, $\Delta G_{coll.disp.}$) is lower than the free energy of separate phases (oil and water, ΔG_{ow}), so the self-emulsification of these formulations are thermodynamically favourable ($\Delta G_{coll.disp.} < \Delta G_{ow}$). The situation is reversed for nanoemulsions: the free energy of the colloid dispersion is higher compared with the separated phases ($\Delta G_{coll.disp.} > \Delta G_{ow}$), so the creation of nanoemulsion is energetically unfavourable (unstable thermodynamics) *(Fig.7.)*.

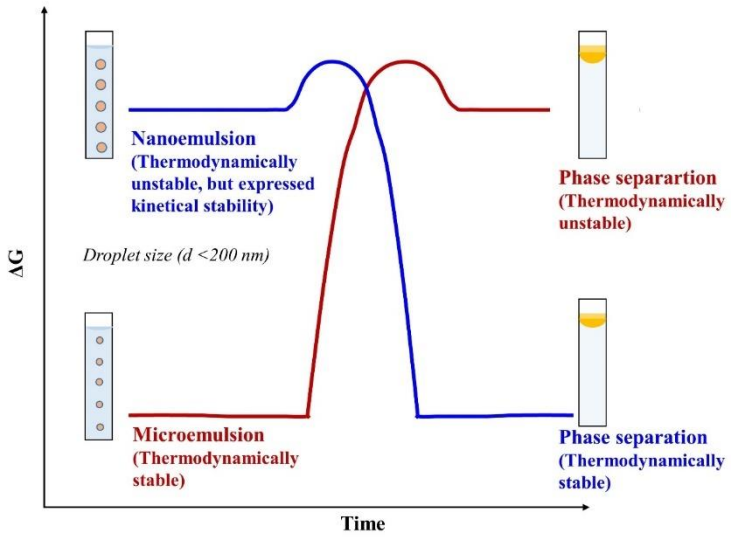

Figure 7. Demonstration of the free energy (ΔG) of nanoemulsion and microemulsion compared to the phase separated state. Microemulsions have a lower free energy than the phase separated state, whereas nanoemulsions have a higher free energy. *(self-made)*

In spite of their thermodynamic instability, nanoemulsions are able to put up aggregation resistance for months during storage; the system will persist in a metastable state. If there are sufficient energy barriers separating the two phases, the coalescence of nanoemulsified dispersion will be slow and sustained. The height of the needed energy barrier is mainly determined by physicochemical phenomena that prevent the droplets from coming into close proximity, such as repulsive hydrodynamic and colloidal (e.g., steric, electrostatic) interactions operating between droplets (89) . In general, it can be

concluded that the higher the energy barrier is, the more expressed the kinetic stability. There are a lot of various physicochemical phenomena which can lead to the breakdown of a nanoemulsion (e.g. flocculation, creaming, Ostwald-ripening, coalescence) (90). The role of stabilizer excipients such as weighting agents, surface active agents, texture modifiers, polymers is essential in the long-term stability of colloidal dispersions (91).

Table V. Comparison of microemulsion and nanoemulsion

Character	**Microemulsion**	**Nanoemulsion**
Thermodynamic stability	Stable	Unstable
Kinetic stability	Unstable, but compensated	Metastable, steric and electrostatic repulsive forces
Morphology	Disparate (e.g. spherical, lamellar, cylinder)	Spherical
Composition	Higher emulgent/oil ratio Emulgent with low molecular mass	Lower emulgent/oil ratio Proteins, polymers, emulgents with high molecular mass
Optical properties	Clears up around 200 nm, turns transparent under 60 nm	
Particle-size distribution	Single, narrow peak, low polydispersity	Multiple, broad peaks, relative high polydispersity

From the point of view optical properties, the droplet size is decisive: the system begins to clear up around 200 nm and turns transparent under 60 nm (92). Nanoemulsions tend to have spherical structure because of the large Laplace pressure. Within that size range the surface tension (γ: N/m) is high, while particle radius (r: m) is low, therefore - according to Law of Laplace ($\Delta P = \frac{2\gamma}{r}$)- significant Laplace pressure can be detected. A sphere has the lowest interfacial area and concomitant surface tension for a given volume of material, that is the reason behind nanoemulsions favoured character (86).

Microemulsions exhibit a wide range of shapes (e.g. worm-like, bicontinuous sponge-like, liquid crystalline, or hexagonal, spherical swollen micelles). Influencing factors are type and quantity of incorporated oil and surfactant, and the ideal curvature of utilized surfactant(s) *(Tbl. V.)* (93). In this thesis I am primarily focus on microemulsions and nanoemulsions that can be used to encapsulate lipophilic components, that consist of small spheroid particles comprised of oil and surfactant molecules dispersed within water. Other kinds of microemulsion systems (e.g. liquid crystalline, worm-like) are out of the scope of this thesis.

It is important to distinguish between microemulsions and nanoemulsions in practice since this predispose their long-term stability, functionality, robustness against altered environmental conditions (temperature, relative humidity, dilution) and bioavailability. Some practical methods provide data which category a colloidal dispersion belongs to. Composition, particle size distribution studies, long-term storage measurements supplemented with altering environmental conditions, particle shape analysis might be constructive for determining the type of system.

1.4.2. Role of excipients in the formulation of SEDDS

The utilized excipients have a definitive influence on self-emulsification, stability and drug delivery *(Fig.8.)*. Chemical structure and concentration of oil and emulgent, oil/emulgent ratio, quality and quantity of co-emulgent, emulgent/co-emulgent ratio, weigh-in order, temperature, ionic strength were shown to have significant effect on the quality of SEDDS (94). It is clear that a lot of parameters must be considered to fulfil the critical quality attributes of SEDDS:

- Solubility of API in the oily phase must be maximal
- Achieve in the various physiological conditions of GIT constant droplet size and stability
- Toxicity, purity, stability, price, acquisition of excipients are important criteria
- Improved bioavailability by reduced droplet size and enhanced absorption via lymphatic transport and solubilisation

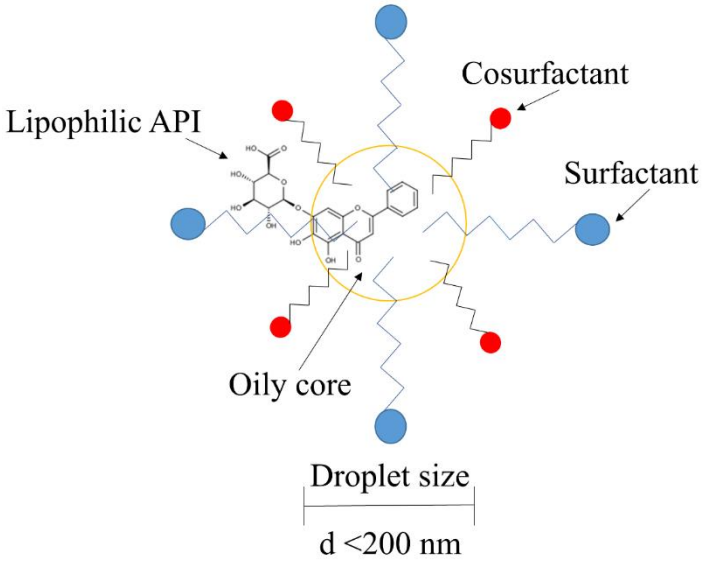

Figure 8. Schematic diagram of o/w nanoemulsified droplet solubilizing lipophilic substance *(self-made)*

1.4.2.1. Oils

Oils are the most significant components of SEDDS, which promote self-emulsification, facilitate drug absorption through the mucosal membrane and allow the dissolution of large amounts of lipophilic substances. The solubilisation capacity of GIT is also enhanced by using lipid components because they stimulate pancreatic and bile juice excretion (95). Oils can be classified as natural, semi-synthetic and synthetic derivates. According to their chemical structure we can distinguish between triglycerides and mixed glycerides (mixture of mono-, di-, and triglycerides) esterificated by medium or long-chained fatty acids (saturated/unsaturated). Natural oils are derived primarily from plant sources comprised of mixtures of triglycerides which contain fatty acids of varying chain lengths and degrees of unsaturation (e.g. soy oil, sunflower oil, coconut oil, olive oil). Their main advantage is the fully digestion and absorption in the GIT mediated by physiological enzymes and therefore they are generally regarded as safe (GRAS). The acceptance of patients is also higher in case of natural medicines and excipients. The low resistance to oxidation and decreased solvent capacity compared to semi-synthetic and synthetic derivates are challenging formulation issues (7).

Semi-synthetic and synthetic oils are partial glycerides, prepared by glycerolises, a transesterification reaction of triglycerides in order to increase the hydrophilic character of natural oils. There are several modified oils on the market: glyceryl-monocaprylocaprate (Capmul® MCM); glyceryl-monostearate (Geleol™, Imwitor® 191, Cutina™ GMS, Tegin™); glyceryl-distearate (Precirol™ ATO 5); glyceryl-monooleate (Peceol™); glyceryl-monolinolate (Maisine™ 35-1); glyceryl-dibehenate (Compritol®888 ATO). PEGylated polyoxylglycerides are also available: oleoyl macrogol-6 glycerides (Labrafil® M 1944CS), lauroyl Macrogol-32 glycerides (Gelucire® 44/14). Numerous research groups investigated the relationship between solubility and bioavailability of API and structure of oil (96–98). The components, process parameters and conclusions were different and therefore does not enable unambiguous interpretation. They pointed out as a collective and general experience that the incorporated active substance has a significant impact on the *in vitro/in vivo* fate of lipid-based DDS.

1.4.2.2. Surfactants

Surfactants are amphiphilic molecules that lower the surface tension, meaning they contain both hydrophilic and hydrophobic groups. Emulsifiers are indispensable components of SEDDS as they strengthen drug absorption by altering the lipid bilayer organization, enhance the lipid-intestinal membrane interactions, dissolve hydrophobic substances between their hydrocarbon chains and moreover kinetically stabilize the droplet size distribution (99). Application of higher surfactant concentrations don't always reduce droplet size of colloidal dispersion, formed after dilution of SEDDS preconcentrate in GIT, but may even increase it. The phenomenon can be attributed to the increased water penetration, and concomitant disruption of interfacial film, which causes oil droplets to be expelled into external water phase (82). Surfactants are classified into cationic, anionic, zwitterionic and non-ionic types. It was revealed that non-ionic surfactants demonstrating lower toxicity and have better tolerability in case of chronic use compared to ionic ones (100). Hydrophilic-lipophilic balance (HLB) is an important indicator for the characterization of surfactants that quantifies the oil and water attracting capacity of the surface-active molecule. Using 30-70 % (w/w) emulgent provides colloidal SNEDDS/SMEDDS dispersions with long-term physical stability and narrow particle-size distributions (101). From the point of view self-emulsification, the preferred HLB value should be higher than 12 (102). The HLB for a mixture of emulsifiers is calculated in proportion to the concentrations. Droplet size analysis was demonstrated as a suitable method for the determination of required HLB value in lemon oil emulsions (103). A special property of non-ionic surfactants is cloud point, the temperature above which the surfactant phase separates and precipitates out of solution. The cloud point is higher than 37 °C in ideal case because of the risk of irreversible phase separation in the body (104). Furthermore, it was demonstrated that several emulgents have an inhibitory impact on different CYP-enzymes and on intestinal P-glycoprotein, which phenomena can be used to enhance the bioavailability in special cases (105). Some of the typically used surface active agents in SEDDS formulations are macrogolglycerol-ricinoleate (Kolliphor® EL), macrogolglycerol-oleate (Labrafil® M 1944 CS), caprylocaproyl macrogol-8 glycerides (Labrasol®), propylene glycol monocaprylate type II (Capryol® 90) polysorbate 20 (Tween® 20).

1.4.2.3. Co-surfactants/Co-solvents

Co-solvents are integral part of SEDDS. They initiate self-emulsification, increase the elasticity of interfacial film, lower interfacial tension, allow the dissolution of remarkable amount of API and prevent formation of liquid crystals (106). Co-surfactants can also be used to fine-tune the formulation phase behaviour, for example, by expanding the temperature or salinity range of microemulsion formation. In general, the optimal applied concentration lies between 20 and 50 %(w/w). Application of co-surfactant is not mandatory at all, several studies focused on cosolvent-free formulations (107, 108). Ethanol, propylene glycol, Transcutol® P and PEG400 are some of the widely used co-surfactants.

1.5. Transformation of liquid SEDDS/SMEDDS/SNEDDS into solid dosage forms

Transforming liquid self-emulsifying preconcentrates to solid carriers is a strategy in lipid-based formulation design, which besides solubility improvement, offers further advantages over liquid systems; increased long-term physicochemical stability, ease to scale up, processability, precise dosing and improved patient compliance (109). However, it is important that the solidification procedure must preserve self-emulsifying properties and small droplet size which have to be demonstrated by reconstitution studies during formulation development. The most relevant solidification methodologies are spray drying, extrusion-spheronization and adsorption onto porous solid carriers (110). Adequate drug loading, compatibility, suitable drug release profile, processability are critical quality attributes of carriers used for converting liquid SEDDS to solid dosage forms (111). Oral delivery of pH-, and enzyme-sensitive biologics may be achieved by solid SEDDS formulated with special environment responsive excipients. The basic methodologies are reviewed briefly below *(Fig.9.)*.

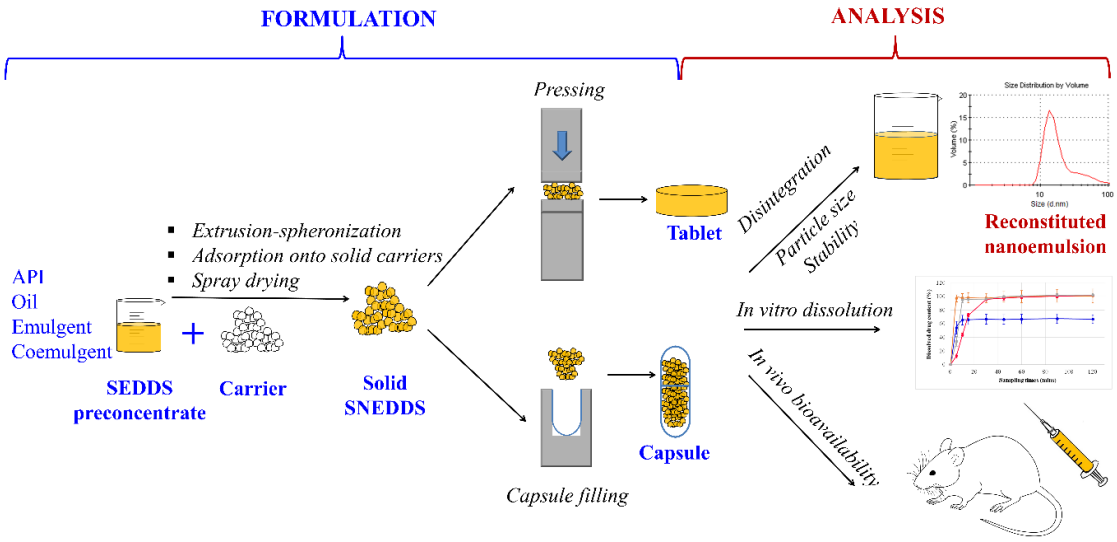

Figure 9. Formulation and analysis possibilities of solid SEDDS *(self-made)*

Extrusion-spheronization

Extrusion-spheronization is an agglomeration technique involving multiple processes for the preparation of matrix pellets. A compromise between the smallest amount of adsorbent material needed and the largest amount of liquid SEDDS required is essential to produce pellets with good physical characteristics and highest possible drug loading (112). Sticking of extrudate, friable and soft pellets, challenging spheronization process and decreased porosity are the main consequences of high liquid SEDDS content (113). Reconstitutability and self-emulsifying properties of matrix pellets were confirmed in several studies (114, 115). The order of components mixing was identified as a critical parameter for a successful extrusion/spheronization process and for the roundness value of pellets (116). Colloidal silicon dioxide, microcrystalline cellulose and lactose were successfully utilized for the preparation of self-emulsifying matrix pellets. HLB value of emulgent in liquid phase influences the processability and mechanical properties of pellets. Matsaridou et al. pointed out that the required water quantity for pelletization rose linearly with increasing HLB values (117). Furthermore, the higher the HLB, the faster the disintegration time. Extrusion-spheronization method is suitable for the production of modified release dosage forms. It can either be carried out by formation of a slowly dissolving matrix structure (e.g. HPMC, PVP) that delay release of the drug or by coating the surface of pellets with gastroretentive polymeric dispersion (118).

Adsorption onto porous solid carriers

The simplest and most intensively investigated method to formulate solid SEDDS is adsorption to highly porous solid carriers. Generally used carriers for adsorption of liquid SEDDS are:

- silicon dioxide; fumed silica with different grades of specific surface (Aerosil®) or micronized amorphous silica with different grades of pore volume (Sylysia®);
- magnesium aluminometasilicate with different surface properties (alkaline or neutral) and particle size (Neusilin®)
- porous dibasic calcium phosphate anhydrous (Fujicalin®) and
- microcrystalline cellulose

Combined application of these carriers have been reported as effective approach for producing solid SEDDS with adsorption method (119). Relative simplicity, absence of organic solvents, easy scale up, high drug loading and small number of solid excipients needed are advantages of adsorption method (120). Drug loading is in close correlation with carrier's oil adsorbing capacity; even loadings up to 80 % have been reported; nevertheless, general value is about 50% (121). Beg at al. evaluated the oil adsorbing capacity of various porous carriers, which declines in the following order: Sylysia® 350 > Neusilin® US2 > Sylysia® 550 > Sylysia® 730 > Aerosil® 200 (122). High drug loading and high oil adsorbing capacity are not associated always with superior bioavailability. Yeom et al. pointed out that SEDDS formulated with low oil adsorbing capacity mannitol had better bioavailability compared to other carriers (123). Particle size, porosity (length and diameter of pores), type and amount of adsorbent along with the specific carrier-SEDDS interactions like wettability play a crucial role in dissolution kinetics and drug release. The effect of wettability, the affinity between lipid components and surface of solid carriers was highlighted by hydrophilic (Aerosil® 200) and hydrophobic porous silica particles (Aerosil® R972) with similar nanostructures (124). The surface interactions were significantly greater between hydrophobic particles and lipid components, which was confirmed by only 33% nifedipine release, compared to 80% of hydrophilic silica particles. Thus, the remarkable hydrophobic forces can be utilized to sustain the solubilisation of lipophilic drugs. However, these interactions have been reported as contraproductive in some cases; the incomplete drug release had to

counterbalance using superdisintegrant in the formulations (125). Complete drug release can be also hampered due to gel formation and clogging of pores (126).

Spray drying

Spray drying is a well-known gentle, rapid, cost-effective and scalable process in pharmaceutical industry, where the dry powder is made from a fluid material by atomization it into a hot drying gas, usually air. For the production of solid SEDDS sufficient carriers are needed that can influence drug release and oral bioavailability of incorporated drug (127). Low yield and the stability issue of volatile cosurfactants (e.g. Transcutol®, ethanol) due to relative high drying temperature must be kept in mind during formulation development (128). Further limiting factor for this technique is the viscosity of SEDDS; it must be low enough to enable spraying onto the carrier. Several hydrophobic (colloidal silica, magnesium stearate) and hydrophilic (e.g. maltodextrin, dextran, HPMC, lactose, poly vinyl alcohol) carriers were investigated for spray dried solid SEDDS. Controlled drug release from solid SEDDS can be obtained by water-soluble carriers, which exert erosion and swelling-dependent drug release mechanisms. Yi et al. prepared nimodipine-loaded solid SEDDS stabilised with HPMC of various viscosities. Formulation with higher HPMC viscosity demonstrated a reduced release rate due to the inhibition of drug diffusion through dense polymer matrix and sustained polymer erosion (129). Prevention of *in vivo* drug precipitation can be achieved by adding polymers like gelatine and Soluplus® to the dispersion to be spray dried (130).

1.6. Cyclodextrin complexation

Cyclodextrins (CDs) are cyclic oligosaccharides composed of α-1,4-linked D-glucopyranose units possessing a hydrophilic exterior and hydrophobic cavity, where lipophilic molecules can form a non-covalently bonded inclusion complex (131). Although they have been discovered in the early 1890s, the attention was drown to CDs in the 1980s with the first application in the pharmaceutical and food industries (132). These molecules can operate and become widespread as excipients throughout the whole industrial and agricultural sector. In pharma industry CDs are used for the improvement of water-solubility and bioavailability of medicinal products. They are used for example in tablets, aqueous parenteral solutions, nasal sprays and eye drop solutions (4). In food

industry their taste masking and flavour stabilizing along with food preservative effect is utilized (133). In agriculture CDs are applied for improvement of the physico-chemical characteristics of pesticides, extension of shelf-life and reduction of environmental pollution (134).

1.6.1. Short history of Cyclodextrins

Antoine Villiers French pharmacist described in 1891 the formation of unexpected crystals with particular properties during a potato starch fermentation reaction by *Bacillus amylobacter*. Villiers concluded that the properties of these special dextrins were very clearly different from those of the various saccharides known at that time (132). The next exciting scientific result of CD research was linked to the work of Austrian Franz Schardinger. In two publications (1903, 1911) he described the preparation, separation and purification of Dextrin A and B, which he classified as cyclic polysaccharides (135). His hypothesis regarded to the cyclic structure of Dextrin A and B was confirmed in 1948 by Freudenberg et al. Friedrich Cramer introduced first the term "cyclodextrin" (1956) and provided numerous data on cyclodextrin host-guest complexes and basic physicochemical characteristics (136). The "CD bomb" was exploded in the 1980's: the nontoxicity of CDs became increasingly accepted, and several manufacturers started to produce and to market CDs. The first CD-containing product, a prostaglandin E2/β-CD (Prostarmon E™) sublingual tablet was launched in Japan, 1976. Since then a great number of patents, publications and products were the outcome of CD inclusion complexes to enhance solubility, improve stability and increase bioavailability of drugs. Today the annual CD production is over 10000 tonnes and CDs can currently be found in over 60 marketed pharmaceutical products *(Tbl. VI.)* (137). Traditionally, CDs are used as excipients, however several research groups all over the world are investigating their potential as active pharmaceutical ingredients. Bridion® (modified γ-CD by placing eight carboxyl thio ether groups at the sixth carbon positions) and HP-β-CD, which are used for reversal of neuromuscular block in anaesthesia and for the treatment of fatal genetic Niemann Pick Type C disease, a cholesterol metabolism disorder, respectively. The latter one has received an orphan drug designation (EU/3/11/895) (138).

Table VI. FDA approved pharmaceutical products with cyclodextrins

Drug	**CD**	**Trade name**	**Dosage form**
Alprostadil	α-CD	Edex®	Injection
Piroxicam	β-CD	Brexin®	Tablet
Omeprazol	β-CD	Omebeta®	Enteric capsule
Metronidazole	β-CD	Flagyl®	Vaginal gel
Aripiprazole	SBE-β-CD	Abilify®	I.m. solution
Ziprazidone	SBE-β-CD	Zeldox®	Capsule
Itraconazole	HP-β-CD	Sporanox®	Oral solution
Mytomicin	HP-β-CD	MitoExtra®	I.v. infusion
Chloramphenicol	RAMEB	Clorocil®	Nasal spray
Minoxidil	γ-CD	Alopexy®	Hair solution

Abbreviations: *HP-β-CD* ((2-hydroxypropyl)-*β*-CD), *RAMEB*-CD (random methylated *β*-CD) (*SBE-β*-CD (sulfobutylether-*β*-CD), I.m. (intramuscular), I.v. (intravenous)

1.6.2. Physicochemical characteristics of Cyclodextrins

Naturally occurring parent CDs are crystalline, homogeneous, nonhygroscopic substances, which are toroidal macro-rings built up from glucopyranose units. α, β, and γ CDs comprise of 6, 7, and 8 glucopyranose units, respectively, and differ in their molecular weight, cavity size, and solubility *(Fig.10/A., Tbl. VII.)*. There are bigger CDs composed of 9 (δ-CD), 10 (ε-CD), and 11 (ζ-CD) glucose units, but their practical suitability is negligible in the field of pharmaceutical sciences (139). The glucopyranose units adopt a $^4C_1$ conformation and orient themselves so that the molecule forms the aforementioned torus-like geometry. The consequence of this geometry is that the CD molecule has a hydrophilic (exterior) surface and a considerably less hydrophilic (interior) microenvironment in its cavity (140).

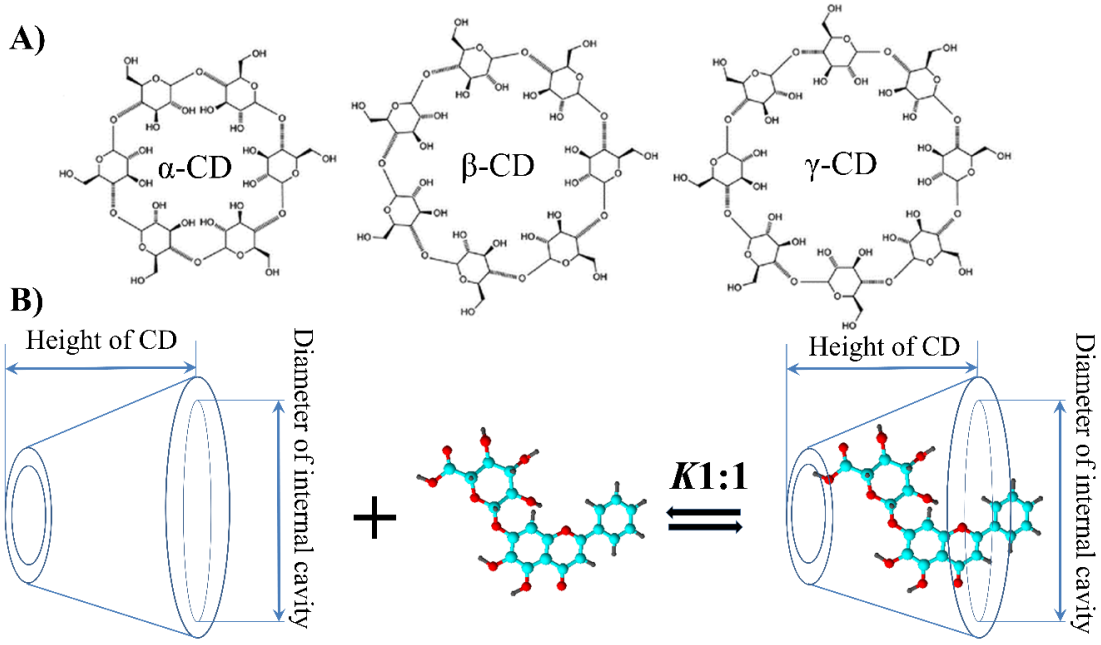

Figure 10. Chemical structure of α-, β-, and γ-CD (A). Schematic demonstration of CD and drug inclusion mechanism (B) *(self-made)*

The polarity of the cavity has been estimated to be similar to that of aqueous ethanolic solution. This attribute gives CDs the opportunity to host molecules possessing low water solubility *(Fig.10/B.)*. All secondary hydroxyl groups are situated on one of the two rims ("wider") of the ring, whereas all the primary ones are placed on the other rim ("narrower") (141). These hydrophilic groups are outside of the molecular cavity, whereas the inner surface has a less hydrophilic character due to the ether-like anomeric oxygen atoms and the skeletal carbon atoms.

Table VII. Physicochemical properties of parent and derivate cyclodextrins *(self-made)*

Property	**α-CD**	**β-CD**	**γ-CD**	**HP-β-CD**	**RAMEB**	**SBE-β-CD**
Glucose units	6	7	8	7	7	7
Molecular weight (g/mol)	972	1135	1297	1135.0 + n·(58.2)	1135.0 + n·(14.1)	1135.0 + n·(158.2)
Internal cavity diameter (nm)	0.57	0.78	0.95	0.78	0.78	0.78
Internal cavity height (nm)	0.78	0.78	0.78	~ 0.78	~ 0.78	~ 0.78
Cavity volume (nm^3)	0.174	0.262	0.472	~0.262	~0.262	~0.262
Solubility (mg/ml)	158	185	232	> 500	>600	>500

Substitution of any of the hydrogen bond-forming hydroxyl groups of native CDs, even by lipophilic functions, results in a dramatic improvement in their aqueous solubility, referred as CD derivates (141). The modification of natural (parent) CDs generally aims at converting them into amorphous, non-crystallisable derivatives, to provide high CD concentration in aqueous solutions. Number of CD derivates exceeds 11.000, but new types are permanently developed (142). At present, α-CD, β-CD, γ-CD, HP-β-CD, RAMEB and SBE-β-CD are used in medicines on the European market (143). According to regulatory requirements, the extent of substitution must be defined to avoid any misunderstandings. Conventionally, the so-called average degree of substitution (DS) is used, which gives the average number of substituted hydroxyls of a glucose unit (142). One of the largest developer, producer and supplier of CD derivates and a pioneer in CD-based innovation is CycloLab, headquartered in Budapest, Hungary.

1.6.3. Formation of drug-cyclodextrin inclusion complex

Cyclodextrin molecules are able to form non-covalently bounded drug-CD complexes and therefore to host lipophilic moieties into the cavity *(Fig.9/B.)*. There is a dynamic equilibrium between the molecules bound in the complex and the free drug molecules in solution. Higuchi and Connors' phase-solubility method is used to study the effect of cyclodextrin concentrations on drug solubility and to describe the complexation process *(Fig.11.)* (144).

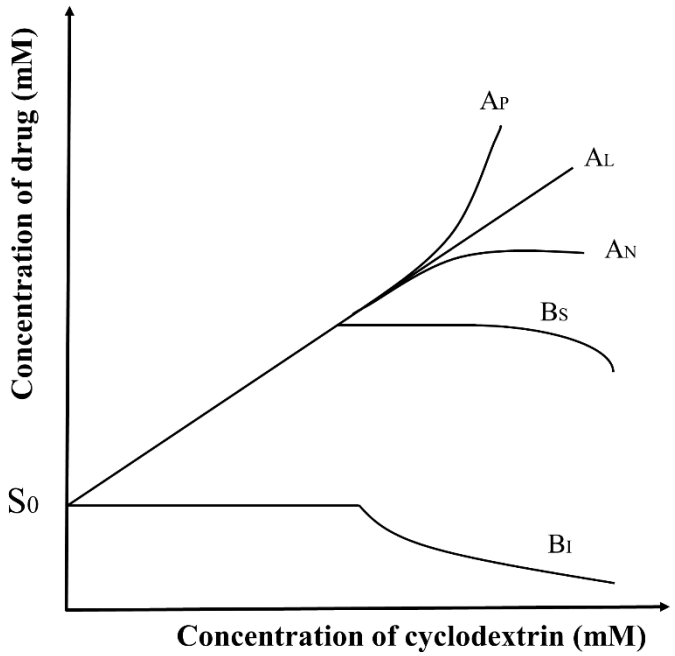

Figure 11. Types of phase-solubility isotherms according to Higuchi and Connors *(self-made)*

Abbreviations: A_L: linear diagram; A_P: positive deviation from linearity; A_N: negative deviation from linearity; B_S: the complex has limited solubility; B_I: insoluble complex; S_0: intrinsic drug solubility.

In cases when the formed complex is insoluble (B_I), the solubility of the guest remains unaltered until all guest molecules converted into insoluble CD complex; thereafter a decrease in the concentration of dissolved drug can be detected. A typical B_S-type solubility curve is, where the initial ascending portion is followed by a plateau region and then a slight decrease in total drug solubility accompanied by precipitation of complex. If the solubility limit of complex is higher than the studied CD concertation range, the isotherm is of type A. A_L-type isotherm describes a linear increase with constant

stoichiometry, while A_P-type represents a positive deviation from linearity indicating a continuous rise in the stoichiometry of complex. A_N-type isotherm can be described by complex processes: either the host ratio within the complex increases or there is a change in solvent-solute interactions (ionization, hydrolysis), or both contribute at the same time (145).

The complex formation is a reversible process and can be described with the following equitation:

$$m \times \mathrm{D} + n \times \mathrm{CD} \overset{K_{m:n}}{\longleftrightarrow} [\mathrm{D}_m\mathrm{CD}_n] \quad (1)$$

where *m* drug molecules (D) associate with *n* cyclodextrin (CD) molecules to form a complex of *m:n* stoichiometry. $K_{m:n}$ is the observed stability constant of the complex, also known as the binding constant, formation constant, or association constant. Rearranging eq. (1) $K_{m:n}$ can be expressed as:

$$K_{m:n} = \frac{[\mathrm{D}_m\mathrm{CD}_n]}{[\mathrm{D}]^m \times [\mathrm{CD}]^n} \quad (2)$$

If the intrinsic solubility (S_0) of drug is defined as drug solubility without CD and the formed complex is D-CD, then:

$$[D] = S_0 \quad (3) \qquad [D]_{Total} = S_0 + [D - CD] \quad (4)$$

where $[\mathrm{D}]_{\mathrm{Total}}$ is the total drug solubility assuming 1: 1 complex stoichiometry. Plotting $[D]_{Total}$ against $[CD]_{Total}$ gives a linear function, where the intercept is S_0, the slope of linear is B. The stability constant ($K_{1:1}$) of drug-CD inclusion complexes can be calculated as

$$K_{1:1} = \frac{B}{S_0 \times (1 - B)} \quad (5)$$

In this thesis all stability constants were calculated using eq. (5).

1.6.4. Toxicological assessment and regulatory status of Cyclodextrins

The safety and toxicity of cyclodextrins depend on the route of administration and dose. Due to their molecular weight and relative high hydrophilicity, CDs are not absorbed from the GIT, therefore oral administration is basically considered as safe. For parenteral use, α-, HP-β-, and SBE-β-CD are approved and regarded as safe. Intravenously administered CDs are rapidly removed from the systemic circulation and are renally excreted (146). In case of heterobranched CD-derivates, a transglycosylation step is possible. The haemolytic effect of CDs has been reported in many *in vitro* publications. Irie and Uekama pointed out that the haemolytic effects of various CD derivatives and parent CDs decrease in the order of β-CD > HP-β-CD ≥ α-CD >> γ-CD, whereas SBE-β-CD was nonhaemolytic (147). However, the clinical relevance of haemolytic side effect is negligible. In animal studies after oral administration α-, β-, HP-β, SBE-β-, and γ-CD mild side effects like soft faeces, diarrhoea or cecal enlargement were observed. These side effects can be attributed to a high intake of poorly indigestible carbohydrates (148). The negative effect of CDs on kidney is well-known for a long time. It was demonstrated that host-guest complexes of cholesterol/CD enter by glomerular filtration and are then taken up by the kidney tubular cells, where the insoluble cholesterol aggregates cause kidney damage (148). It is important to note that the different CDs have different renal toxicity. No observed effect level (NOEL) was shown in case of α-, HP-β-, SBE-β-, and γ-CD administering 75 mg/kg, 50 mg/kg, 80 mg/kg and 200 mg/kg intravenous injection daily for a month in rats, respectively (149, 150). RAMEB and β-CD, however, generates irreversible cell injury and kidney dysfunction and thus are not suitable for medicinal products given intravenously (151). EMA has reported a guideline summarizing the approved cyclodextrin-containing formulations depending on administration route considering the clinical and non-clinical data *(Tbl. VIII.)* (143). Furthermore, it proposes various recommendations for the safe and efficient utilization of cyclodextrins.

Table VIII. Approved cyclodextrin types depending on administration route (143)

Route	**α-CD**	**β-CD**	**γ-CD**	**HP-β-CD**	**RAMEB**	**SBE-β-CD**
Oral		X	X	X		X
Parenteral	X			X		X
Dermal		X	X	X		
Nasal					X	
Ocular		X		X	X	
Rectal		X		X		

The regulatory status of cyclodextrins vary greatly from country to country *(Tbl. IX.)*. In the EU, Japan and USA an approved claim can be found for α-, β-, and γ-CD as food ingredients. Parent cyclodextrins as well as CD derivates are listed as pharmaceutical excipients in the EU, Japan and USA. The monograph of SBE-β-CD is already referenced in the Japanese Pharmaceutical Codex (JPC) and U.S. Pharmacopoeia (USP) and will be included in the European Pharmacopoeia (Ph. Eur.) next year.

Table IX. Regulatory status of cyclodextrins in foods and pharmaceuticals

	Regulatory status in food			**Regulatory status in pharmaceuticals**		
	EU	USA	Japan	EU	USA	Japan
α-CD	Novel food ingredient	GRAS	Natural product	Monograph	Monograph	Monograph
β-CD	Food additive	GRAS	Natural product	Monograph	Monograph	Monograph
γ-CD	Novel food ingredient	GRAS	Natural product	Monograph	Monograph	Monograph
HP-β-CD	-	-	-	Monograph	Monograph	Monograph
SBE-β-CD	-	-	-	-	Monograph	Monograph

Regulation (EC) N° 1223/2009 on cosmetic products is the main regulatory framework for finished cosmetic products when placed on the EU market. CosIng is the European Commission database for information on cosmetic substances and ingredients contained in the Regulation (EC) N° 1223/2009.

According to the database as of 12/12/2019, 12 Cyclodextrins are referred and approved as cosmetic substances (chelating, viscosity controlling, emulsion stabilizing, skin conditioning, absorbing, surfactant) in the EU:

1. Acetyl cyclodextrin
2. Cyclodextrin crosspolymer
3. Cyclodextrin Hydroxypropyltrimonium Chloride
4. Cyclodextrin laurate
5. Dimaltosyl Cyclodextrin
6. Hydroxyethyl Cyclodextrin
7. Hydroxypropyl Cyclodextrin
8. Maltosyl Cyclodetrin
9. Methyl Cyclodextrin
10. Sodium Cyclodextrin Butylsulfonate
11. Sodium Cyclodextrin Sulfate
12. Sodium Hydroxypropyl Cyclodextrin Octenylsuccinate

1.6.5. Methods of preparation of inclusion complexes

In the scientific literature one can find numerous approaches for the preparation of drug-CD inclusion complexes. On the one hand, the selected method along with the process parameters applied considerably influences the final product. On the other hand, an optimized and efficient complexation is needed for the demanded improved dissolution rate and greater bioavailability enhancement (152). The most popular techniques available for the inclusion preparation can be divided on the basis of complex state; a) methods in solution, b) methods in semisolid state and c) methods in solid state *(Fig.12.)*.

Methods in solution

There are extensive data about the different solution methods, where drug and CD is perfectly dissolved in purified water and/or organic solvents. Temperature, pH and ionic strength are critical parameters for the appropriate interaction between the compounds. One option is the rapid cooling down of equilibrated mixture to precipitate out of solution the complex (153). Similarly, precipitation of drug–CD complex can be achieved by

adding antisolvent, which precipitates the complex. Other opportunity is the removal of solvent(s) from the system via solvent evaporation (154), spray drying (155, 156) or freeze drying (157, 158). Appreciable drawback of these procedures is the general organic solvent demand and time-consuming attribute. When using organic solvents, the formulation has to be always evaluated for residuals.

Methods in semisolid state

Hot-melt extrusion (HME) is a recognized, continuous process for manufacturing of solid dispersions and innovative dosage forms. HME is also a suitable method for creating paste-like extrudates containing drug-CD complexes. The API, CD and amorphous polymer are fed into the extruder, conveyed, exposed to shear inside the extruder and subsequently the extrudate is pressed out through a die. Yano and Kleinebudde used HP-β-CD to improve the dissolution behaviour of indomethacin by HME (159). Thiry et al. studied HME to form CD-itraconazole (ITZ) complexes using different CDs in a 1:1 (CD:ITZ) molar ratio (160). It was revealed that the polymer is not only a matrix forming agent, but also increase the stability of inclusion complex (161).

Simple kneading is a possibility to formulate a homogenous pasty product, where the drug-CD physical mixture is kneaded with moistening agent (water/ethanol) in a high-shear granulator (industrial scale) or in a mortar (laboratory scale). This is followed by drying and sieving of the powder. Nonetheless, such a method often results a low complexation ratio (153).

Methods in solid state

The complexation process can be initiated by microwave irradiation (MWI), by gentle heating or by mechanochemical activation through grinding with mortar-pestle combination or with different types of mills. The disadvantage of thermal stimulation is the potential degradation of API. Grinding, on the other hand, gives the opportunity to be a cheap, fast and highly effective method for the formulation of drug-CD inclusion complexes in the solid state, generally without using of organic solvents. He et al. carried out the molecular encapsulation of rifampicin into HP-β-CD by simple manual grinding using mortar and pestle creating an amorphous product with 2.5 times higher solubility and enhanced antimicrobial activity (162) . The complex preparation is also feasible by

planetary ball mills operated with alternating periods (overall time from 1 to 5 h) to prevent overheating and rotation speed of 400-600 rpm (156).

Methods in solution

Crystallization

a) Cooling
b) Antisolvent
c) Co-Evaporation
d) Spray drying
e) Freeze-drying

Methods in semisolid state

a) Hot-melt extrusion
b) Kneading

Methods in solid state

Thermal activation

- Microwave irradiation
- Heating

Mechanochemical activation

- Planetary ball mill
- Tumbling ball mill
- Vibrational mill
- Physical blending

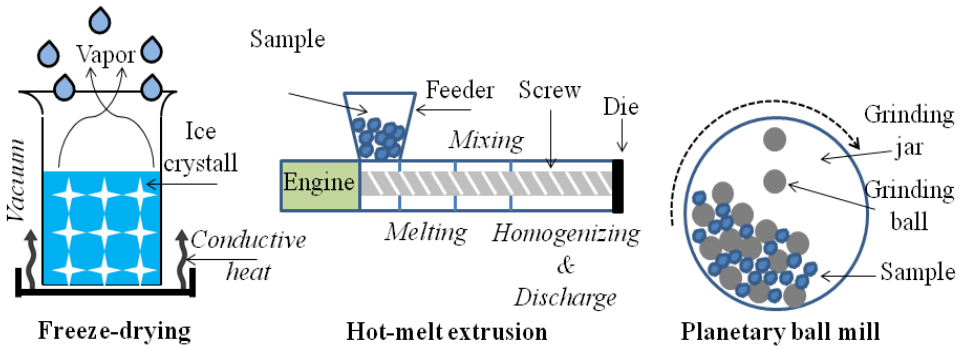

Figure 12. Frequently used formulation processes of drug-CD inclusion complex *(self-made)*

Li et al. used planetary ball mill for the preparation of bisacodyl-β-CD complex, where the process parameters were 5 h process time (5 min run and 1 min pause) at 400 rpm in 50 ml agate jar. The end product was fully amorphous and indicated better solubility compared to complexes formulated by co-evaporation or freeze-drying (163). High-energy vibrational mills and tumbling ball mills are seldom used for this purpose.

1.6.6. Pharmaceutical application of cyclodextrins

The complex-forming ability, special shape and structure along with the extensive formulation possibilities laid the foundation of cyclodextrin application in field of pharmaceutical technology and industrial pharmaceutics. Cyclodextrins were first described by Villiers in 1891, however, the first pharmaceutical product including cyclodextrin as excipient was marketed 85 years later in Japan (*see detailed in Section 1.6.1.).* 130 years after their discovery a marked progress has been made, but CDs are still regarded as pharmaceutical excipients of enormous unexploited potential (137).

The most characteristic application field of CDs is the solubility enhancement of lipophilic drugs with poor water solubility. Furthermore, wettability of apolar surfaces, dissolution time and complex stability is also increased. API-CD complexes compared to other solubilization techniques have several beneficial properties:

- Due to the lack of surfactants, the tissue irritation and further side effects can be avoided.
- The risk of precipitation on dilution in GIT juices is practically negligible.
- Numerous administration routes can be applied (e.g. per oral, dermal, ocular, parenteral, nasal, as well as drug targeting formulations).
- Inside the cavity of CD, acid sensitive drugs can be stabilized and protected.
- In this context, a reliable, non-invasive delivery of proteins (e.g. insulin) and formulation of CD-siRNA-conjugates have been successfully demonstrated.

In addition, the CD complexation is utilized in many more fields of pharmaceutical technology and analytics:

- Tissue toxicity and irritative potential of drugs are reduced.
- Physical, chemical and photochemical stability are ameliorated.
- Odour and taste masking effect.
- Shelf-life and effect of volatile substances (aromatics, fragrances, essential oils) are sustained.
- Cyclodextrin crosspolymers due to their swellability have a potential as disintegrants of solid dosage forms.

- CDs are naturally chiral molecules; therefore, they are the most frequently used chiral additives for the separation of various enantiomers.
- In the elimination of residual solvents, impurities, degradation products CDs are often involved.

2. Objectives

The main objective of this work was to formulate and develop baicalin-loaded DDS in order to counterbalance the negative physicochemical and pharmaceutical properties of baicalin. For this challenging task, the preformulation studies of the drug were put in the focus, which provided strong basis for the development, optimization and comparison of baicalin-cyclodextrin inclusion complexes and of baicalin-loaded self-emulsifying DDS. Considering the above mentioned, my aims were the followings:

1. Quantify the most important biorelevant physicochemical properties of baicalin in terms of acid/base, lipophilicity and thermodynamic solubility in different compendial and physiological media. Explore its polymorphism and crystal structure, crystal habit, particle size, thermal behaviour.
2. Preparation and comparative evaluation of various baicalin-CD inclusion complexes. In order to reveal the molecular interactions inside the cavity and to characterize the 3D geometry of the complex, each species was subjected to phase solubility, ^{1}H NMR and 2D ROESY experiments along with molecular modelling of the binding pattern into cyclodextrins. Comparison of computational study and experimental results were also in my interest.
3. Enhance the poor aqueous solubility and dissolution rate via a liquid self-nanoemulsifying drug delivery system. Find an optimized carrier system for baicalin, and to analyse and characterize the reconstituted nanoemulsion using AFM, droplet size, and Zeta-potential measurements, long-term stability tests, and *in vitro* dissolution studies. Elaborate a sample preparation method for AFM imaging of nanosized droplets was also a substantial goal.
4. Transform liquid self-emulsifying preconcentrates to solid carriers and prepare self-nanoemulsifying matrix pellets by extrusion-spheronization method. Identify the critical process parameters and reveal the relationships. Analyse the physical state of baicalin in the solid dosage form and follow the incidental alteration(s) in time. Examine the drug release and the reconstitutability of droplets by *in vitro* dissolution studies at pH 1.2 and pH 6.8.

3. Methods

*3.1.*Materials

Baicalin (batch number:BA-16118) was supplied by Actin Chemicals, Inc. (Chengdu, China). Sodium taurocholate, lecithin, pepsin, indicator molecules for the NMR-pH titrations (TRIS, acetamidine hydrochloride and 1-methylguanidine hydrochloride) were purchased from Sigma-Aldrich (Budapest, Hungary), the deuterated solvent D_2O from VWR International (Debrecen, Hungary) and the DMSO-d_6 from Euriso-top (Saint-Aubin, France). The following materials were donated by Gattefossé (Saint Priest, France) and were used as received: Capryol® 90 (Propylene glycol monocaprylate), Labrafac™ Lipophile WL 1349 (Medium-chain triglycerides), Labrafil® M 1944 CS (Oleoyl polyoxyl-6 glycerides), Labrasol® (Caprylocaproyl polyoxyl-8 glycerides), Lauroglycol™ 90 (Propylene glycol monolaurate), Maisine® CC (Glyceryl monolinoleate), Peceol™ (Glyceryl monooleate (type 40)), Transcutol® P (Dyethylene glycol monoethyl ether). Kolliphor® EL (Polyoxyl 35 hydrogenated castor oil), Kolliphor® RH40 (Polyoxyl 40 hydrogenated castor oil), Olive oil, Emprove® (Absolute ethanol) were purchased from Sigma Aldrich (St. Louis, USA). Sunflower oil was supplied by Hungaropharma (Budapest, Hungary). GalenIQ™ 800 (Isomalt) was kindly gifted by Beneo Palatinit GmbH (Mannheim, Germany). Avicel® PH 101 was supplied by DuPont Nutrition & Biosciences (Midland, USA). All CDs (α-CD, β-CD, γ-CD, (2-hydroxypropyl)-β-CD (HP-β-CD), random methylated β-CD (RAMEB-CD) and sulfobutylether-βCD (SBE-β-CD)) were kindly donated by Cyclolab R&D Ltd. (Budapest, Hungary). Other chemicals of analytical grade were obtained from commercial suppliers and used without further purification. Bidistilled water was used for all NMR solutions; for solubility analysis, freshly prepared distilled water was applied.

3.2. Preparation of compendial and biorelevant media

The pH value of each solution was controlled with a Hanna® pH 210 microprocessor pH meter (Hanna Instruments, USA) and media were prepared according to literature at room temperature (27).

A total of 0.94 g of 1 M HCl and 0.35 g of NaCl were diluted and dissolved to 1000 ml with distilled water and used as simulated gastric fluid (SGF) with pH 1.2. A total of 250 ml of 0.2 M K_2HPO_4 and 77 ml of 0.2 M NaOH were homogenized and diluted to 1000 ml with distilled water. This medium served as simulated intestinal fluid (SIF) with pH 6.8.

Blank buffer of FaSSGF pH 1.6 (1.99 g NaCl dissolved in 900 ml distilled water, adjusted the pH to 1.6 with 1 M HCl and filled to 1000 ml with distilled water) and phosphate buffer pH 6.5 (0.42 g NaOH pellets + 3.95 g NaH_2PO_4 monohydrate + 6.19 g NaCl dissolved in 900 ml distilled water, adjusted the pH to 6.5 with either 1 M NaOH or 1 M HCl and filled to 1000 ml with distilled water) were prepared as stock solutions.

FaSSGF was produced from blank buffer of FaSSGF pH 1.6, which was completed by 0.08 mM sodium taurocholate, 0.02 mM lecithin, 0.1 mg/ml pepsin and has osmolality of 120 ± 2.5 mOsmol/kg. To obtain the FaSSIF medium, 100 ml of blank phosphate buffer (pH 6.5) was made up by 3 mM sodium taurocholate and 0.75 mM lecithin. FaSSIF has an osmolality of 270 ± 10 mOsmol/kg.

3.3. Preformulation studies

3.3.1. Determination of Thermodynamic Solubility by Saturation Shake-Flask Method

The thermodynamic solubility of baicalin in various media was determined by saturation shake-flask method based on the method of Baka et al. (164). Briefly, 10 mg of baicalin was added to 5 ml of each solvent in sealed vials. All samples were stirred (approx. 500 rpm) and thermostated (IKA RT-5 power heatable magnetic stirrer, IKA Work Inc., USA) at 37 ± 0.5°C for 24 h allowing it to achieve thermodynamic equilibrium. After this period, 24 h of sedimentation cycle was adopted without stirring at 37 ± 0.5°C. To improve the efficacy of phase-separation, the saturated supernatant of samples was centrifuged at 14,000 rpm for 15 min (Herolab MicroGen 16, Herolab GmbH, Wiesloch,

Germany). The aliquots (250 µl) taken for solubility experiments were suitably diluted with blank buffers and the absorbance was measured at λ = 316 nm by UV spectroscopy (Agilent 8453 UV-Visible Spectrophotometer, Agilent Technologies Ltd., USA). The drug exhibited absorption maxima (λ_{max}) at 214, 279 and 316 nm in distilled water. Ideally, λ_{max} selected for the analysis of drug should not show any interference due to solvents and excipients present in the dissolution medium. At 279 nm, baicalin showed higher molar absorptivity; however, this wavelength was not selected for the quantification of the drug because there was interference of excipients in biorelevant media at this wavelength. In the solubility study, thus, λ_{max} 316 nm was selected for the quantification of baicalin. In case of the distribution study, the above-mentioned obstacle did not appear, so λ_{max} 279 nm could be easily used. All experiments were repeated three times and results were calculated from the linear calibration curve of baicalin in each media. Data are expressed as mean ± SD (µg/ml).

3.3.2. Acid-base properties

NMR-pH titrations were performed on a Varian VNMRS spectrometer (600 MHz for ^{1}H). Spectra were recorded at 25°C. Titrations were carried out in solutions containing 95% (v/v) H2O and 5% (v/v) D_2O, with the addition of small amounts of 0.1 M HCl and NaOH. One molar NaOH and solid NaOH crystals were also used to achieve highly basic pH values. The ionic strength was kept at 0.15 M by the presence of NaCl. The concentration of baicalin and its methyl ester was 1.0×10^{-3} M and ascorbic acid was used in large excess (5.0×10^{-3} M) to prevent the oxidation of the studied catechol molecules in alkaline solutions. The sample volume was 600 µl. NMR spectra were referenced to the internal standard DSS (sodium 3- (trimethylsilyl)-1-propanesulfonate). The water signal was suppressed by presaturation. Spectra were processed with VNMRj 3.2a software. pH values were read on a Metrohm 2.780.0010 precision pH meter with a 6.0258.600 Unitrode glass Pt 1000 electrode (Metrohm AG, Herisau, Switzerland). The pH-potentiometric system was calibrated using pH 1.68, 4.01, 6.87, 9.18 aqueous buffer solutions. In highly basic solutions, pH was measured by NMR-pH indicator molecules as well to avoid the uncertainty of the glass electrode pHmeter readings in such solutions (165). The concentration of these pH indicators was 1.0 mM. For the analysis of NMR

titration curves of proton chemical shifts versus pH, the software Origin Pro 8 (OriginLab Corp., Northampton,MA, USA) was used.

3.3.3. Distribution Coefficient Measurements by the Stir-Flask Method

The distribution coefficients were calculated from the absorbance of the molecules before and after partitioning at several octanol/water phase ratios (166). For the pH control, a pH 7.40 phosphate buffer and a standardized HCl solution were used, with an ionic strength of 0.15 M in both cases. The pH of the phosphate buffer was measured using a Metrohm 6.0204.100 combined pH glass electrode and a Metrohm 780 pH meter. The concentration change of baicalin was followed by UV-absorbance measurements. Because of the poor water solubility in acidic solutions, the absorbance of the octanol phase (with an initial baicalin concentration of 4.2×10^{-5} M) had to be monitored in the partition experiments with 0.15 M HCl. However, at pH 7.40, the solubility in water was high enough to follow the concentration change of baicalin in the aqueous phase, starting from the initial concentration of 5.6×10^{-5} M. Several water/octanol phase ratios were used, depending on the pH and the expected log D value, to ensure that the absorbance of baicalin after partitioning should become approximately half as much as the original value before partitioning. Then, the two phases were intensively stirred for 2 h in thermostated double-walled glass cells at constant temperature (25 ± 0.1°C). After separation of the equilibrated phases and centrifugation, the concentration of baicalin was determined by UV spectrophotometry (Perkin-Elmer Lambda 15) at several values at 279 nm (λ_{max}). The distribution coefficients were calculated from the absorbance of baicalin before and after partitioning.

3.3.4. Crystal habit

The external shape and morphology of individual crystals were characterized by Scanning Electron Microscopy (SEM). SEM images were collected from the surface of individual particles operating JSM 6380LA Series Scanning Electron Micrpscope (JEOL Inc., USA). Accelerating voltage varied from 5 kV to 10 kV and spot size from 8 to 10 depended on the electrostatic charge-up of microstructured surface. 100–500 times of zoomed in images have been taken for particle size determinations and 1000–3000 times for particle surface comparisons.

3.3.5. Particle size analysis

Particle size of baicalin was determined by Laser Diffractometry (LD) method with the instrument Mastersizer 2000 laser diffractometer (Malvern Instruments Ltd., UK). Sample preparation involved dispersing 3.00 w/w% baicalin and 0.50 w/w% Polysorbate 80 solution into demineralized water and dilute it to 100.0 ml. The dispersion was poured into Mastersizer Hydro SM small volume dispersion unit at a mixing speed of 1500 rpm, which yielded 10 % laser obscuration. Sample absorbance was measured prior particle sizing by an 8453-type, single beam UV-Vis spectrophotometer, (Agilent Technologies, USA) on wavelength λ_{max} = 633 nm, which is the wavelength of red He-Ne laser beams, found in instrument Mastersizer 2000 laser diffractometer. Laser diffraction measurement was performed based on Mie scattering theory, pre-set measurement parameters including refractive index of baicalin 1.739, refractive index of dispersant water 1.333 were utilized with general purpose measurement enhanced sensitivity mode, which is suitable for sample characterizations containing irregular shaped particles. Every sample was measured five times individually and the mean ± standard deviation values are reported. Each measurement took 20 seconds to perform suggested by the Malvern diffraction application v.5.60.10.0 (Malvern Instrument Ltd., UK), to allow slow moving larger aggregates to pass through the detector array.

3.4. Baicalin-Cyclodextrin inclusion complexation

3.4.1. Phase solubility studies

The phase solubility studies were carried out according to the method of Higuchi-Connors (167). Experimentally, an excess amount of baicalin (10 mg, 2.25 mM) was added to increasing concentrations (5, 10, 20, 40, 80 mM) of various distilled water-based CD stock solutions at pH 4.5 (in case of β-CD—because of its low aqueous solubility—1.25, 2.5, 5, 7.5, 10 mM stock solutions were prepared). The vials were agitated by ultrasonication (Branson 5200, Danbury, USA) for 4 h followed by 72 h of equilibration phase (25°C). After sedimentation, the saturated supernatant was taken and centrifuged at 14,000 rpm for 15 min with Herolab MicroCen 16 centrifuge (Herolab GmbH, Wiesloch, Germany). Samples were suitably diluted with distilled water and drug concentration was obtained via UV spectroscopy at wavelength 279 nm (Agilent 8453 UV-Visible Spectrophotometer, Agilent Technologies Ltd., USA). All experiments were

repeated three times and results were calculated from the linear calibration of baicalin in distilled water ($R^2 = 0.9992$). Assuming 1:1 complex stoichiometry, the stability constants ($K_{1:1}$) of baicalin-CD inclusion complexes were calculated based on phase solubility diagrams according to Higuchi-Connors (eq. 5).

3.4.2. Signal Assignment of Baicalin and Characterization of Baicalin-Cyclodextrin Inclusion Complexes Using ^{1}H NMR and 2D ROESY Experiments

Assignment and CD complexation NMR experiments were recorded at 25°C on a Varian Mercury Plus spectrometer at 400 MHz. For complete signal assignment, 15 mg of baicalin was dissolved in 0.6 ml DMSO-d_6 and transferred to 5 mm NMR tube. For the investigation of inclusion complexes, cyclodextrin was dissolved in 0.7 ml D_2O and baicalin was dissolved in 0.3 ml DMSO-d_6; these two stock solutions were mixed and sonicated; after 72 h, an aliquot of 0.6 ml was transferred into a 5-mm NMR sample tube. The resulting solution was at 2.5 mM concentration for both compounds. Reference baicalin solution was made by the same method without CD. In the beginning of the experiments, minimal precipitation was observed. Therefore, the concentration of baicalin in the final solution was reduced from 10.0 to 2.5 mM, in which concentration was still enough for the characterization of baicalin-cyclodextrin inclusion complexes and gave sufficient signal/noise ratio. Chemical shifts are given in ppm and are referenced to the residual solvent signal (DMSO-d_6: δH = 2.50 ppm; δC = 39.50 ppm). For investigation of inclusion complexes, ^{1}H spectrum was taken from 64 scans, 24 k data points, the sweep width was 6400 Hz. For the ROESY spinlock, a mixing time of 400 ms was used; the number of scans was 16 and 4 k time domain points and 256 increments were applied. For complete assignment, 32 scans, 32 k data points and 6400 Hz spectral width were used for ^{1}H measurement and 16,384 scans, 64 k data points and 24,154 Hz sweep width were applied for ^{13}C measurement. In case of the gHSQC spectrum, data points were acquired with 1 k × 512 and 4 scans were used. In the gHMBC experiment, 1 k × 256 data points and 8 scans were applied. gCOSY measurement was taken from 1 k × 256 data points and 8 scans. The processing was carried out by using a cosinebell window function, single zero filling and automatic baseline correction.

3.4.3. Molecular Modelling of the Binding into Cyclodextrin

All computations were carried out with the Gaussian09 program package (Gaussian Inc., USA, Wallingford CT, 2009) using convergence criteria of 3.0×10^{-4}, 4.5×10^{-4}, 1.2×10^{-3} and 1.8×10^{-3}, for the gradients of the root mean square (RMS) force, maximum force, RMS displacement and maximum displacement vectors, respectively. The 3D structures of various cyclodextrin structures, like β-CD, γ-CD, RAMEB-CD and SBE-β-CD as well as their complexed forms with baicalin were optimized at B3LYP/6-31G(d) level of theory and compared to each other (168).

3.5. Liquid Self-nanoemulsifying Drug Delivery Systems

3.5.1. Solubility Studies

The thermodynamic solubility of baicalin was determined in distilled water, different oils, emulgents, and co-emulgents by saturation shake-flask method with minor modifications (164). Firstly, an excess amount of baicalin was added to 2 g of each excipient in sealed vials. All samples were stirred (approx. 500 rpm) and thermostated (IKA RT-5 power heatable magnetic stirrer, IKA Work Inc., Wilmington, DE, USA) at 37 ± 1 °C for 24 h. Secondly a cycle of sedimentation (to achieve separation of the excess solid from the solution) was carried out for 24 h at 37 ± 1 °C. To improve the efficacy of phase-separation, the saturated supernatant of samples was centrifuged at 14,000 rpm for 15 min using a centrifuge (Herolab MicroGen 16, Herolab GmbH, Wiesloch, Germany) followed by removal of the incidentally undissolved baicalin from the supernatant by filtering it with a nylon membrane filter (0.22 μm, 25 mm, FilterBio® NY, Labex Ltd., Budapest, Hungary). Samples were suitably diluted with absolute ethanol and drug concentration was obtained via UV spectroscopy at wavelength 279 nm using equivalent proportions of excipients as blank (Agilent 8453 UV-Visible Spectrophotometer, Agilent Technologies Ltd., Santa Clara, CA, USA). All experiments were repeated three times and results were calculated from the linear calibration of baicalin in absolute ethanol ($R^2 = 0.9991$). Data are expressed as mean ± SD (μg/mL).

3.5.2. Screening of Surfactants for Emulsifying Ability

Various surfactants (Capryol® 90, Kolliphor® EL, Kolliphor® RH 40, Labrafil® M 1944 CS, Labrasol®, Lauroglycol™ 90) were screened for emulsification ability with the selected oily compound. According to pre-formulation experiments, different oil:emulgent w/w ratios (1:3, 1:4, 1:5, 1:6) were created, and selection of the emulgent was based on the results of droplet size and transmittance analysis. Briefly, 1 g of pre-concentrate was prepared in sufficient quantities, gently stirred, and heated to 37 ± 1 ˚C, promoting the homogenization process. The isotropic mixture, 0.1 mL, which was accurately weighed and diluted to 100 mL with distilled water, yielded fine emulsions. Emulsions were equilibrated for 2 h at room temperature before measuring their transmittance by Agilent 8453 UV-Visible Spectrophotometer at wavelength 633 nm using distilled water as blank. The droplet size (Z-avg) distribution and polydispersity index were measured by dynamic light scattering (DLS) method with the instrument Zetasizer Nano ZS™ (Malvern Instruments Ltd., Malvern, UK). Measurement settings were: automatic mode, NIBS (none-invasive-back-scattering) 173˚, 30 sub runs/measurements, run duration of 10 s, automatic laser position selected, 4.65 mm position from the bottom of the cuvette, attenuation setting of attenuator 9 was selected automatically. Five measurements with 30 runs were performed for every sample and the mean ± SD values are reported in this article for all DLS parameters, including intensity-weighted mean hydrodynamic diameters (Z-avg) and polydispersity index (PDI).

3.5.3. Construction of Ternary Phase Diagram

In order to identify the self-nanoemulsifying compositions with the desired droplet size (Z-avg < 200 nm), a ternary phase diagram was constructed (169). For every mixture, the surfactant and co-surfactant (S_{mix}) ratios were varied from 1:1, 1:2, 1:3, and 2:1. 2 g of the oil and S_{mix} in different w/w ratios (1:9, 1:8, 1:7, 1:6, 1:5, 1:4, 1:3, 1:2, 1:1, and 2:1) were measured, blended for 1 h at approximately 500 rpm (IKA RT-5 power heatable magnetic stirrer), and heated at 37 ± 1 ˚C. Compositions were evaluated for nanoemulsion formation by dropping 100 µL of each of the 40 mixtures in glass beakers containing 100 mL distilled water that was maintained at 37 ± 1 ˚C, followed by Z-avg measurements (for setting parameters see *Section 3.5.2.*). All experiments were repeated three times and

the ternary phase diagram was constructed using the ProSim ternary diagram drawing application (ProSim, Toulouse, France).

3.5.4. Preparation of Self-Nanoemulsifying Formulations without (SNEDDS) and with Baicalin (BSNEDDS)

In all cases, oil, emulgent, and co-emulgent were thermostated at 37 ± 1 ˚C and stirred (approximately 500 rpm) in different w/w ratios by a heatable magnetic stirrer. After a 1-h homogenization cycle, they were stored at room temperature in sealed vials until further use. BSNEDDS were prepared by the above-mentioned method, but at the end of the homogenization cycle, baicalin was added to the optimized pre-concentrate (C = 2.5 mg/mL).

3.5.5. Optimization of SNEDDS Preconcentrates

In order to reduce the number of trials needed in the optimization of SNEDDS formulation, and to characterize the relationship between the formulation factors and the output variables, a response surface methodology based on Face Centered Central Composite Design was utilized. The amount of oil and S_{mix} ratio can significantly influence the quality and performance of a nanoemulsion, so different oil:S_{mix} (1:8, 1:6, 1:4) ratios and emulgent:co-emulgent (1:1, 2:1, 3:1) ratios were analyzed as formulation variables (X_1, X_2). In the study, a three-level (coded as +1, 0, −1) factorial design for the optimization of two variables with 13 runs (5 centre points) was applied. Droplet size (Y1), transmittance (Y2), Zeta-potential (Y3), and PDI (Y4) were selected as responses. Experiments were run in random order to increase the predictability of the model. The modelling of corresponding response surfaces was carried out using second order models, which can describe the surface curvature with the following polynomial equation:

$$Y = b_0 + b_1 x_1 + b_2 x_2 + b_{12} x_1 x_2 + b_{11} x_1^2 + b_{22} x_2^2 \quad (6)$$

where Y is the dependent variable; b_0 the intercept is the arithmetic average of all quantity outcomes of 13 runs; x are the independent variables (x_1 oil:S_{mix} ratio, x_2 emulgent:co-emulgent ratio) and b parameters mark the regression coefficients characterizing the main (b_1, b_2), the quadratic (b_{11}, b_{22}), and the interaction effects (b_{12}). A substantial goal of

an optimization process is to find the most desirable set of conditions. Optimization of multiple responses was carried out by graphical optimization, which set minimum or maximum limits for each response then created an overlay graph highlighting an area of desired operability. The optimization and statistical experiments were designed and evaluated using the Design-Expert® software, version 7.0.0 (Stat-Ease® Inc., Minneapolis, MN, USA, 2005). In the doctoral thesis a 95% confidence interval and a corresponding 0.05 significance level was used. In all cases, when the p value was less than (or equal to) 0.05, then the null hypothesis was rejected and the result was regarded as statistically significant.

3.5.6. Characterization of Optimized BSNEDDS

3.5.6.1. Droplet size, Transmittance, PDI, and Zeta-Potential Measurements

Droplet size, transmittance, and PDI were determined according to *Section 3.5.2*. Zeta-potential was measured using the Zetasizer Nano ZS™ (Malvern Instruments Ltd., Malvern, UK) by diluting 0.1 mL of optimized BSNEDDS with 100 mL of distilled water. The evaluation was based on Laser Doppler Micro-electrophoresis using the Smoluchowski model. The selection of the attenuator level and the position of the optics was set automatically. The instrument was operated by automatic selection of voltage based on the measured conductivity of the sample. The analysis was carried out at 37.0 °C in clear, disposable folded-capillary zeta cells. Five measurements with minimum 10 runs/sample were performed for each sample, the mean values ± SD (mV) are reported.

3.5.6.2. Determination of the Thermodynamic Solubility of Baicalin in Optimized SNEDDS

2 g of selected oil, emulgent, and co-emulgent were thermostated and homogenized (37 °C, approximately 500 rpm, 1 h) in optimized ratios by a heatable magnetic stirrer. An excess amount of pure baicalin was added to the best pre-concentrate in sealed vials. Henceforth, the investigation was fulfilled as detailed in *Section 3.5.1*.

3.5.6.3. Cloudpoint Measurement

Cloudpoint is the temperature above which an aqueous solution of a water-soluble surfactant becomes turbid. The optimized formula was diluted with distilled water to 100

times and placed in a water bath where the temperature was increased gradually (1.0 °C/min). Cloudpoint was recorded as the temperature at which the diluted formulation turned cloudy (visual perception).

3.5.6.4. Effect of Dilution on Droplet Size and PDI

The optimized formulation was evaluated for robustness of dilution. The pre-concentrate was diluted to 50, 100, 500, and 1000 times by distilled water in 100 mL Erlenmeyer-beakers with continuous stirring at 37 ± 1 °C. Distribution parameters were measured using the dynamic light scattering method as described above *(Section 3.5.2.)*.

3.5.6.5. Long-Term Physical Stability of Nanoemulsions

0.2 mL of optimized BSNEDDS was dropped by automatic pipette into 100 mL distilled water at 37 ± 1 °C, with continuous stirring for 1 h at approximately 500 rpm (IKA RT-5 power heatable magnetic stirrer). After several minutes of mild stirring, an intrinsic droplet size and PDI were measured by Zetasizer Nano ZS™ (for setting parameters see *Section 3.5.2.*). The Erlenmeyer flask with stopper was stored at room temperature and protected from direct sunlight until further investigation. Determinations were performed at 37.0 °C throughout the storage time (1 day, 3 days, 7 days, 14 days, 21 days, 28 days).

3.5.6.6. Atomic Force Microscopy

Sample Preparation for AFM Imaging

The BSNEDDS preconcentrate was diluted 10^7 -fold with distilled water. Five μL of this emulsion was dropped on a freshly cleaved mica surface and was frozen by pouring approximately 30 mL liquid N_2 onto it. The sample was immediately placed in the lyophilisation chamber (CoolSafe™ 110-04 freeze dryer, ScanVac, Lillerød, Denmark), pre-cooled to −60 °C, and lyophilized at the following parameters: 10 min freezing at −40 °C, then drying at 0.020 hPa vacuum chamber pressure for 18 h. The shelf temperature was set at 15 °C for 1 h, 20 °C for 1 h, 30 °C for 8 h, and 40 °C for 4 h. Freeze-dried samples were stored protected from light at ambient humidity at 25 ± 1 °C and examined within 4 h of the end of the lyophilisation process.

AFM Imaging and Analysis

Lyophilized samples were imaged in non-contact mode with a Cypher S instrument (Asylum Research, Santa Barbara, CA, USA) at 1–2 Hz line-scanning rate in air using a silicon cantilever (OMCL AC-160TS, Olympus, Tokyo, Japan) and oscillated at its resonance frequency (typically 300–320 kHz). Temperature during the measurements was 29 ± 1 ˚C. Images were analyzed by using the built-in algorithms of the AFM driving software (IgorPro, WaveMetrics Inc., Lake Oswego, USA). AFM amplitude-contrast images are shown in this paper. To determine height variations, height-contrast data were used.

*3.6.*Preparation of self-nanoemulsifying matrix pellets (SNEMPs)

SNEMPs were prepared by extrusion-spheronization method using MCC alone (BSNEDDS-MCC) or with the combination of isomalt, (BSNEDDS-MCCIsm). Two different formulas were created according to *Table X*.

Table X. Composition of liquid BSNEDDS preconcentrate and two SNEMPs expressed in % (w/w)

	BSNEDDS	**BSNEDDS-MCC**	**BSNEDDS-MCCIsm**
Baicalin	2.5	1.25	0.83
Peceol™	13.93	6.965	4.64
Kolliphor® EL	55.71	27.855	18.57
Transcutol® P	27.86	13.93	9.29
MCC	-	50	33.33
Isomalt	-	-	33.33

The batch size was 50 g in all cases. The powders were accurately weighed and blended in a mortar with a porcelain pestle for 10 minutes. BSNEDDS was added slowly to the powder with thorough mixing of the components until the liquid preconcentrate was completely adsorbed. For a successful process, 4 g demineralized water was added to the mass. The wet mass was extruded using a single-screw extruder with the rotation speed of 60 rpm (screw length: 60 mm, diameter: 20 mm) (Caleva Multi Lab extruder, Caleva

Process Solutions Ltd., England) equipped with standard die plate of 1 mm diameter and 1 mm depth holes. The extrudates were then spheronized for 4 minutes at 1000 rpm in a 105-mm radial plate spheronizer using a saw-toothed frictional plate (Locost Kft, Hungary). The pellets were stored in drying chamber at 40 °C until further analysis.

3.7. Physical characterization of SNEMPs

3.7.1. Flow properties

The flowability of matrix pellets were evaluated by measuring the flow rate through an orifice and calculating the Carr's index and Hausner ratio using the bulk and tapped density results.

The flow rate of the pellets was recorded as the ratio of mass (g) to time (s) using standard ASTM glass funnel with an orifice diameter of 10 mm (n = 3). 50 g of pellets were weighed in and introduced into the funnel. The funnel was standing on a horizontal surface fixed to a holder and a piece of paper was placed under it by maintaining about 10 cm gap between the paper and tip of the funnel. The time needed for flowing 50 g pellets through the oriface was recorded.

Bulk and tapped density were obtained using STAV 2003 Stampfvolumeter (J.Engelsmann AG.,Germany) equipped with Omron HFCX-A4 counter. 50 g of pellets from each formulation were weighed in and introduced into the dry graduated 250-cm^3 cylinder (readable to 2 cm^3). The bulk and tapped density were determined according to Ph.Eur.9.0. by the formula m/V_0. Hausner ratio was calculated as the ratio of tapped density to bulk density, whereas Carr's index was calculated as the difference between tapped density and bulk density divided by tapped density and expressed as percent.

3.7.2. Friability

For friability testing, 10 g of pellets were accurately weighed and introduced into the friabilator (Erweka TA3R, Erweka GmbH, Germany). A drum, with 100 mm internal radius, a depth of 35 mm and subject to minimum static build-up was used. The pellets were tumbled at each turn of the drum on 12 pieces of straight projections with sizes of 35×35×3 mm. These 12 projections extend from the outer wall to the middle of the drum. The investigation took 10 minutes with the rotation speed of 20 rpm. Particles smaller than 0.20 mm were regarded as attrition and friability was calculated as the weight loss of sample (%) after agitation. The measurement was repeated three times.

3.7.3. Shape analysis

One hundred pellets were randomly chosen from each batch to be analyzed. The pellets were placed on nonshiny black surface serving as the background. The pellets were illuminated from the top using cold white coherent fibre optic light (20V/150W, 50/60 HZ, 3200 K, 450.000 fc illumination intensity) of Volpi Intralux 5000-1 cold light source (Volpi, Switzerland). Photomicrographs of pellets were taken with a digital camera (Coolpix 4500, Nikon, Japan) linked to a stereomicroscope (SMZ 1000, Nikon, Japan). One pixel corresponds to 3.048 μm. The images produced were digitized and analyzed using the computer program Image Pro® Plus 4.5 (Media Cynerbetics, USA). In this study, the pellet size and shape were characterized by roundness, aspect ratio (AR) and $Feret_{max}$ diameter.

3.7.4. Residual water content

The water content of the dried pellets was determined using a Karl Fischer titrator (787KF Titrino, Metrohm AG, Switzerland). Prior to the titration of the samples the water equivalency factor of Hydranal was determined using sodium tartarate (Hydranal-water standard, Sigma–Aldrich Chemie GmbH, Germany). The solvent was extra dry methanol, which was titrated with Karl Fischer reagent (Hydranal-composite-5) before the measurement. 120 mg of pellets were accurately weighed, dispersed (15 sec at 15.000 rpm) and titrated with the reagent three individual measurements.

3.8. Solid state characterization of SNEMPs

3.8.1. FT-IR

Physicochemical properties of pure baicalin, various carriers, physical mixtures, BSNEDDS-MCC and BSNEDDS-MCCIsm pellets were examined using Jasco FT/IR-4200 spectrophotometer (Jasco Products Company, USA) which was equipped with Jasco ATR PRO470-H single reflection accessory. The measurements were performed in absorbance mode. The spectra were collected over a wavenumber range of 4000 and 400 cm^{-1}. After 50 scans at a resolution of 4 cm^{-1}, the measurements were evaluated with the FT-IR software (Spectra Manager-II, Jasco).

3.8.2. Raman spectroscopy

The above-mentioned samples were analyzed using dispersive Raman spectroscopy with proprietary fluorescence rejection equipped with CCD detector (Bravo Handheld Raman Raw Material Analyzer, Bruker Optics Inc., USA). The measurements were carried out at room temperature in 5 ml volumetric vials with screw-caps. The spectra were obtained in the range 3200-300 cm^{-1} with spectral resolution 10-12 cm^{-1}. The laser excitation wavelength was 700-1100 nm (DUO LASER™). The analysis was assessed with OPUS 7.8 spectroscopy software (Bruker Optics Inc., USA).

3.9.In vitro dissolution study and reconstitution properties of SNEMPs

Dissolution testing was performed using Hanson SR-8 Plus™ Dissolution Test Station (Hanson Research, USA) by paddles method (USP apparatus 2) with 50 rpm at 37 ± 0.2 °C. The formulations were screened in 500 ml aqueous-based dissolution media at pH=1.2 (Ph.Eur.9) and pH=6.8 (Ph.Eur.9). Pure baicalin, liquid BSNEDDS, BSNEDD-MCC and BSNEDDS-MCCIsm pellets were exposed to the media and at predetermined time-points, 5 ml of samples were withdrawn and filtered through 10 μm pore size membrane full flow filters from the media by Hanson AutoPlus Multifill collector (Hanson Research, USA). After every sampling, media replacement was accomplished with 5 ml of fresh buffer solution. Dissolution studies were completed three times and the cumulative drug release (%) ± SD was analysed by UV-Vis spectrophotometry at 279 nm against equivalent proportions of excipients as blanks. Withdrawn and filtered samples at 120 minutes were characterized for droplet size and PDI as described for liquid BSNEDDS in *Section 3.5.2*. 24 hours visual observation was fulfilled for any precipitation or phase separation.

4. Results

4.1. Preformulation studies

4.1.1. Determination of Thermodynamic Solubility by Saturation Shake-Flask Method

Baicalin is a weak triprotic acid (pK_{a1}: 4.21, pK_{a2}: 8.56, pK_{a3}: >14) with remarkable pH-dependent solubility. The water solubility of baicalin was determined in distilled water (67.03 ± 1.60 μg/ml), which is in close agreement with literature data (25). The difference could be explained by dissimilar sample preparation methods, in particular, equilibration time. In the highly acidic environment of stomach, the neutral form of baicalin is overwhelmingly dominant, so the measured solubility can be considered as the intrinsic solubility of baicalin (11.64 ± 0.44 μg/ml) at pH 1.2 SGF. As the pH increases, the ionization processes contribute significant solubility improvement (10504 ± 330 μg/ml) at pH 6.8 SIF, where baicalin exists decisively in monoanionic form ($[H_2B]^-$: 98.0%). Significant solubilizing impact of FaSSGF (33.21 ± 0.72 μg/ml) was found to be correlated to compendial pH 1.2 SGF. The ~3-times increase in solubility can be explained by the presence of surface-active agents (lecithin, taurocholate) in FaSSGF. Surprisingly, FaSSIF did not live up to our expectations. Instead of a remarkable solubilizing effect, a minor decrease (8111 ± 472 μg/ml) of thermodynamic solubility was found correlated to compendial pH 6.8 SIF *(Tbl. XI.)*. Similar results were observed in the case of weakly acidic furosemide and niflumic acid by Takács-Novák et al (18). The solubility of acidic zafirlukast was also negatively influenced by interactions of bile salt and soy lecithin, whereas the amphiphilic molecules exhibited significant positive effect for the weak base carvedilol (170). The phenomena could be explained by the fact that taurocholate and lecithin micelles possess net negative charge, thus an electrostatic repulsion exists between the solute anion and the micelle. In the case of neutral and cationic APIs repulsive forces can be neglected.

Table XI. Thermodynamic solubility (μg/ml) of baicalin in various compendial and biorelevant media

Medium	**AVG**	**SD**
Aqua dest.	67.03	1.60
pH=1.2 (SGF)	11.64	0.44
pH=6.8 (SIF)	10504	330
pH=1.6 (FaSSGF)	33.21	0.72
pH=6.5 (FaSSIF)	8111	472

4.1.2. Acid-base properties

In baicalin there are 12 protons connected to carbon atoms, but in ^{1}H NMR spectra only the singlets of H8 and H3 on ring A, and the doublet of the aromatic H2',6' protons can be easily assigned, while the other aromatic protons occur in complex spectrum of multiplets. The protons of the monosaccharide unit overlap with each other and with the signals of the antioxidant ascorbic acid. The suppression of the large water signal also interferes with the observation of certain NMR signals. Thus, during the NMR-pH titration we followed the above mentioned three chemical shift signal sets.

Since protonation processes are instantaneous on the NMR chemical shift time scale, the observed chemical shift (δ^{obsd}) of a certain nucleus can be expressed as a weighted average of chemical shifts of the non-, mono-, di- and triprotonated forms of baicalin (B):

$$\delta^{\mathrm{obsd}} = \delta_{\mathrm{B}^{3-}} x_{\mathrm{B}^{3-}} + \delta_{\mathrm{HB}^{2-}} x_{\mathrm{HB}^{2-}} + \delta_{\mathrm{H_2B}^{-}} x_{\mathrm{H_2B}^{-}} + \delta_{\mathrm{H_3B}} x_{\mathrm{H_3B}} \quad (6)$$

where weighting factors are mole fractions that can be expressed in terms of stepwise protonation macroconstants and the actual hydrogen ion concentration.

For example, $x_{H_2B^-}$ is:

$$x_{H_2B^-} = \frac{K_1K_2[H^+]^2}{1+K_1[H^+]+K_1K_2[H^+]^2+K_1K_2K_3[H^+]^3} \quad (7)$$

Combining and rearranging Eq. (6) and (7) yields Eq. (8) that can be directly fitted to the ^{1}H-NMR titration curve of each nucleus observed.

$$\delta^{obsd} = \frac{\delta_{B^{3-}}+\delta_{HB^{2-}}K_1[H^+]+\delta_{H_2B^-}K_1K_2[H^+]^2+\delta_{H_3B}K_1K_2K_3[H^+]^3}{1+K_1[H^+]+K_1K_2[H^+]^2+K_1K_2K_3[H^+]^3} \quad (8)$$

The logarithms of the obtained protonation constants correspond to the negative logarithms of dissociation constants, namely pK_{a1}=logK_3, pK_{a2}=logK_2 and pK_{a3}=logK_1 (17).

The NMR-pH titration curves can be seen in *Figure 13*, while the obtained dissociation constants are summarized in *Table XII*. The titration curves show that each observed nucleus displays chemical shift changes upon dissociation of each acidic proton.

The methyl ester of baicalin has no free carboxyl functional group, therefore two dissociation constants could be fitted only. The obtained pK_a values are demonstrated in *Table XII*.

Table XII. Acid dissociation constants of baicalin and its methyl ester

	Baicalin		**Baicalin methyl ester**	
	AVG	**SD**	**AVG**	**SD**
pK_{a1}	4.21	0.02	8.78	0.05
pK_{a2}	8.56	0.03	> 14	-
pK_{a3}	> 14	-	-	-

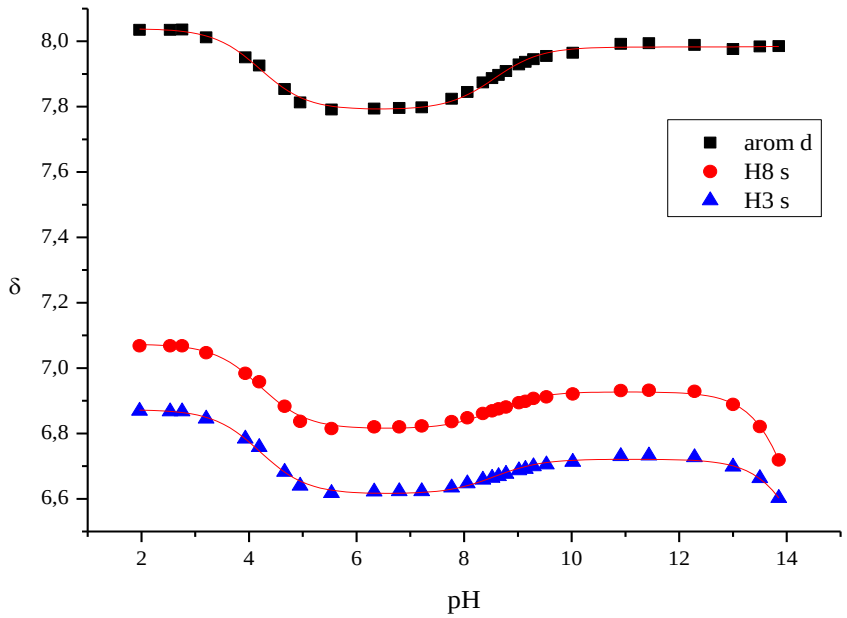

Figure 13. NMR-pH titration curves of the H2',6' (arom d) and H8 and H3 protons of baicalin. Computer fits of Eq. (8) are shown in solid lines.

The first acid dissociation constant (pK_{a1}) obviously belongs to the carboxyl group of baicalin, because the methyl ester derivate (without a free carboxyl group) has no dissociation constant in the acidic region. Furthermore, two independent studies established that the UV spectrum of baicalin shows no profound absorption variation, just a slight increase in absorption intensity upon the increasing solubility of baicalin in less acidic solutions (19, 171). The two phenolic hydroxyl groups on C5 and C6 on ring A would cause a marked bathochromic shift upon their deprotonation (172).

Thus, pK_{a2} of baicalin and the analogous pK_{a1} of baicalin methyl ester belongs to one kind of the phenolic hydroxyl groups. The second phenolic hydroxyl deprotonation takes place above pH 14, but the exact value of the pK_{a3} of baicalin (or the analogous pK_{a2} of its methyl ester) cannot be determined with sufficient certainty. Due to the reasons below:

- the pH value of highly alkaline solutions can only be determined with indicator molecules, like 1-methylguanidine, but their chemical shift is also influenced by the changing ionic strength and solvation at these extreme pH values (173).
- the chemical shift of baicalin is also influenced by the changing ionic strength and solvation above pH 13, apart from the concurrent deprotonation.

- the rapid oxidation of baicalin above pH 13, even in the presence of a large excess of ascorbic acid, makes the observation of its signals very difficult and uncertain.

The high pK_{a3} values (above pH 13) of other biologically active catechols, like dopamine and epinephrine can be determined only with uncertainty for similar reasons (174).

A UV-pH titration attempted to determine the pK_{a2} and pK_{a3} values of baicalin, and claimed the 7.6 and 10.1, respectively (19). However, these results are highly dubious in light of the oxidizability of baicalin in alkaline solutions. Namely, the change in the UV-spectra of baicalin is not only the result of protonation, but also that of the decomposition. With the help of ascorbic acid, we could prevent this oxidative process, and during NMR study we could also monitor the pH range where the molecule has remained intact. The stability issues of baicalin were evaluated in buffered aqueous solutions at different pHs (2.0, 3.0, 4.5, 6.8, 7.4 and 9.0) and temperatures (4, 25 and 40 °C). Acidic environment and low temperature were protective factors to preserve the integrity of baicalin (30).

The knowledge of pK_a values allows the calculation of species distribution diagram of baicalin *(Fig. 14/A)*.

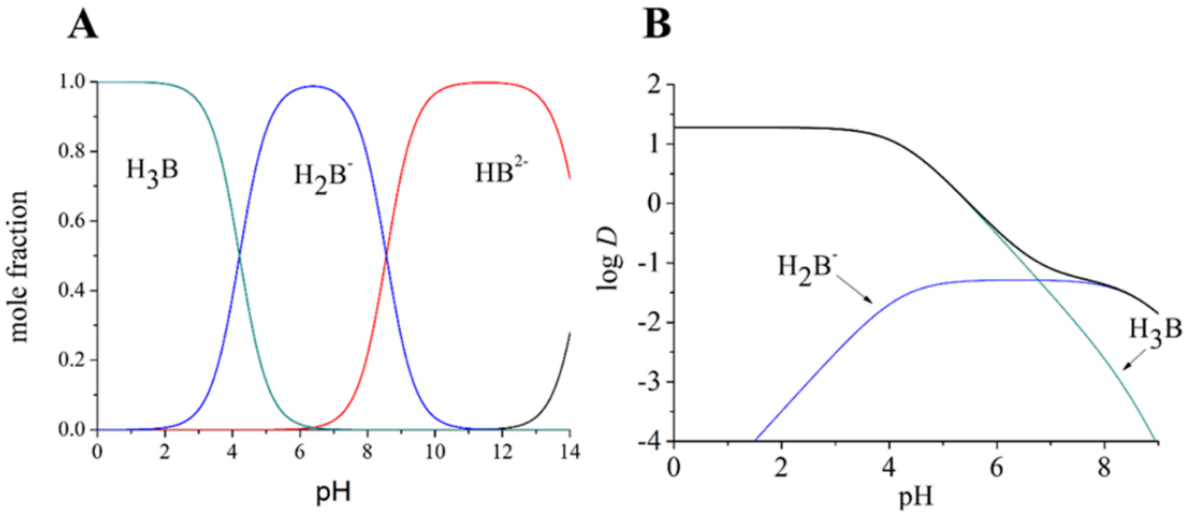

Figure 14. The species distribution diagram (A), and the lipophilicity profile of baicalin (B)

The neutral form of baicalin (H_3B) is dominant up to pH 4.21. The monoanionic form (H_2B^-) reaches its maximum at the pH of blood (pH 7.40), with 93.5%. The dianionic form (HB^{2-}) becomes the dominant one above pH 8.56, while the trianionic form (B^{3-}) starts to appear only in extremely alkaline solutions that have little relevance to biochemical or physiological processes.

4.1.3. Distribution Coefficient Measurements by the Stir-Flask Method

When more than one electrical species is present in solution, the observed ratio of concentrations in partition experiments is the distribution coefficient (*D*), which takes into account the intrinsic species-specific lipophilicity of the various electrical species present (P_i), and their mole fractions in the aqueous phase (x_i).

For baicalin, the pH-dependent distribution coefficient is the sum of four products:

$$D_{(pH)} = \Sigma x_i P_i = x_{B^{3-}} P_{B^{3-}} + x_{HB^{2-}} P_{HB^{2-}} + x_{H_2B^-} P_{H_2B^-} + x_{H_3B} P_{H_3B} \quad (9)$$

where x_i mole fractions are pH-dependent quantities, while P_i parameters are pH-independent ones. The lipophilicity profile (the variation of log *D* as a function of the aqueous pH) of a drug is essential in understanding its pharmacokinetic behaviour (175).

The log *D* value of 1.28 (0.08) measured with a standardized 0.15 M HCl solution characterizes the log *P* value of the neutral form. In such acidic solutions it is the dominant species and exhibits obviously higher lipophilicity than the anionic forms. In a previous study the log *P* of baicalin was reported to be "1.27 (pH 7)". It is not exactly clear what the authors meant by this, probably they calculated the log *P* of baicalin from a log *D* measured at pH 7 (19).

However, our log *D* value of -1.22 (0.02) measured with a pH 7.40 phosphate buffer is a composite one, where contributions of both the neutral and the monoanionic forms are important and comparable. The relative concentration of the dianionic form is only 6.5% here, and due to its obviously smaller partition coefficient it can be neglected at this physiological pH. Thus Eq. (9) can be simplified as

$$D_{(pH\,7.40)} = x_{H_2B^-} P_{H_2B^-} + x_{H_3B} P_{H_3B} \quad (10)$$

The mole fraction data can be calculated similarly as shown in Eq. (7), thus the partition coefficient of the anionic form can be obtained. The log *P* value of the anion turns out to be -1.28, thus there is a 2.56 log unit difference between the lipophilicity of

the neutral and the anionic form. For phenols the typical difference in the octanol/water system is around 3 log units, further verifying our results (175). These partition coefficients allow the construction of the lipophilicity profile of baicalin, which can be seen in *Figure 14/B*. The broad black line is the overall lipophilicity profile of the molecule, the sum of the contributions of its two important species. The distribution coefficient becomes monotonically smaller as the pH is increased. The contribution of the neutral form is dominant up to pH 6.77, but at higher pH values the anionic form is the more important one for the distribution coefficient.

4.1.4. Crystal habit

SEM displayed micro scaled plates with angular edges in case of baicalin crystal's *(Fig.15, Fig.16.)*. This physical property predicts poor flowability and processability. Anisotropy during compression may significantly affect negatively the overall mechanical properties of the compact (176).

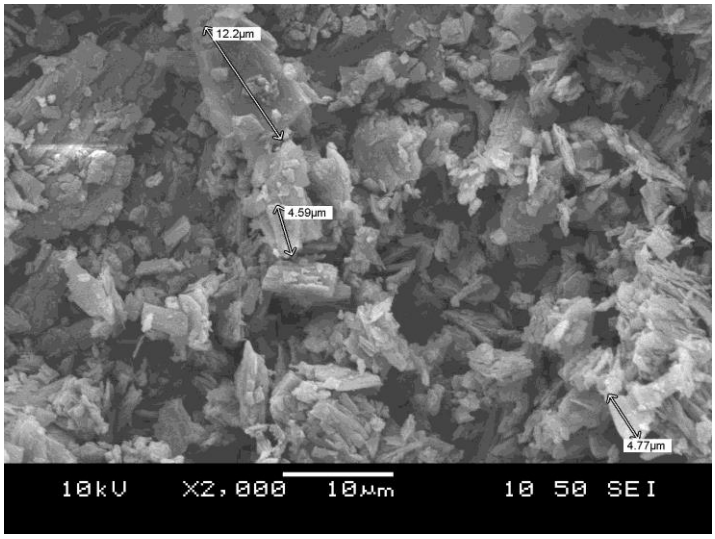

Figure 15. SEM image of baicalin crystals (2000x magnification)

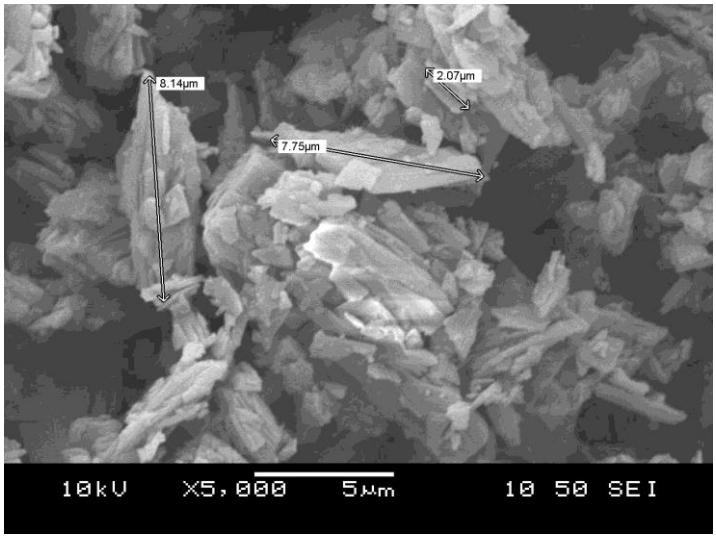

Figure 16. SEM image of baicalin crystals (5000x magnification)

4.1.5. Particle size analysis

The particle size of pure baicalin followed a bimodal distribution characterized by an expressed peak between 0.5-100 μm and a mild second peak between 100-300 μm *(Fig.17.)*. The average surface weighted mean particle size (D [3,2]) measured by laser diffraction was 4.99 ± 0.126 μm. The d (0.1), d (0.5) and d (0.9) values were 1.821, 5.757 and 23.223, respectively. This number indicates the diameter of a particle at which 10%, 50% or 90% of the particles in the sample are smaller. SEM results are comparable with values obtained by laser diffraction method, both suggest a particle size on the bottom of μm scale *(Section 4.1.4.)*. The particle size distribution of the drug substance may have significant effects on final drug product performance (e.g., dissolution, bioavailability, content uniformity, stability, etc.) and have impact on safety, efficacy, and quality of the drug product. If the particle size is critical, the International Conference on Harmonization (ICH) guideline Q6A provides guidance on when and how a particle size specification should be considered (177).

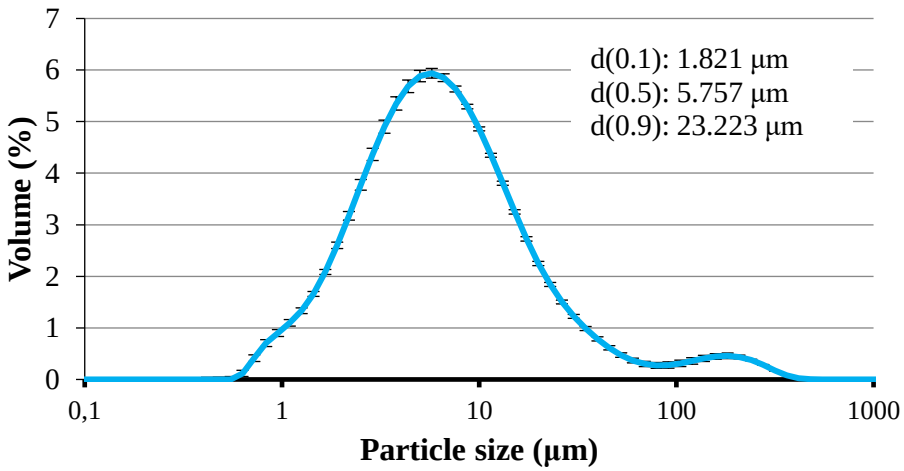

Figure 17. Particle size distribution of baicalin

The Span is the measurement of the width of the distribution. The narrower the distribution, the smaller the span becomes. The span is calculated as:

$$Span = \frac{d(0.9) - d(0.1)}{d(0.5)} \quad (11)$$

Baicalin demonstrated a high Span value (3.718 ± 0.158) indicating a wide particle size distribution. In the scientific literature and regulatory guidelines there is no acceptance limit for Span.

4.2. Baicalin-cyclodextrin inclusion complexation

4.2.1. Phase solubility studies

Phase solubility analysis can provide valuable information about changes in drug solubility when it interacts with different concentrations of CDs. Since the changes of physicochemical and biological properties of a drug are dependent on the stability constant of CD complexes, it is essential to determine this parameter accurately (178).

The phase solubility profile of baicalin- α-cyclodextrin complex showed a typical B_S-type solubility curve, where the initial ascending portion is followed by a plateau region and then a slight decrease in total baicalin solubility accompanied by precipitation of complex. Baicalin- *β-, γ-, HP-β-, RAMEB-, SBE-β-*CD complexes revealed a linear enhancement in solubility of baicalin upon addition of increasing amounts of CD *(Fig. 18.)*. This indicates that the complexation belongs to the A_L-type, assuming 1:1 binding stoichiometry. 5.47 times solubility enhancement was demonstrated by γ-CD encapsulation (67.03 μg/mL vs. 366.64 μg/mL) compared to solubility of baicalin in DW. In case of RAMEB, SBE-β-CD and HP-β-CD the solubility improvement was significant, but less expressed, 2.88-, 2.55-, and 1.59 times, respectively. The inclusion complex of α-, and β-CD didn't reveal significant solubility enhancement. Based on Equation (5), the apparent stability constants ($K_{1:1}$) of host-guest complexes were calculated *(Tbl. XIII.)*.

Table XIII. Apparent stability constants ($K_{1:1}$) and types of phase solubility diagrams of baicalin-CD systems at 25 °C

CD	$K_{1:1}$	Type
α	-	B_S
β	70.1	A_L
γ	**329.8**	**A_L**
HP-β	76.2	A_L
RAMEB	240.9	A_L
SBE-β	102.9	A_L

The largest $K_{1:1}$ was found in case of *γ*-CD (329.8 M^{-1}), that can well be explained by the fact that *γ*-CD is neutral and has wide internal cavity (8 glucopyranoside units). The order of stability constants was as follows: *γ*-CD > *RAMEB*-CD > *SBE-β*-CD > *HP-β*-CD > *β*-CD. The three most promising CDs were selected and examined further (*see in following sections*).

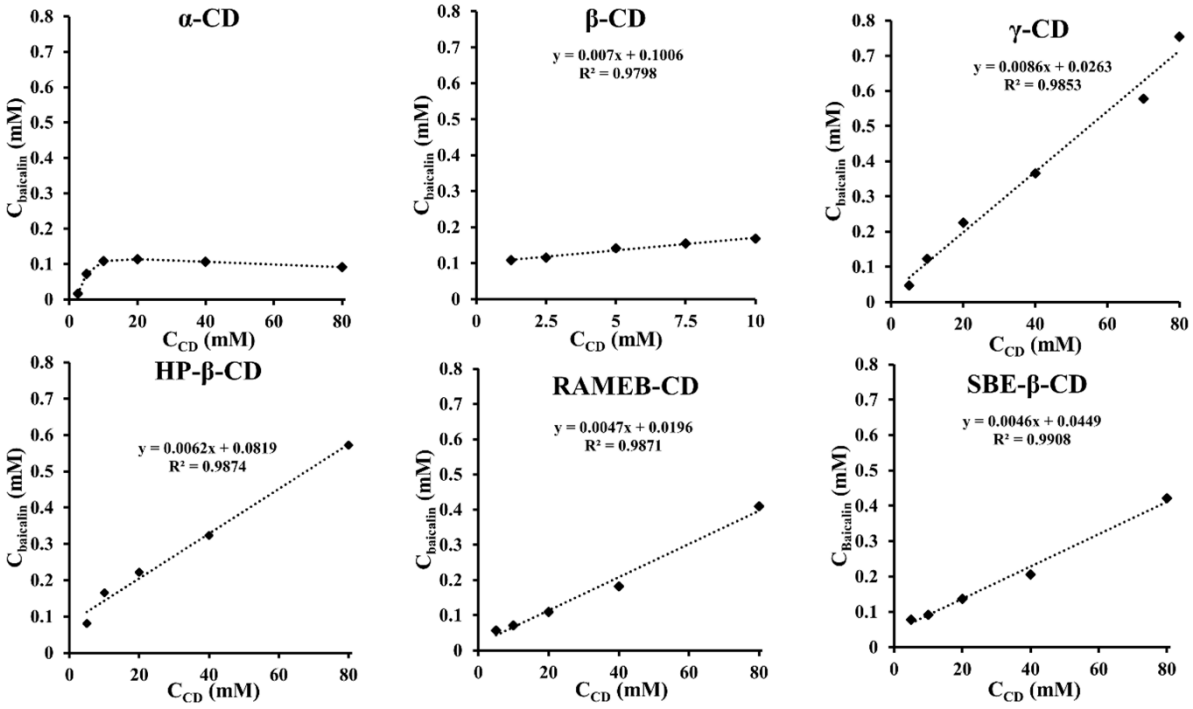

Figure 18. Phase solubility profiles of baicalin and various CDs

4.2.2. Signal Assignment of Baicalin and Characterization of Baicalin-Cyclodextrin Inclusion Complexes Using ^{1}H NMR and 2D ROESY Experiments

The NMR analysis of baicalin was carried out in DMSO-d_6 for complete assignment and published data were completed and corrected (179, 180) *(Fig.19.)*. The ^{1}H NMR chemical shifts are in δ ppm (DMSO-d_6, 400 MHz): 13.50-12.12 (1H, brs, COOH); 12.60 (1H, brs, C-5-OH); 8.70 (1H, brs, C-6-OH); 8.07 (2H, dm, *J*=7.4 Hz, H-2',6'); 7.67-7.54 (3H, m, H-3',4',5'); 7.05 (1H, s, H-8); 7.02 (1H, s, H-3); 6.05-4.65 (1H, brs, C-4"-OH); 5.53 (1H, d, *J*=3.9 Hz, C-2"-OH); 5.34 (1H, d, *J*=3.7 Hz, C-3"-OH); 5.25 (1H, d, *J*=7.4 Hz, H-1"); 4.08 (1H, d, *J*=9.5 Hz, H-5"); 3.52-3.26 (3H; m; H-2",3",4"). ^{13}C NMR data in δ ppm (DMSO-d_6, 100 MHz): 182.6 (C-4); 170.1 (C-6"); 163.6 (C-2); 151.3 (C-7); 149.2 (C-9); 146.8 (C-5); 132.1 (C-4'); 130.9 (C-1'); 130.6 (C-6); 129.2 (C-3',5'); 126.4 (C-2',6'); 106.1 (C-10); 104.8 (C-3); 99.9 (C-1"); 93.7 (C-8); 75.5 (C-5"); 75.3 (C-3"); 72.8 (C-2"); 71.3 (C-4").

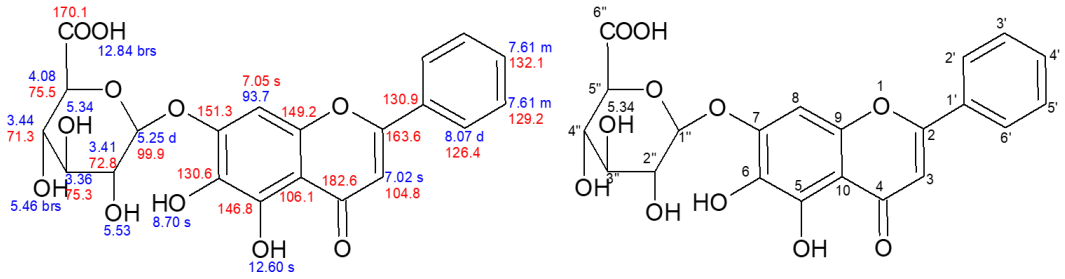

Figure 19. Total signal assignment of baicalin and numbering of the molecule (blue values: ^{1}H NMR chemical shifts, red values: ^{13}C NMR chemical shifts; in δ ppm; 400/100 MHz; 25°C)

To obtain direct evidences for the interaction between baicalin and CDs, ROESY experiments were also carried out. In the case of γ-CD unequivocal interaction was seen for H-3 protons of the CDs and aromatic protons (H-2',4' and H-3',5') of baicalin *(Fig.20.)*. Weaker, but appreciable cross-peaks were shown also for H-5 protons of γ-CD with the aromatic protons (H-2',4' and H-3',5') and between H-3 of γ-CD and H-3 of baicalin. Interestingly, H-8 of baicalin had crosspeak only with H-5".

For RAMEB-CD cross-peaks between the same moieties were found but at lower intensity *(Fig.21.)*. The baicalin-SBE-β-CD complex gave only the H-3 (baicalin) – H-3 (CD) interaction near to the noise *(Fig.22.)*.

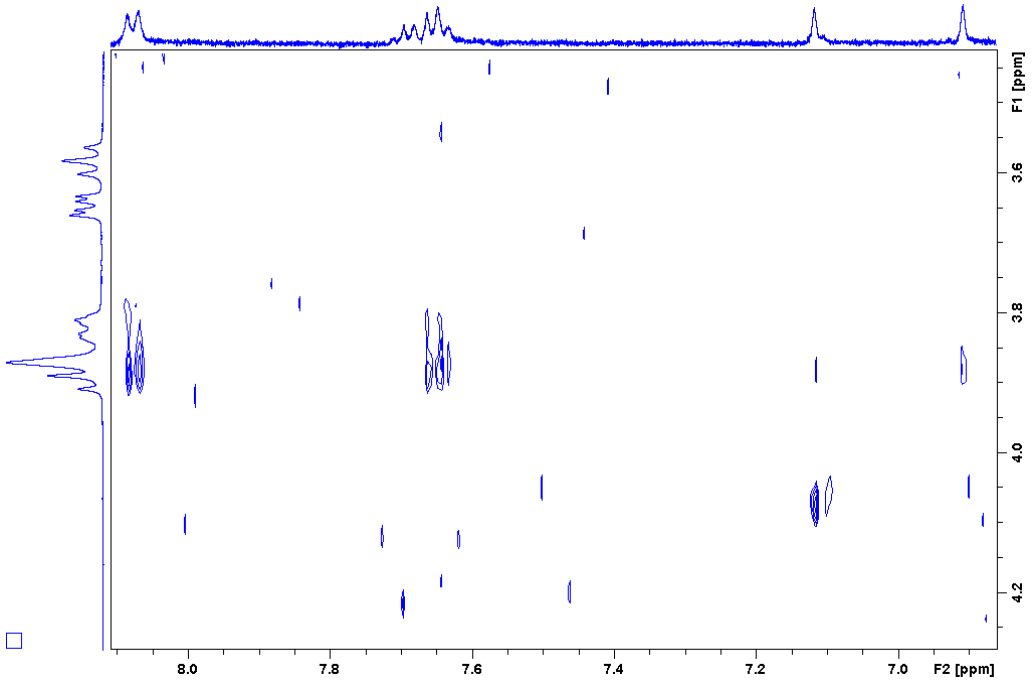

Figure 20. 2D ROESY NMR spectrum of Baicalin-γ-CD complex; 400 MHz; 25 °C

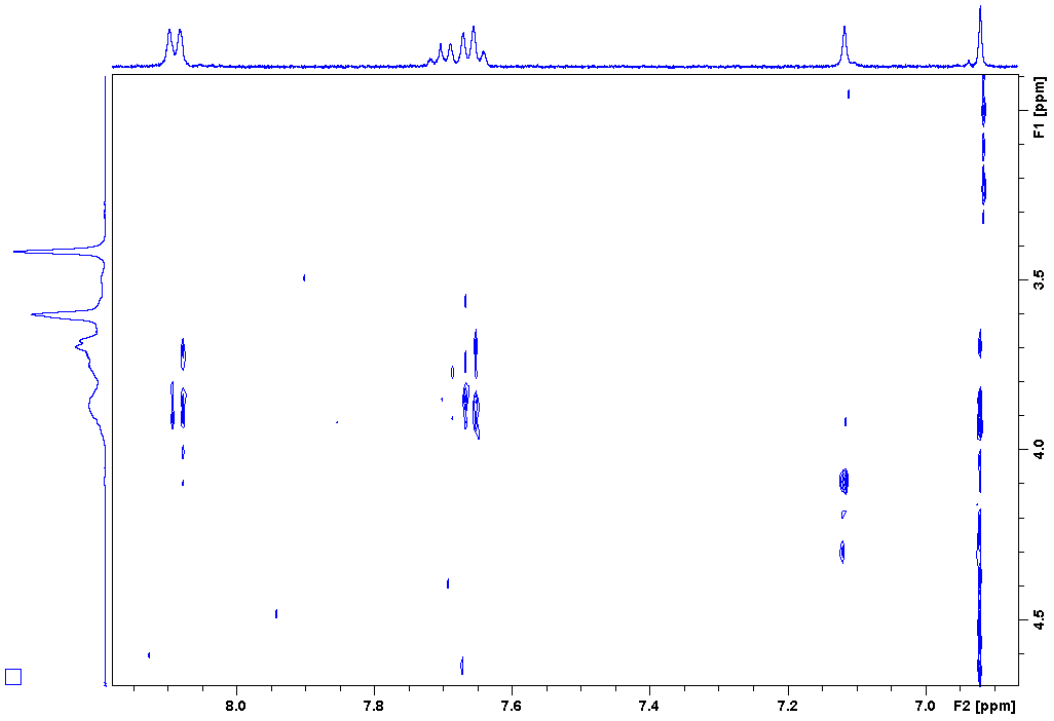

Figure 21. 2D ROESY NMR spectrum of Baicalin-RAMEB-CD complex; 400 MHz; 25 °C

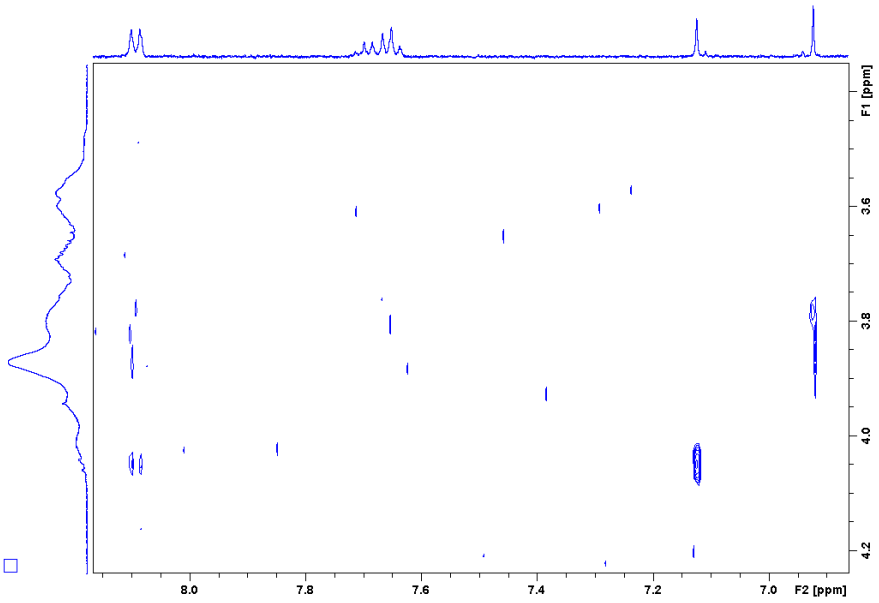

Figure 22. 2D ROESY NMR spectrum of Baicalin-SBE-β-CD complex; 400 MHz; 25°C

Proton chemical shifts in 1D ^{1}H NMR spectra also differ before and after forming inclusion complexes *(Tbl. XIV., Fig. 23.)*. All protons of the A, B and C rings were affected by the interaction with CDs. Most promoted chemical shift change was found for the γ-CD complex: ca. 0.1 ppm for H-3 and H-2',6'; ca. 0.06 ppm for H-8 and H-3',4',5'. In case of SBE-β and RAMEB-CD inclusion complexes the chemical shift changes were in the range of 0.01-0.02 ppm.

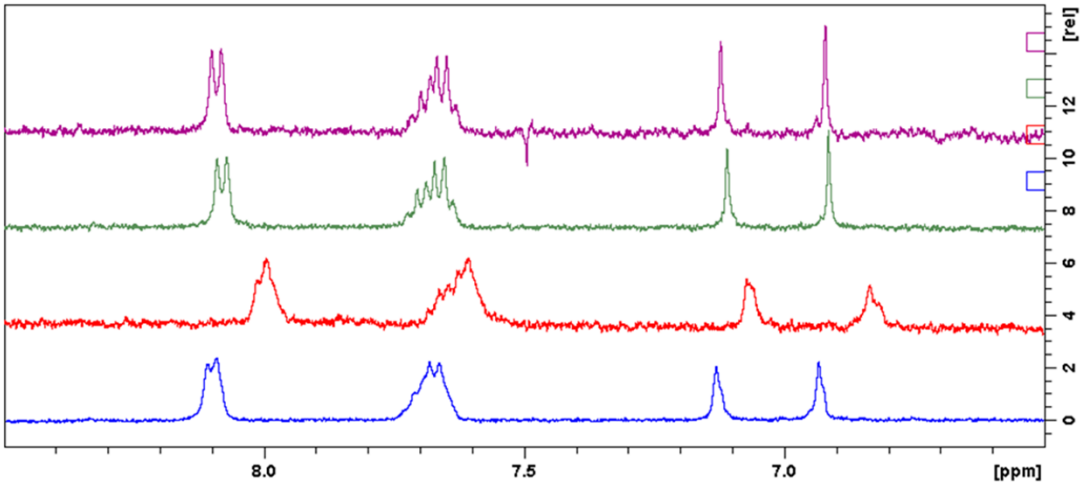

Figure 23. ^{1}H NMR spectra of baicalin (blue), baicalin-γ-CD (red), baicalin-RAMEB-CD (green) and SBE-β-CD (purple); 400 MHz; 25 °C

Most clear evidences about complexation could be gained from the sample with γ-CD. ROESY and ^{1}H NMR results suggest that H-2',6' and H-3 are inserted into the cavity, because these protons underwent the largest chemical shift change in 1H spectrum, and NOE interactions could also be developed with H-3 of CD. H-3',4',5' show also NOE correlation with H-3 of CD, but a decreased chemical shift change could be detected, thus these protons are in the cavity, but near the rim of the CD and became not significantly shielded. Since aromatic protons have more intensive through-space interaction with H-3 of CD, than H-5 protons, it could be concluded, that the aromatic moiety is closer to the wide rim. Concerning the complexation with RAMEB-CD, analogous interactions could be observed as in case of solution with γ-CD, but weaker NOE interactions and moderate chemical shift changes could be observed. The results for baicalin-SBE-β-CD suggest only weak interaction between baicalin and the CD.

Table XIV.^{1}H NMR chemical shifts of baicalin in its solution and inclusion complexes; 400 MHz; 25 °C

	Baicalin	***γ*-CD + Baicalin**		***RAMEB*-CD + Baicalin**		***SBE-β*-CD + Baicalin**	
	δ (ppm)	δ (ppm)	Δδ (ppm)	δ (ppm)	Δδ (ppm)	δ (ppm)	Δδ (ppm)
H-3	6.9331	6.8348	-0.0983	6.9145	-0.0186	6.9211	-0.0120
H-8	7.1301	7.0652	-0.0649	7.1096	-0.0205	7.1223	-0.0078
H-3',-4',-5'	7.6811 7.76-7.60	7.6240 7.72-7.55	-0.0571	7.6721 7.7434-7.6028	-0.0090	7.6652 7.7365-7.5939	-0.0159
H-2',-6'	8.0986	8.0043	-0.0943	8.0799	-0.0187	8.0908	-0.0078

4.2.3. Molecular Modelling of the Binding into Cyclodextrin

In the structures of CD, three different hydroxyl groups can be distinguished, two at the upper ring, and one at the bottom ring for each hexose unit. According to computational study at B3LYP/6-31G(d) level of theory, anionic baicalin molecule docks and accommodates differently into the *β*-CD and *γ*-CD. In the most preferred arrangement of the baicalin in *β*-CD, it breaks one of the weak hydrogen bonds (HB) of *Type-I* OH at the upper ring and forms a strong HB (*Bonding-A*) with the carboxylate group of baicalin on *ring-III*, as illustrated in *Figure 24*. The carbonyl group on the *ring-I* also forms a weak interaction with a neighbouring C–H of the opposite hexose.

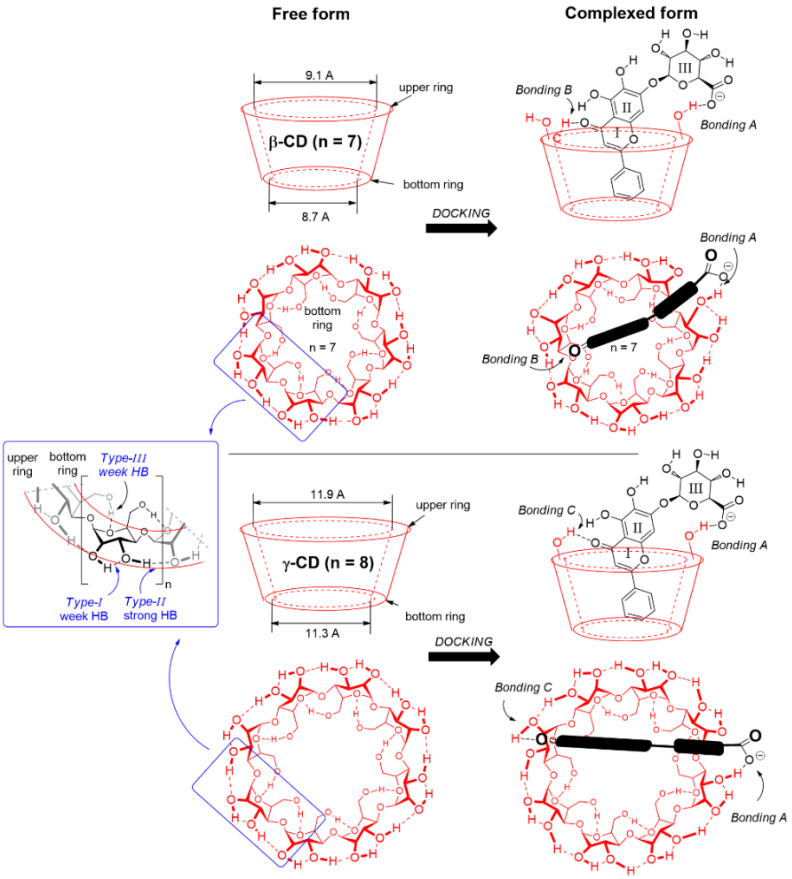

Figure 24. Different bonding types between baicalin and β-, γ-CDs. For β -CD, the bonding pattern consists of Bonding-A and Bonding-B, while for γ-CD it is Bonding-A and Bonding-C obtained by B3LYP/6-31G(d) level of theory.

The bonding pattern is different with *γ*-CD. Beside the same *Bonding-A*, the carbonyl group on the *ring-I* forms a much stronger HB with the *Type-II* OH group at the opposite

site (*Bonding-C*). This difference can be revealed in their bonding energy values, listed in *Table XV*. The calculated complexation energy in vacuum is –162.4 kJ mol^{-1} for *β*-CD, while it is significantly stronger for *γ*-CD (–181.5 kJ mol^{-1}), exhibiting 19.1 kJ mol^{-1} beneficial energy difference in favour of *γ*-CD. This bonding pattern difference can be explained in terms of the diameter, related to the respective 7 and 8 glucose units in *β*- and *γ*-CD cyclodextrins. The strongest interaction is forming between the carboxylate and one of the OH groups of CD (*Bonding-A*), making a strong and rigid anchor. In the case of even number (n = 8; *γ*-CD), the opposite site provides beneficial OH group for the baicalin carbonyl (*Bonding-C*), while for odd number (n = 7; *β*-CD), the opposing wall can offer only a C–H group (*Bonding-B*).

Table XV. Energy differences of the complexation process of the four types of cyclodextrins (β-CD, γ-CD, RAMEB-CD and SBE-β-CD) obtained by B3LYP/6-31G(d) level of theory

	Complexation energy (ΔE; kJ mol^{-1})	**$\Delta\Delta E$; kJ mol^{-1} relative to *β*-CD**
β-CD	–162.4	0.0
γ-CD	–181.5	–19.1
RAMEB-CD	–164.2	–1.8
SBE-β-CD	–41.0	+121.4

To model the partially methylated cyclodextrin, we constructed the model of *RAMEB*-CD according to literature data (181). Here, the seven hydroxyl groups (OH; *Type-III*) at the bottom ring are completely methylated, while five out of the total of 14 the OH groups (*Type-I* and *II*) are methylated at the upper ring randomly. As *Figure 25* illustrates, the original cone shape of the *β*-CD has significantly changed by the partial methylation. Namely, the narrower bottom ring of the *β*-CD became extended and forms a loose ring structure. It makes significantly larger room to accommodate of the baicalin molecule. However, the *RAMEB*-CD still provides enough hydroxyl groups at the upper ring to form strong hydrogen bonding (*Bonding-A*), like the original *β*-CD, as illustrated in *Figure 25*. The apolar bottom part of the CD can interact more comfortably with the phenyl substituent of the drug molecule. The computed complexation energy is little bit lower, than that for *β*-CD, which can support the experimental findings.

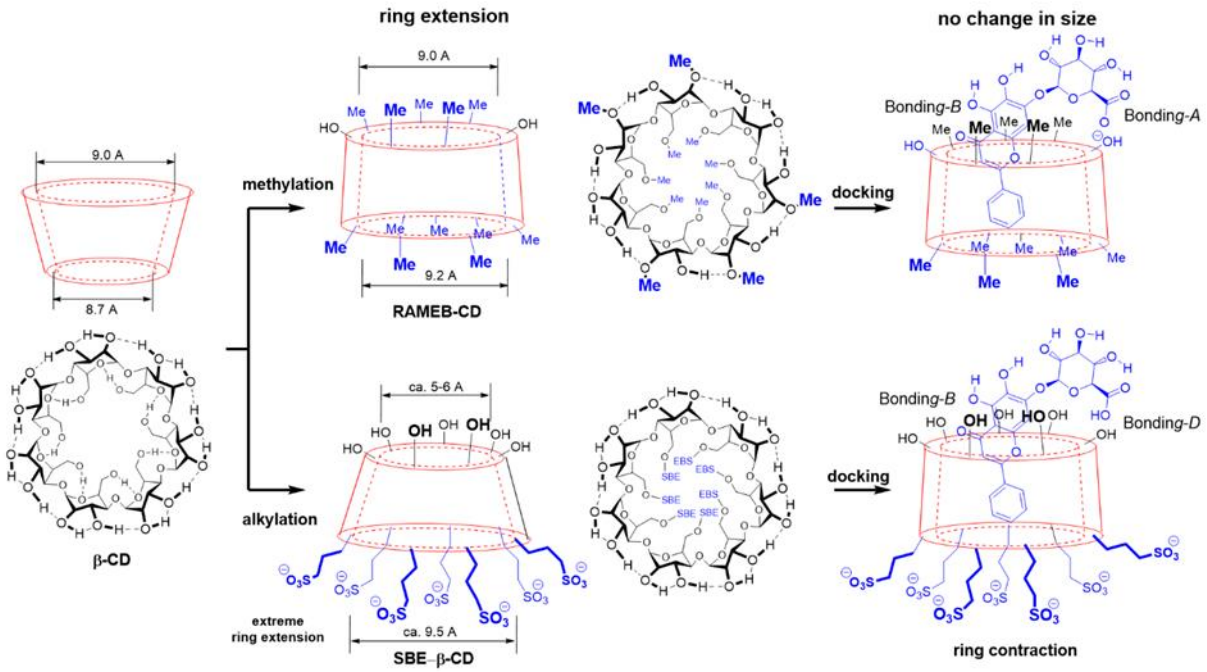

Figure 25. Shapes of the two modified β-cyclodextrins (RAMEB-CD and SBE-β-CD), obtained by B3LYP/6-31G(d) level of theory. On the right-hand side structures represent the different bonding patterns between baicalin and modified β-CD. RAMEB-CD and SBE-β -CD consist of Bonding-A + Bonding-B, and Bonding-B + Bonding-D

The seven sulfobutylether groups in *SBE*-β-CD typically replace the seven *Type-III* OH groups. Supposing a complete deprotonation of the sulfonic acid, the seven anionic sulfonate groups expand the cyclodextrin ring extremely, due to the Coulomb repulsion of the anions. This effect opens the bottom end of the CD and closes the upper ring. During the complexation, the neutral form of baicalin needs to re-open the upper ring to get into the hole and forms a similar HB with one of the Type-I OH, but here the COOH points to the CD-OH (*Bonding-D*). The computed energy is far less beneficial, than that of for *β*-CD, which should not be realistic, compared to the experimental result. Here, the neglect of the whole solvent environment overestimates the coulomb repulsion, which lowers the level of reliability. The calculated complexation energies refer to vacuum, while in case of phase-solubility and NMR studies a complex solvent system was utilized. The energy-minimised structures of CD complexes are demonstrated in *Figure 26.*

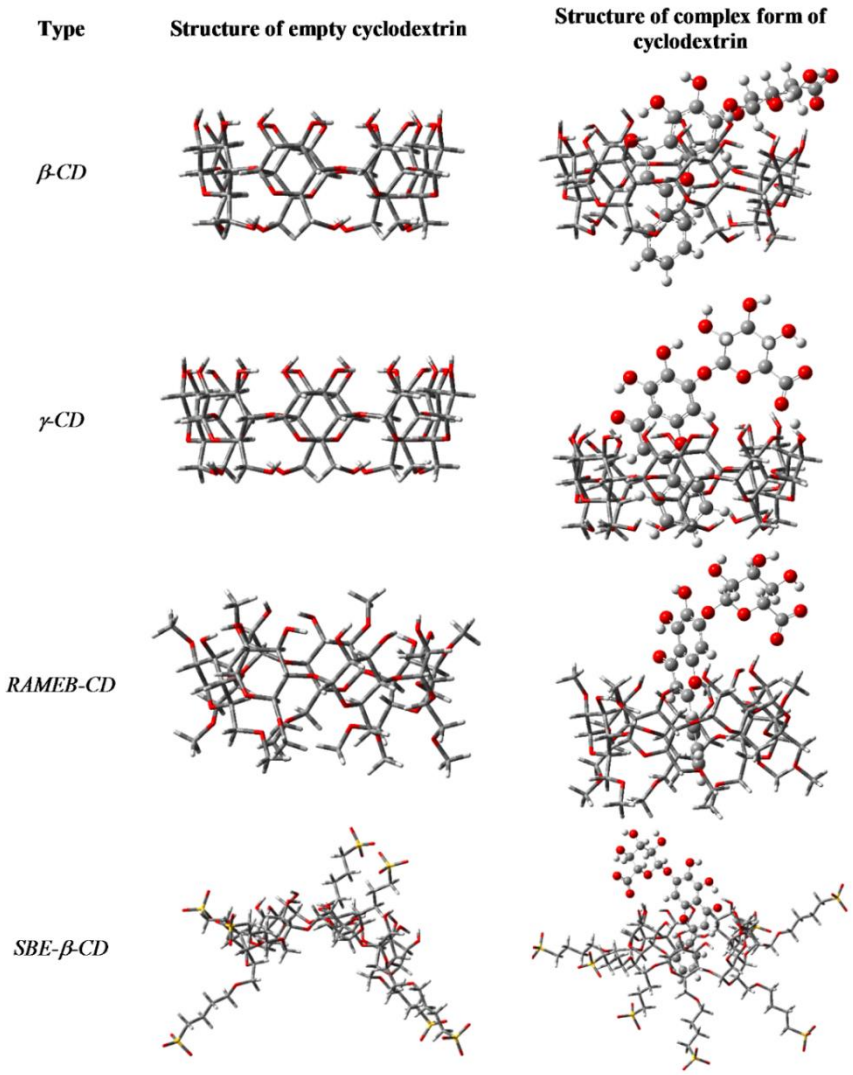

Figure 26. Optimized structures of various cyclodextrins and their complexed forms at B3LYP/6-31G(d) level of theory

*4.3.*Liquid Self-nanoemulsifying Drug Delivery Systems

4.3.1. Solubility Studies

Oil represents one of the most important excipients in SNEDDS formulations. To achieve optimal drug loading, it is essential to choose the oil having greatest solubilizing capacity (182). Amongst the various oils that were examined, Peceol™ showed significantly the highest solubilizing capacity (719.1 ± 83.05 µg/ml) for baicalin followed by Labrafac™ Lipophile WL 1349 and Maisine® CC. The investigated natural oils were unsuitable to dissolve target amount of baicalin. This observation is in accordance with literature (183).

Based on solubility studies, Peceol™ was the ideal choice as oily phase. Selection of surfactant depends on several factors such as solubilizing capacity for the API, the efficiency and rapidity to emulsify the oil and safety (106). Non-ionic surfactants are considered less toxic than ionic ones. Due to these considerations we analyzed five non-ionic surfactants with various HLB values. The highest solubility of baicalin was obtained in Labrasol® (3609.4 ± 277.39 µg/ml) followed by Kolliphor® EL and Labrafil® M 1944 CS. Solubility studies are necessary, but not sufficient conditions for selecting an emulgent, so Kolliphor® EL, Labrafil® M 1944 CS and Labrasol® were tested further for emulsification ability (see *Section 4.3.2.*) (184). The role of the co-surfactant together with the surfactant is to lower the interfacial tension, and to facilitate dissolving large amount of API in the oily phase (182). Drug absorption and dispersibility can be also improved by prudent selection of co-emulgent (82). Transcutol® P, an ether derivate revealed extreme high (13742.5 ± 691.74 µg/ml) solubilizing capacity, and were chosen therefore as co-surfactant for further investigations. The results of solubility study are presented in *Figure 27.*

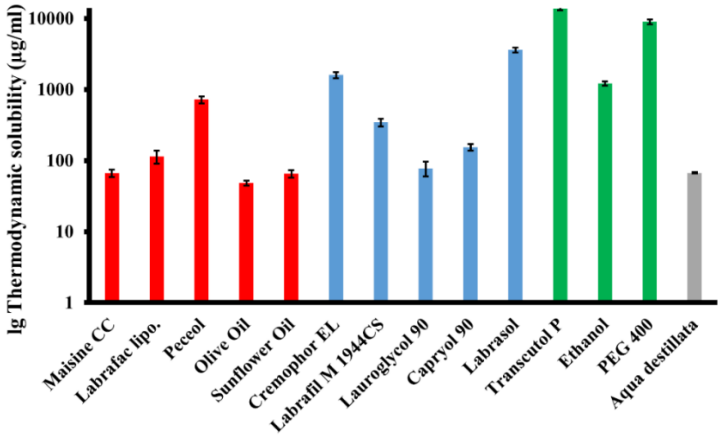

Figure 27. Thermodynamic solubility of baicalin in various oils (red), emulgents (blue), co-emulgents (green) and distilled water (gray). (Mean ± SD; n=3)

4.3.2. Screening of Surfactants for Emulsifying Ability

Three emulgents with various molecular structure and HLB-value were chosen to screen their ability to emulsify the oily phase by droplet size (*Fig.28/A*) and turbidity analysis (*Fig.28/B*). The droplet size of emulsions of Labrasol® and Kolliphor® EL demonstrated reduction with increased emulgent content, while Labrafil® M 1944 CS did not indicate any significant droplet size shift mixed with various oil ratios. All Labrasol® containing formulations proved unacceptable self-emulsification efficiency and turbid systems were generated. Kolliphor® EL showed the best emulsification ability and produced the most desired droplets with 151 ± 1.2871 nm. Turbidity analysis revealed a clear augmentation of transmittance with increased oil:emulgent ratios for Kolliphor® EL and Labrasol®, however Labrafil® M 1944 CS expressed a sharp decline. It has been reported, that the required HLB value to form o/w nanoemulsion is greater than 10 (185). The very poor emulsifying ability of Labrafil® M 1944 CS can be attributed to its low HLB-value (HLB=3). Labrasol® (HLB=14) exhibited better affinity for the oil phase compared to Labrafil® M 1944 CS, although the best compatibility was shown with Kolliphor® EL (HLB=12). This indicates that nanoemulsification was also influenced by other factors besides of HLB value, such as the chemical structure, saturation and chain length of surfactant (186).

We have selected Kolliphor® EL giving the greatest transmittance and lowest droplet size with increased oil:emulgent ratios. In consideration of the aforementioned results and observations, we can conclude that Peceol™, Kolliphor® EL and Transcutol® P is the best choice for designing baicalin containing SNEDDS.

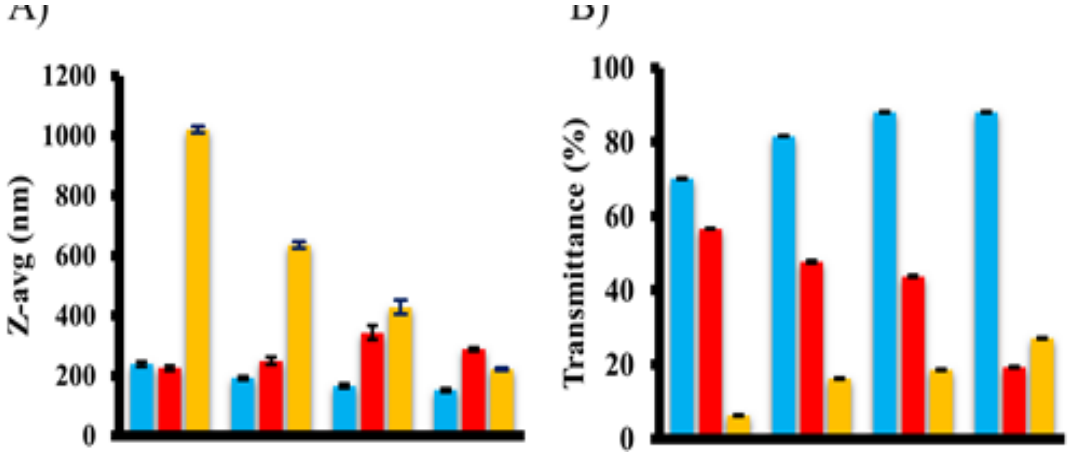

Figure 28. Emulsification ability of Kolliphor® EL (blue), Labrafil® M 1944 CS (red) and Labrasol® (yellow) with Peceol™ at different w/w ratios characterized by droplet size (A) and transmittance (B) analysis. (Mean ± SD; n=3)

4.3.3. Construction of Ternary Phase Diagram

The ternary phase diagram of different formulations of SNEDDS prepared by varying the concentration of Peceol™, Kolliphor® EL and Transcutol® P is demonstrated in *Figure 29*. The ternary phase diagram was constructed based on solubility and emulsification studies to identify the nanoemulsifying region (Z-avg < 200 nm, T% > 90%), and the composition also helps to determine the concentration range of components for the formation of a nanoemulsion. Compositions containing more than 22% oil phase were found to be out of nanoemulsifying region. It was observed, that at least 40% surfactant is required for producing droplets under 200 nm.

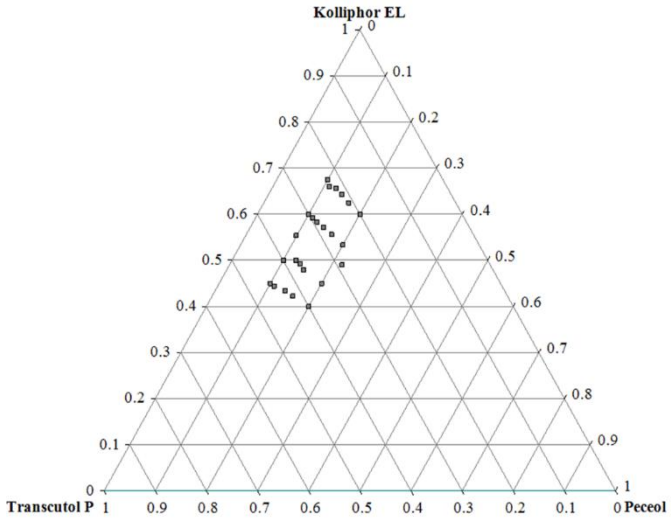

Figure 29. Ternary phase diagram of Peceol™, Kolliphor® EL and Transcutol® P based on droplet size and transmittance analysis. The area bordered by grey squares represents the self-nanoemulsifying region. (n=3)

4.3.4. Optimization of SNEDDS Preconcentrates

Independent variables and their levels and dependent variables with goals used in Face-centered experimental design is indicated in *Table XVI*. Thirteen experiments were designed to understand the influence of formulation variables (oil:S_{mix} and emulgent:co-emulgent ratios) affecting droplet size, transmittance, Zeta-potential and PDI (*Tbl. XVII*). The values of responses Y1 (Z-avg (nm)), Y2 (Transmittance (%)), Y3 (Zeta-potential (mV)) and Y4 (PDI) ranged from 20.3 to 200.8 nm, 78.7 to 100%, -33.8 to -15.9 and 0.25 to 0.69, respectively. The ratio of maximum to minimum for responses Y1, Y2, Y3 and Y4 was found to be 9.892, 1.271, 0.47, and 2.76, respectively. Power transformation was

not required for these responses, no aliases were found for Quadratic model, and in all cases the Sequential Model Sum of Squares detected the Quadratic model as significant. The models were validated by one-way analysis of variance (ANOVA), lack of fit and R^2 tests. The Model F values for responses Y1, Y2, Y3, and Y4 were 120.36, 66.24, 50.03, and 47.72, respectively, which implied that models were significant. The final polynomial equations and a summary of the regression analysis on all the responses are presented in *Tab. XVIII*. The main effects (b_1, b_2) represent the average result of changing one variable at a time from its low level to its high level while the other is kept fixed. The interaction term (b_{12}) show how Y1-Y4 change when two variables are simultaneously changed, while the quadratic terms (b_{11}, b_{22}) symbolize nonlinearity. The positive sign of the coefficients indicates synergistic effect on responses, while the negative sign expresses antagonistic effect. Our analysis also revealed non-significant lack of fit test results (p>0.05) for all the measured responses, which strengthened the reliability of the models.

Table XVI. Independent variables and their levels (A) and dependent variables with goals (B) used in Face-centered experimental design

A)		**Levels**		
Independent variables	**Symbol**	**-1**	**0**	**+1**
Oil:S_{mix} ratio	X1	1:8	1:6	1:4
Emulgent:co-emulgent ratio	X2	1:1	2:1	3:1

B)		
Dependent variables	**Symbol**	**Goal**
Z-avg (nm)	Y1	Y1 <200 nm
Transmittance (%)	Y2	Y2 >90%
Zeta-potential (mV)	Y3	Y3 >±20 mV
PDI	Y4	Y4 <0.400

Table XVII. Experimental matrix and observed responses

Std	Run	X1: Oil:S_{mix}	X2: Emulgent: co-emulgent	Y1: Z-avg (nm)	Y2: Transmittance (%)	Y3: Zeta-potential (mV)	Y4: PDI
10	1	0	0	99.5	96.7	-27.4	0.46
7	2	0	-1	138.4	97.7	-22.1	0.48
1	3	-1	-1	27.7	99.9	-17.8	0.28
8	4	0	1	84.4	97.5	-33.8	0.54
12	5	0	0	94.1	96	-28.6	0.49
4	6	1	1	136.2	88.6	-25.5	0.69
3	7	-1	1	20.3	100	-25.7	0.25
9	8	0	0	95.5	97.8	-27.7	0.46
2	9	1	-1	200.8	78.7	-15.9	0.54
6	10	1	0	141.3	82.6	-19.1	0.59
13	11	0	0	98.9	96.8	-27.1	0.41
5	12	-1	0	23.7	100	-23.3	0.27
11	13	0	0	97.9	96.1	-27	0.44

Analysis of standardized main effects (only significant values p <0.05 are discussed) showed that droplet size (Y1) was affected by synergistic effect of oil:S_{mix} ratio, antagonistically influenced by emulgent:co-emulgent ratio, interaction term between oil:S_{mix} and emulgent:co-emulgent ratio, and quadratic terms of oil:S_{mix} ratio. Transmittance (Y2) was synergistically affected by emulgent:co-emulgent ratio and interaction between oil:S_{mix} and emulgent:co-emulgent ratio, and an antagonistic effect was found with oil:S_{mix} ratio. In the case of Zeta-potential (Y3) we found a positive correlation with oil:S_{mix} ratio and its quadratic term, and a negative correlation with emulgent:co-emulgent ratio. PDI (Y4) showed significant synergistic effect with oil:S_{mix} ratio and emulgent:co-emulgent ratio. Based on these results, it is obvious, that all the factors contribute in determining the characteristics of SNEDDS.

Table XVIII. Summary of results of regression analysis for responses Z-avg, Transmittance, Zeta-potential and PDI with R^2, Adj-R^2 and Pred-R^2 tests. (statistical significance indicated by * ($p < 0.05$))

Source	Z-avg (nm)	Transmittance (%)	Zeta-potential (mV)	PDI
b_0	+ 97.24	+ 96.74	- 27.61	+ 0.46
b_1	+ 67.77*	- 8.33*	+ 1.05*	+ 0.17*
b_2	- 21.00*	+ 1.63*	- 4.87*	+ 0.030*
b_{12}	- 14.30*	+ 2.45*	- 0.43	+ 0.045*
b_{11}	- 14.91*	- 5.58	+ 6.54*	- 0.045
b_{22}	+ 13.99	+ 0.72	- 0.21	+ 0.035
R^2	0.9885	0.9793	0.9728	0.9730
Adj-R^2	0.9803	0.9645	0.9533	0.9537
Pred-R^2	0.8887	0.8222	0.7732	0.9047

Analysis of standardized main effects (only significant values $p < 0.05$ are discussed) showed that droplet size (Y1) was affected by synergistic effect of oil:S_{mix} ratio, antagonistically influenced by emulgent:co-emulgent ratio, interaction term between oil:S_{mix} and emulgent:co-emulgent ratio, and quadratic terms of oil:S_{mix} ratio. Transmittance (Y2) was synergistically affected by emulgent:co-emulgent ratio and interaction between oil:S_{mix} and emulgent:co-emulgent ratio, and an antagonistic effect was found with oil:S_{mix} ratio. In the case of Zeta-potential (Y3) we found a positive correlation with oil:S_{mix} ratio and its quadratic term, and a negative correlation with emulgent:co-emulgent ratio. PDI (Y4) showed significant synergistic effect with oil:S_{mix} ratio and emulgent:co-emulgent ratio. Based on these results, it is obvious, that all the factors contribute in determining the characteristics of SNEDDS.

Response surface method (RSM) designs help to quantify the relationships between one or more measured responses and the vital input factors. The generated 3D plots show how any of two factors affects the response. *Figure 30/A*, displays the effect of oil:S_{mix} (X1), emulgent:co-emulgent (X2) and their interaction on droplet size (Y1). When both oil:S_{mix} (1:8) and emulgent:co-emulgent was at low (1:1), mean droplet size of 27.7 ± 0.12 nm was observed.

By increasing oil content while keeping X2 at 1:1, droplet size was risen to 200.8 ± 1.64 nm. As the amount of surfactant and co-surfactant mixture increases, so decreases the droplet size. It can be attributed by the fact, that the strong localization of surface-active agents at the oil–water interface reduces the interfacial free energy. The higher the oil content, the more extensive the total interfacial area to be stabilized, and the amount of surfactant molecules are not sufficient to cover the oil droplets and lower interfacial tension at o/w interface. The lowest droplet size (20.3 ± 0.08) was achieved at low oil:S_{mix} level (1:8) and at high emulgent:co-emulgent ratio (3:1). The 3D response surface plot of transmittance is demonstrated in *Figure 30/B.*

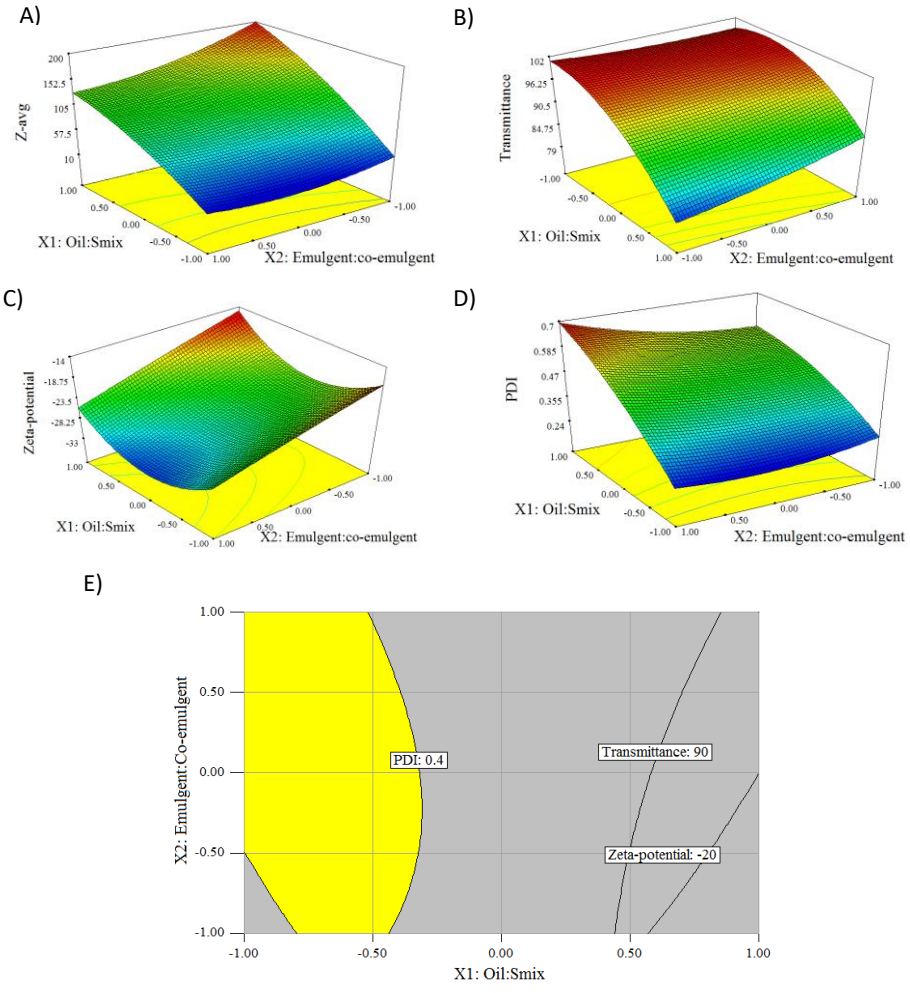

Figure 30. 3-D response surface plots for effect of oil:S_{mix} ratio and emulgent:co-emulgent ratio on Z-avg (A), Transmittance (B), Zeta-potential (C) and PDI (D). Overlay plot (E) for various oil:S_{mix} and emulgent:co-emulgent ratios, where the area that satisfies the constraints is yellow, while the area that does not meet criteria is grey.

Formulations are considered transparent if the percentage transmittance is above 90%, which is due to the fact that droplet size is not larger than 25% of the wavelength of incident light (187). Lower oil:S_{mix} ratios were favourable for producing -irrespective to the emulgent:co-emulgent ratio- perfectly transparent nanoemulsions (100% and 99.9%). As the amount of oil decreases in the formulation, the transmittance increases and vice versa. Examining the responses, the minimum transmittance value (78.7 ± 0.08%) was detected at high level of oil:S_{mix} and at low level of emulgent:co-emulgent. *Figure 30/C* illustrates the relationship between oil:S_{mix} and emulgent:co-emulgent ratios on Zeta-potential. The lowest Zeta-potential (-33.8 ± 0.83 mV) was observed at middle level of oil:S_{mix} and high level of emulgent:co-emulgent ratio. This electrokinetic potential was decreased by decreasing the ratio of co-surfactant. This phenomena might be explained by the insufficient co-surfactant concentration, because the co-surfactant plays a special role in reduction of interfacial tension and providing flexibility of the interfacial film (182). The highest Zeta-potential (-15.9 ± 0.72) was detected at high oil:S_{mix} and low emulgent:co-emulgent level. This result –besides the low Transcutol® P concentration- can be explained by the chemical structure of Peceol™. The oil composed of carboxyl groups of fatty acids, and in solutions it can be deprotonate to carboxylate anions (188). The analysis of PDI (*Fig.30/D*) pointed out parallel relationships with the droplet size measurements and also supplementing some differences as well. Emulgent:co-emulgent ratio influenced slightly the polydispersity indices, while effect of various oil:S_{mix} ratios were significant on PDI. The narrowest droplet size distribution was 0.25 and found when oil:S_{mix} was at low level and emulgent:co-emulgent was high. We can conclude, that higher oil content of the preconcentrate produces nanoemulsion with wider droplet size distribution. The desired PDI value should be less than 0.400, which implies a uniform particle size distribution (189).

All the measured responses were graphically optimized using the optimization module of the software. With multiple responses it is necessary to find regions where requirements simultaneously meet the critical properties. By superimposing or overlaying critical response contours on a contour plot it is possible to visually search for the best compromise. The minimum and maximum acceptable responses were determined according to the scientific literature: droplet size <200 nm, transmittance >90%, Zeta-potential <±20 mV, PDI <0.40. The overlay plot can be seen in *Figure 30/E*.

We selected our optimized formulation from the middle of the yellow labelled area of the overlay plot. The optimized SNEDDS contains Peceol™ (14.29%, w/w), Kolliphor® EL (57.14%, w/w) and Transcutol® P (28.57%, w/w). The predicted values for responses Y1, Y2, Y3 and Y4 were 59.63 nm, 99.51%, -26.50 mV and 0.36, respectively. Three batches of the optimized formulation were prepared and measured 52.87 ± 0.5322 nm, 99.87 ± 0.18%, -25.42 ± 0.710 mV and 0.335 ± 0.004. The predicted and observed values of responses were in very close correlation, indicating the reproducibility of the model.

4.3.5. Characterization of Optimized BSNEDDS

4.3.5.1. Droplet size, Transmittance, PDI, and Zeta-Potential Measurements

The droplet size, transmittance, PDI and Zeta-potential of optimized BSNEDDS was measured. It is well-known fact, that droplet size is an essential feature, and can significantly influence the *in vivo* fate of a nanoemulsion. The globule size of emulsion also determines the rate and extent of drug release (190). The Z-avg was highly desirable with 86.75 ± 0.3553 nm, likewise PDI value with 0.403 ± 0.007, indicating that the system had narrow droplet size distribution and anticipating an improved drug release. Transmittance of diluted sample was 99.93 ± 0.13%. In general, when the Zeta-potential of an emulsion is high (> ± 20 mV), the repulsive forces exceed the attractive forces, resulting in a relatively stable system. The long-term stability of a nanoemulsified system can be estimated by examine the fluctuation of Zeta-potential (191). The Zeta-potential of optimized BSNEDDS was -24.3 ± 1.44 mV and the specific conductivity was found to be 0.0135 ± 0.002 mS/cm.

4.3.5.2. Determination of the Thermodynamic Solubility of Baicalin in Optimized SNEDDS

The thermodynamic solubility of baicalin in optimized SNEDDS was 2714.3 ± 113.8 µg/ml. It indicates 40.5-times solubility improvement correlate with solubility in distilled water (67.3 ± 1.6 µg/ml).

4.3.5.3. Cloudpoint Measurement

A special property of non-ionic surfactants is cloudpoint, the temperature above which the surfactant phase separates and precipitates out of solution. The cloudpoint is higher than 37 °C in ideal case because of the risk of irreversible phase separation in the body (104). The cloud point for BSNEDDS was 71-73 °C providing stabile nanoemulsion *in vivo* at physiological temperature.

4.3.5.4. Effect of Dilution on Droplet Size and PDI

After oral administration of SNEDDS, nanoemulsion formation upon dilution takes place *in vivo*. It is relevant aspect to demonstrate that uniform nanoemulsions are formed in terms of various dilutions and these nanoemulsified systems do not show any sign of phase separation and/or precipitation. The drug may precipitate *in vivo* at higher dilutions which might significantly affect drug absorption (192). All emulsions were found to be in the acceptable nanoemulsion region (Z-avg <200 nm, T >90%, PDI <0.4), proving their robustness to dilution. After 24 hours of inspection, neither phase separation, nor precipitation was observed. *In vitro* results showed that BSNEDDS upon different dilutions forms uniform nanoemulsions and drug solubility in BSNEDDS was adequate (no precipitation).

4.3.5.5. Long-Term Physical Stability of Nanoemulsions

The long-term physical stability of BSNEDDS was evaluated by droplet size, PDI measurements and macroscopic observation for a month. Various physicochemical phenomena can lead to the breakdown of a nanoemulsion (e.g. creaming, flocculation, Ostwald ripening), but these undesirable mechanisms can be identified. There was no significant change in droplet size and/or PDI over the investigated period comparing to initial values. The visual observation revealed no phase separation, creaming or precipitation. The O/W baicalin containing nanoemulsion demonstrated high physical stability. The results of long-term stability study are illustrated in *Table XIX*.

Table XIX. Results of long-term stability analysis of liquid BSNEDDS formula (Mean ± SD; n=3)

Storage intervals (days)	**Z-avg (nm)**	**PDI**
0	81.24 ± 0.17	0.406 ± 0.007
1	80.14 ± 0.08	0.405 ± 0.006
5	79.23 ± 0.14	0.379 ± 0.002
7	82.37 ± 0.10	0.400 ± 0.002
21	79.53 ± 0.05	0.443 ± 0.003
28	80.86 ± 0.28	0.3890.003

4.3.5.6. Atomic Force Microscopy

Lyophilized nanodroplets dispersed homogeneously on mica surface showing no signs of aggregation (*Fig.31/A*). They appeared as circular objects with smooth surface and rounded topography (*Fig.31/B*), which corresponds well to what one would expect from a surface adsorbed droplet. Height of particles followed a slightly right skewed distribution (*Fig.31/C*). Lack of outstandingly large particle sizes indicate that droplets did not coalesce during sample preparation. Mean height of droplets (±SD) was 15.4 ± 9.0 nm what was lower than the diameter (52.87 ± 0.5322 nm) obtained from DLS data. This may stem from two factors: *(1)* Flattening of emulsion droplets on mica surface, or *(2)* the fact that DLS yields the hydrodynamic size of the droplets, which is bigger than the real particle diameter. [Since the diameter of surface adsorbed droplets is about two times larger than their height (*Fig.32/A)* at first sight one would think there was a considerable flattening indeed. However, tip convolution artefact on its own can result in this extent of artefactual apparent widening of vesicle diameter being the tip radius approx. 9nm.]

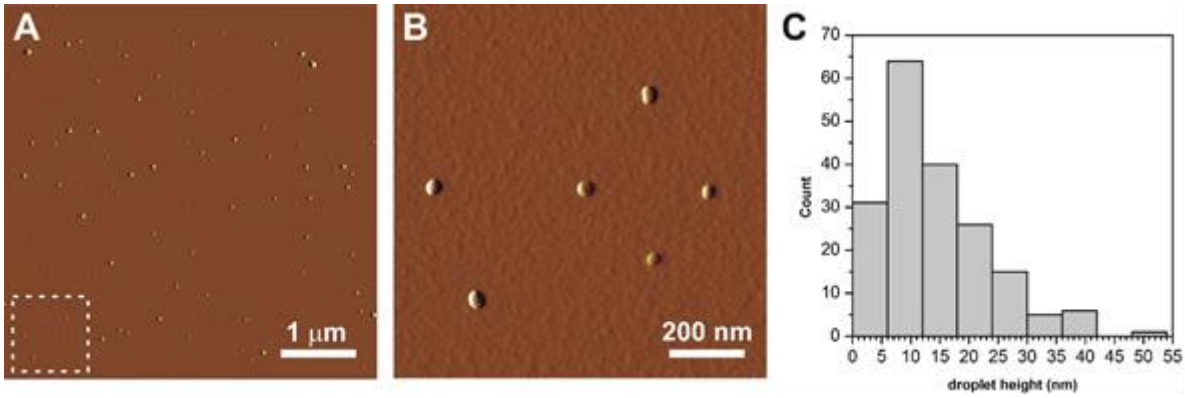

Figure 31. AFM amplitude-contrast images of surface absorbed lyophilized oil droplets (A). Area marked by dashed line is shown in (B). (C) Height distribution of droplets (n=122).

To estimate the diameter of the original, fluid phase emulsion droplets, volume of surface-adsorbed droplets was determined. From this, the real diameter of fluid phase droplets could be calculated, assuming that they have spherical shape and there is no volume change upon surface-adsorption. Estimated fluid phase droplet radius showed an apparent normal distribution with 23.6 ± 12.0 nm as mean ± SD *(Fig.32/B)*. This value falls somewhat closer to the DLS size, the difference between them might be attributed to the hydrodynamic overestimation of particle size by the DLS method.

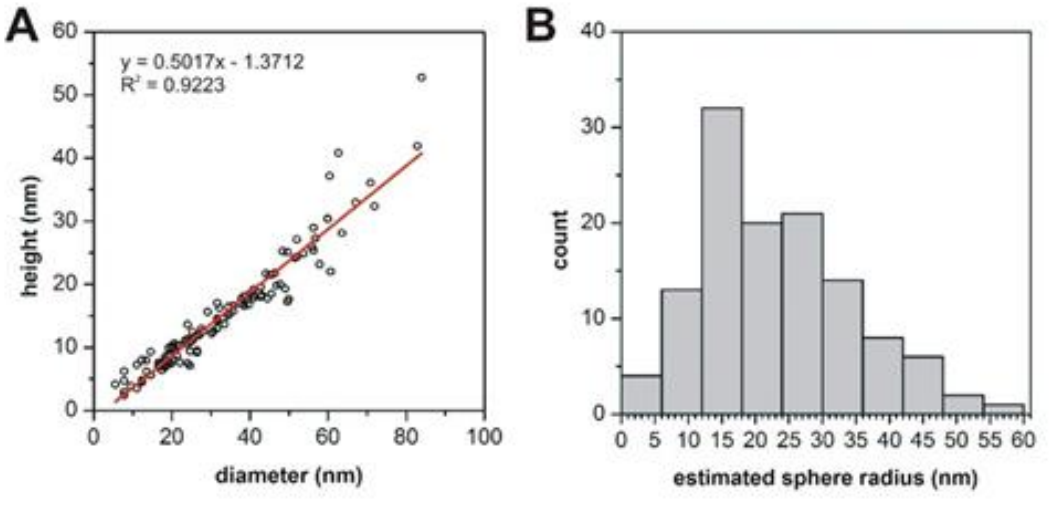

Figure 32. Correlation between the height and diameter of surface-adsorbed oil droplets (A). Histogram of estimated radius of oil droplets in fluid phase (B). Estimation based on volume of surface-adsorbed droplets. (n=122)

*4.4.*Physical characterization of SNEMPs

4.4.1. Flow properties

The flowability of pellets were evaluated by different methods in order to characterize the formulation for this property as precisely as possible. Flow properties of pellets are of primary importance for precise dosing in case of capsules and tablets, mixing and handling processes. The flow through an orifice showed that BSNEDDS-MCC and BSNEDDS-MCCIsm formulations have similar and excellent flow properties. Carr's index calculated from bulk and tapped density values ranged from 6.81% to 8.33%, while Hausner-ratio ranged from 1.16 to 1.19 for BSNEDDS-MCCIsm and BSNEDDS, respectively. These values indicate excellent flow characteristics and low interparticle interactions of the investigated formulations. We can conclude that in the case of baicalin containing matrix pellets the addition of isomalt slightly improves the flowability. The summary of flow properties can be seen in *Table XIX*.

4.4.2. Friability

Pellets with good physical properties have low friability. It is a convenient factor to predict pellet behaviour during film coating, compressing, capsule filling and packaging. The friability of BSNEDDS-MCCIsm and BSNEDDS-MCC was 0.042% and 0.045%, respectively *(Tbl. XIX.)*. There aren't any standardized methods in Ph.Eur.9. for testing friability of pellets, consequently there is no official acceptance limit value. The formulations showed indurate structure, a negligible amount of attrition was generated by agitation.

4.4.3. Shape analysis

The roundness and AR are informative shape parameters, while the maximum Feret diameter can be used to demonstrate the mean particle size of pellets (193). The upper limit for aspect ratio is 1.20, roundness close to 1 expresses an ideal sphere as was previously reported (194). The average value of AR was 1.12 for BSNEDDS-MCCIsm and 1.11 for BSNEDD-MCC, whereas the average roundness was 0.90 and 0.91, respectively. The results of shape parameters of matrix pellets indicated spherical structure. *Table XX.* demonstrates the size and shape analysis of various spheres. Representative stereomicroscopic pictures of different pellet formulations can be seen in *Figure 33.*

Table XX. Summary of physical characterization of BSNEDDS-MCCIsm and BSNEDDS-MCC matrix pellets (Mean ± SD; n=3)

	BSNEDDS- MCCIsm	**BSNEDDS-MCC**
Bulk density (g/cm^3)	0.45 ± 0.007	0.61 ± 0.009
Tapped density (g/cm^3)	0.48 ± 0.008	0.67 ± 0.011
Carr's index (%)	6.81 ± 0.14	8.33 ± 0.17
Hausner-ratio	1.16 ± 0.107	1.19 ± 0.11
Flowability (g/s)	6.02 ± 0.205	6.88 ± 0.213
Friability (%)	0.042 ± 0.35	0.045 ± 0.21
Res. water content (%)	3.947 ± 0.104	2.586 ± 0.251
Feret$_{max}$ (mm)	1.49 ± 0.072	1.33 ± 0.067
AR	1.12 ± 0.08	1.11 ± 0.06
Roundness	0.90 ± 0.07	0.91 ± 0.05

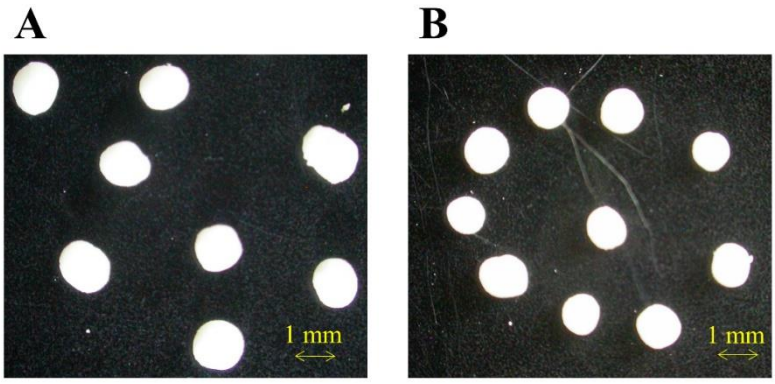

Figure 33. Morphological characteristics of BSNEDDS-MCCIsm (A), BSNEDDS-MCC (B) pellet cores captured by stereomicroscope

4.4.4. Residual water content

It was pointed out that the differences in the residual water content of the two formulations was slight, indicating that the drying process of BSNEDDS-MCCIsm/BSNEDDS-MCC spheres efficiently removed the free water added during the initial wet massing stage, in spite of the various amount of added water during the preparation step of pellets. Residual water content determined by Karl Fischer titration method was in case of BSNEDDS-MCCIsm 3.947 ± 0.104%, while for BSNEDDS-MCC 2.586 ± 0.251% was registered.

4.5. Solid state characterization of SNEMPs

4.5.1. FT-IR

The changes in crystallinity and the alteration of intermolecular (drug-excipient, excipient-excipient) interactions can be detected by Fourier-transformed infrared spectroscopy (195). FT-IR spectra of baicalin, MCCIsm, MCC, BSNEDDS-MCCIsm and BSNEDDS-MCC pellets are shown in *Figure 34*. The following characteristic peaks were identified for pure baicalin: phenolic –OH group at 3491 and 3552 cm^{-1}, -OH at 3373 cm^{-1}, -COOH at 1726 cm^{-1}, C=C of phenyl at 1608, 1573 and 1498 cm^{-1}, carbonyl C=O at 1656 cm^{-1} and C-O-C of ether at 1065 cm^{-1}. Examining the spectra of MCC typical absorption peaks of cellulose at 1430, 1158, 1044, 1025 and 1000 cm^{-1} can be identified corresponding the results with the literature (196). Analysis of MCCIsm mixture showed the characteristic peaks of microcrystalline cellulose and isomalt. The assignment of bands is very difficult due to several overlapping bands and intensive hydrogen bonding. For isomalt the followings were identified: C-C skeletal stretching band at 1087 cm^{-1}, C–OH stretching band for aliphatic secondary OH-group together with C–O–C ring stretch at 1159 cm^{-1} and vibration of C-O-C ring at 935 cm^{-1}. The characteristic absorption bands of baicalin disappeared in spectra of BSNEDDS-MCCIsm and BSNEDDS-MCC pellets, suggesting the crystalline-amorphous phase transition of baicalin.

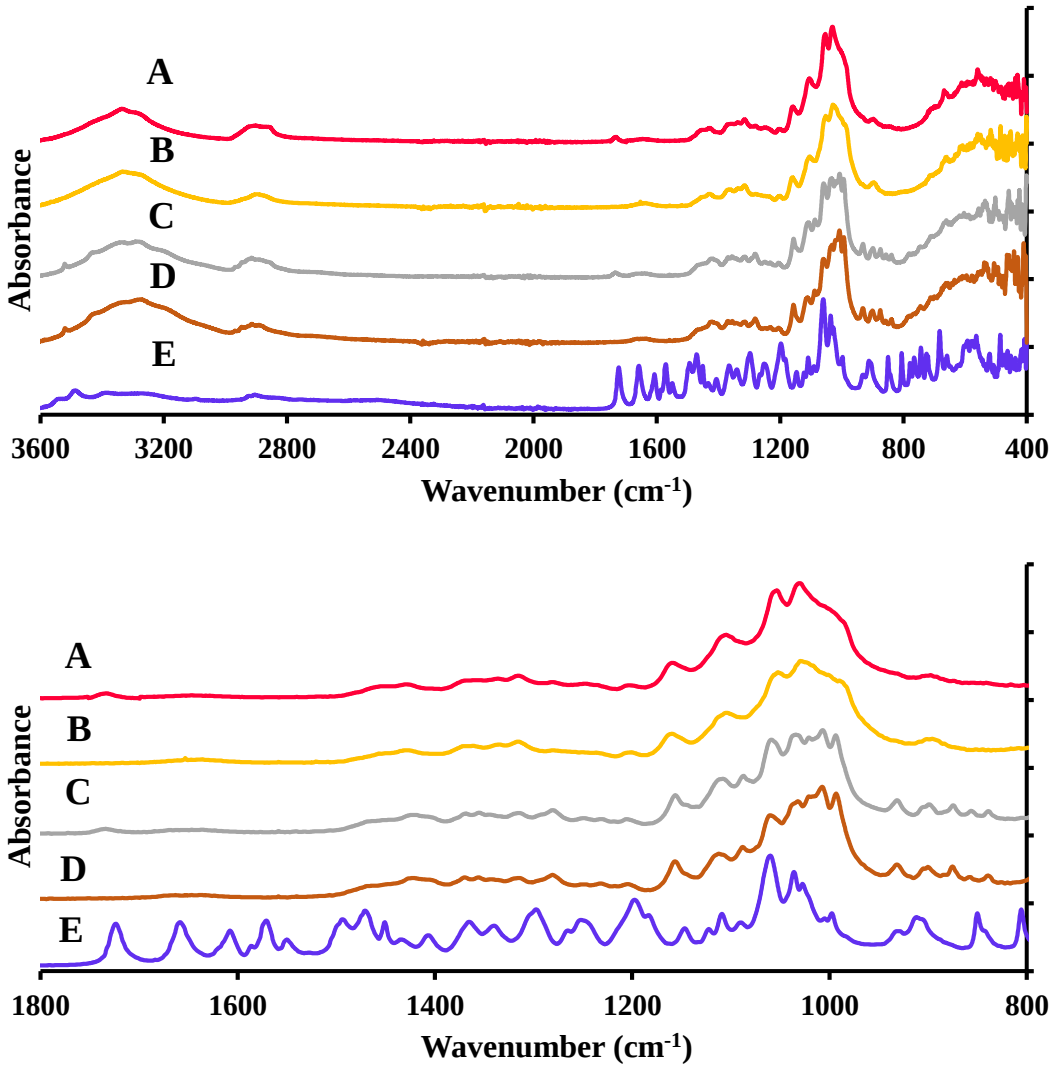

Figure 34. FT-IR spectra of BSNEDDS-MCC (A), MCC (B), BSNEDDS-MCCIsm (C), MCCIsm (D) and baicalin (E). 400-3600 cm^{-1} (top) and 800-1800 cm^{-1} (below)

4.5.2. Raman spectroscopy

The above-mentioned materials and formulations were analysed by Raman spectroscopy, the complementary technology of IR. Vibrational characterization of the samples is represented in *Figure 35.* As baicalin possesses very low symmetry, its FT-IR and Raman spectra are quite similar in appearance with slightly more bands present in the IR spectrum and some differences in relative intensities. The difference in number and intensity of the bands is the consequence of the Raman scattering effect itself (197). Characteristic peaks of baicalin can be found in physical mixture, proposing its crystalline

state. Typical absorption peaks of baicalin cannot be recognized in BSNEDDS-MCCIsm and BSNEDDS-MCC, verifying and supporting the results of DSC and FT-IR analysis.

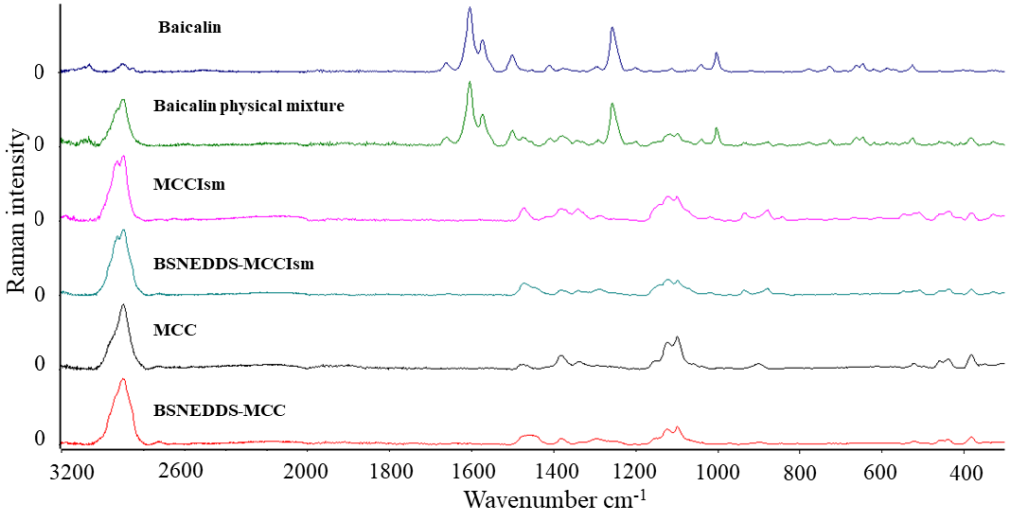

Figure 35. Raman spectra of Baicalin, Baicalin physical mixture, MCCIsm, BSNEDDS-MCCIsm, MCC and BSNEDDS-MCC

4.6.In vitro dissolution study and reconstitution properties of SNEMPs

In vitro release profiles of pure baicalin, BSNEDDS preconcentrate, BSNEDDS-MCCIsm and BSNEDD-MCC at pH 1.2 dissolution medium are shown in *Figure 36/A*. Baicalin instantaneously released from BSNEDDS. Pure drug showed slower dissolution (5.77 ± 3.77%) for the initial period of 5 minutes. After the disintegration period of solid formulations, whole amount of baicalin was dissolved in case of BSNEDDS-MCCIsm and BSNEDDS-MCC within 10 minutes. *Figure 36/B* represents dissolution profiles of baicalin, BSNEDDS, BSNEDDS-MCCIsm and BSNEDD-MCC at pH 6.8 dissolution media. BSNEDDS dissolved total amount of its drug content within 5 minutes. BSNEDDS-MCCIsm has disintegrated faster compared to BSNEDDS-MCC because of the hydrophilic property of isomalt. Self-nanoemulsifying formulations significantly improved the dissolution and dissolution rate of drug comparing to pure form of API. The optimized solid BSNEDDS-MCCIsm released 100% of incorporated baicalin within 10 minutes irrespective to pH value of dissolution media.

The liquid and two solid formulae showed spontaneous nanoemulsification and there was no sign of phase separation or phase inversion of nanoemulsion after storage of 24 h. The

reconstitution was successful because of the low PDI values in both dissolution media for each formulation indicating narrow droplet size distribution. It was also observed that the mean droplet size increased with the solidification of BSNEDDS but it was far below 200 nm (*Tbl. XXI.*). On the grounds of *in vitro* dissolution studies and reconstitution analysis we can declare that remarkable dissolution improvement was achieved and total amount of incorporated baicalin released from homogeneous size distribution nanoemulsified droplets.

Table XXI. Z-avg and PDI values of different liquid and solid formulations at pH=1.2 and pH=6.8 measured during reconstitution analysis (Mean ± SD, n=3)

Z-avg (nm)

	SNEDDS	*BSNEDDS*	*BSNEDDS-MCCIsm*	*BSNEDDS-MCC*
pH=1.2	50.41 ± 0.321	84.93 ± 0.323	132.1 ± 0.152	131.1 ± 0.264
pH=6.8	52.84 ± 0.632	86.67 ± 0.295	132.9 ± 0.208	139.3 ± 0.472

PDI

pH=1.2	0.231 ± 0.01	0.321 ± 0.002	0.396 ± 0.005	0.383 ± 0.002
pH=6.8	0.217 ± 0.01	0.347 ± 0.003	0.411 ± 0.007	0.331 ± 0.01

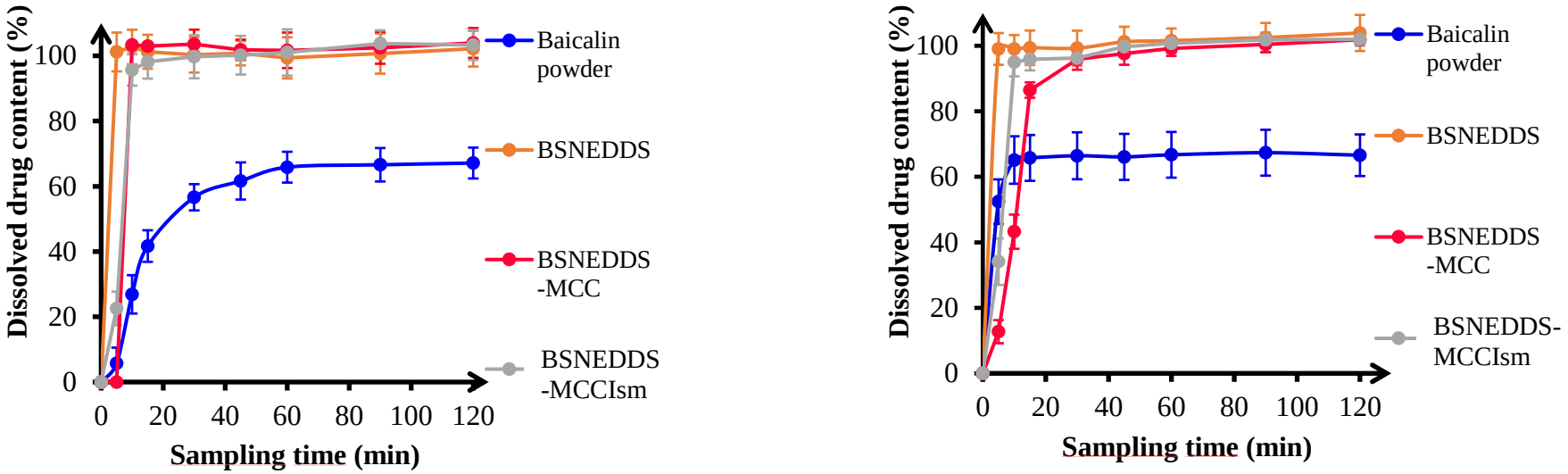

Figure 36. *In vitro* dissolution profile of baicalin powder, BSNEDDS, BSNEDDS-MCC and BSNEDD-MCCIsm at pH 1.2 (left) and at pH 6.8 (right)

5. Discussion

*5.1.*Preformulation studies

Preformulation is an integral part of formulation design and lays down foundation for transforming a new drug entity into a DDS. Numerous articles in topics of formulation development and solubility enhancement of baicalin were published, but the most important physicochemical properties influencing the pharmacokinetic and pharmaceutical behaviour of drugs like acid-base properties, lipophilicity, solubility, crystal size, crystal habit were not investigated yet in a comprehensive study. This thesis filled that gap and it can provide useful and necessary information for the development of baicalin-loaded formulations. Baicalin has low and pH-dependent solubility, low lipophilicity, bad flowability due to anisometric crystal habit, which predicts dubious processability and bioavailability. Therefore, the adequate delivery of baicalin requires a safe, effective, and stable pharmaceutical formulation.

*5.2.*Baicalin-cyclodextrin inclusion complexation

The present work could demonstrate for the first time that γ-cyclodextrin can enhance remarkably the low solubility of baicalin compared to parent α-, and β-CDs and their derivates. There is a different bonding and docking pattern with γ-CD, which can be explained in terms of the diameter, related to the respective 7 and 8 glucopyranose units in *β*- and *γ*-CD. The difference is that *γ*-CD provides an extra beneficial –OH group for baicalin's carbonyl group. The study of Li et al. didn't investigate more CDs, just HP-β-cyclodextrin was used (198). The research aimed to characterize the effect of preparation method for the delivery of complexed baicalin via supercritical fluid encapsulation and solution mixing. They found more favourable properties in case of complexation (e.g. particle size and baicalin solubility) prepared by supercritical fluid extraction compared to conventional solution mixing. In this thesis the conventional solution mixing was utilized but considering the effectivity of supercritical fluid encapsulation, it would be interesting to check and expand this technique to γ-CD complexes in the future. Jing et al. investigated the complexation effect of maltosyl-β-CD on baicalin along with NMR molecular modelling studies (199). In accordance with my findings they suggested that the phenyl moiety is buried deeper than the chromen moiety stabilized via hydrogen

bonds and hydrophobic interactions. The CD complexation of baicalin is underrepresented in the scientific literature; it is promising –in the view of above-mentioned results and considering the large number and types of various CD derivates- to undertake more detailed examinations for the delivery of baicalin and other phytopharmacons.

*5.3.*Liquid Self-nanoemulsifying Drug Delivery Systems

Self-nanoemulsifying systems are able to create colloid dispersion *in vivo* and deliver the molecule entrapped in nanodroplets to the place of absorption. A thorough and detailed analysis is needed to fulfil all critical quality requirements of self-emulsifying systems like drug loading, droplet size, Zeta-potential, long-term stability and dissolution. The selection of oil, emulgent and co-emulgent is also plays a prominent role. The formulation optimization of baicalin-loaded preconcentrates was carried out using face-centered experimental design. I attach great importance to the mathematical description of various phenomena, because they can be quantitatively characterized and disguised interactions can be also highlighted. Oil:surface active agent ratio and emulgent:co-emulgent ratio had a significant impact on all critical quality attributes of nanodroplets. The optimization and formulation development of BSNEDDS resulted in a 40-times solubility enhancement and significant dissolution improvement in case of baicalin. For the very first time, our research group captured these nanodroplets by AFM imaging. The sample preparation was a great challenge, which stems from two facts: 1. the tip of cantilever removed the weakly bonded droplets from sample surface. 2. The droplets were extremely exposed to coalescence due to the high surface energies. Freeze-drying and the use of liquid N_2 eliminated these undesired phenomena. The self-emulsifying approach seems to be very promising, therefore, the quality control, scaling up, industrial implementation, regulatory aspects must be clarified in the future.

*5.4.*Self-nanoemulsifying matrix pellets

Self-emulsifying matrix pellets combine the benefits of liquid SEDDS (e.g. enhanced solubility and bioavailability, improved dissolution) with those of solid dosage forms (e.g. higher stability and reproducibility, better patient compliance, easier administration, modified release). Several formulation aspects must be considered in order to ensure

successful development. During my experiments, MCC demonstrated the most desired properties; it showed adequate oil adsorbing capacity (more than 1.5-times its own weight), nevertheless, it released the bonded drug rapidly in the dissolution medium. The preparation of spherical pellets possessing acceptable physical characteristics was also possible. One of the greatest challenges was the selection of ideal powder/oily preconcentrate ratio for extrusion-spheronization; as the ratio was increased, so decreased the physical stability and processability; the result of lower ratio was a sticky, paste-like extrudate, which gave during spheronization process undesired pellets with high diameter and high friability. The application of isomalt slightly accelerated the disintegration time of pellets due to its hydrophilic nature, however, the oil adsorbing capacity of MCC-Ism powder mixture was significantly decreased, which is not beneficial from the point of view drug loading. The ideal mass ratio was 1/3-1/3-1/3 in case of BSNEDDS-MCC-Ism and 1/2-1/2 in case of BSNEDDS-MCC, respectively. BNSEDDS-MCC as well as BSNEDDS-MCCIsm revealed remarkable dissolution improvement and after disintegration of matrix pellets nanodroplets were generated.

5.5. Comparison of baicalin-CD inclusion complexes and baicalin-loaded SNEDDS

Considering the experimental data, it can be concluded that both the cyclodextrin complexation and the nanoemulsification remarkably enhanced the poor water solubility of baicalin, which is one of the most noteworthy result in this thesis. However, the extent of solubility improvement is different in favour of the lipid-based system. As we talk about two totally different formulation approach and the fundamental physicochemical mechanisms are also working another way, this result is not surprising. It is a possible future direction to extend the investigated CD candidates to realize higher water solubility gain and better stability. The comparison of formulated dosage forms -which have a great impact on patient compliance and industrial feasibility- demonstrates that the lipid-based direction is further advanced than the cyclodextrin-based DDS. In case of SNEDDS, the solidification and the preparation of matrix pellets having good flowability, stability, and in vitro dissolution are already performed. Nevertheless, a lyophilisation and/or spray drying step is necessary regarding the CD research direction to develop a stable and sustainable dosage form. Furthermore, a crucial question has to be answered using in vivo

studies; how can the formulations perform in living organisms with the above detailed solubility and permeability improvement?

5.6. Comparison the two formulations presented in the thesis with the formulations already published in scientific literature

In *Table II* a detailed summary can be found about the innovative formulation possibilities for enhancing the oral bioavailability of baicalin. Indicative examples could be: solid dispersion, liposomes, mixed micelle system or thermosensitive hydrogel. It is clear that each examined innovative formulation can enhance the solubility and/or permeability of baicalin. However, the applied methods and excipients, stability of formulation, costs, industrial feasibility, expected patient-compliance and possible administration route are different. Liposomes, mixed micelle systems, nanoparticles are prone to stability issues, and the industrial scaling-up can be also a challenging task. Nanoemulsions, microemulsion and cyclodextrin complexes as liquid DDS demonstrate limited stability, the patient-compliance is also questionable, and sustainable packaging devices are needed. In case of baicalin this is the first research, which aimed to create solidified self-emulsifying system. Patient-compliance, diverse dosage forms (capsule, tablet, sachet, straw), ease to scaling-up, modified release, appropriate stability are all the advantages of pharmaceutical pellets. The solidified nanoemulsion-based system demonstrated in this thesis may be eligible to fit in the exacting requirements of industrial sector and modern, health-minded patient.

6. Conclusions

The main objective of this work was to formulate and develop baicalin-loaded DDS in order to counterbalance the negative physicochemical and pharmaceutical properties of baicalin. All of the proposed goals were achieved in this study and many further relationships were identified and analysed. In the introduction as well as in the experimental section several challenges and questions were highlighted, which are fundamental, in my view, for the quality control and successful formulation of cyclodextrin and nanoemulsion-based DDS. Based on the results, the following conclusion can be drawn:

1. Baicalin has promising pharmacological effects, but it demonstrates low water solubility and low lipophilicity, which hampers its oral bioavailability (BCS IV). Significant, pH-dependent solubility was found, which can be explained by the fact that the molecule has three acidic functional groups (pK_{a1}: 4.21, pK_{a2}: 8.56, pK_{a3}: >14). The neutral (transportable) form is dominant up to pH 4.2, but in acidic environment its solubility is so low, that the oral delivery of baicalin might be problematic. However, in case of biorelevant conditions (FaSSGF), the presence of neutral emulsifying agents and fatty acids had a significant positive impact on the solubility of baicalin; this beneficial drug-food interaction could be exhausted in liberation and absorption processes (drug intake with/after meal). The molecule decomposes above 50 °C and in alkaline solutions, which are restrictive factors considering further processability.
2. Six different CD derivates were examined to study the solubility enhancement of baicalin along with stability and geometry of inclusion complexes. Molecular modelling analysis pointed out different binding patterns and complexation energy for each baicalin-CD complex. In accordance with the previous hypothesis, thermodynamically the most favourable complex proved to be baicalin-γ-CD host-guest complex ($\Delta E = -181.5$ kJ mol^{-1}), which fact was confirmed by phase-solubility (≈ 5.5 times solubility enhancement) and NMR spectroscopic measurements. The preliminary studies showed that it makes sense to continue the CD project with more detailed and deeper *in vitro* and *in vivo* investigations.

3. Dissolution kinetics of baicalin was improved in a self-nanoemulsifying system taking different types of oils, surfactants, co-surfactants, and ideal ratio of components into consideration, based on response surface methodology, using a central composite experimental design. The best composition contains Peceol™ (14.29%, w/w), Kolliphor® EL (57.14%, w/w), and Transcutol® P (28.57%, w/w). Droplet size was measured by DLS method and verified by AFM, together with morphological characterization. A new sample preparation method gave the opportunity to analyse the freeze-dried samples without any signs of aggregation of droplets. Droplet size after dispergation of BSNEDDS pre-concentrate was highly desirable, with 86.75 ± 0.3553 nm; the Zeta-potential was -24.3 ± 1.44 mV, which is also acceptable. The results proved that the low aqueous solubility and dissolution rate of baicalin can be significantly improved by the optimized BSNEDDS formula. The pre-concentrate showed very rapid emulsification (within seconds) and nanosized droplets were generated.
4. Transformation of liquid BSNEDDS preconcentrate to different solid carriers and the preparation of self-nanoemulsifying matrix pellets were carried out by extrusion-spheronization method. The selection of MCC and isomalt as carriers was an ideal choice as both of the pellet formulas prepared using them demonstrated sufficient physical characteristics. BSNEDDS-MCC and BSNEDDS-MCCIsm had spherical shape, narrow particle size distribution, excellent flow, low friability. The only difference was the slightly accelerated disintegration time in case of BSNEDDS-MCCIsm because of the hydrophilic nature of isomalt. FT-IR, Raman vibrational spectroscopic characterization techniques demonstrated the amorphous physical state of baicalin in solid formulations, which is partially responsible for the enhanced dissolution behaviour. *In-vitro* dissolution studies showed significant, pH-independent dissolution rate and saturation solubility improvement (100%, within 15 minutes). On reconstitution investigations it was pointed out that baicalin is released from the solid dosage form in colloidal dispersion that had an average size of 130-140 nm. These results indicate the significance of solid self-nanoemulsifying systems, which are suitable for the oral delivery of pharmacons possessing low solubility and dissolution rate.

7. Summary

One of the most tremendous challenges faced by pharmaceutical scientists is the improvement of poor solubility and/or permeability and the concomitant low bioavailability of new chemical entities. Baicalin is a bioactive flavonoid extracted from the root of *Scutellaria Baicalensis.* Numerous pharmacological effects of this phytopharmacon were reported (e.g. antioxidant, anxiolytic), nevertheless the inappropriate biopharmaceutical properties hamper its oral delivery. In this thesis the physicochemical analysis of baicalin was demonstrated along with the development and examination of suitable oral DDS, which are able to counterbalance the challenging pharmaceutical attributes of this natural herb medicine. Firstly, the thorough characterization of baicalin was carried out in terms of acid-base properties, biorelevant solubility, lipophilicity, crystal size and crystal habit. Secondly, six baicalin-cyclodextrin inclusion complexes, as possible carriers, were formulated and examined with different theoretical and experimental methods. NMR, thermodynamical calculations and molecular modelling indicated that γ-CD is suitable as a host molecule for baicalin and significantly improves its solubility. In the third section the focus was put on self-nanoemulsifying systems, where response surface methodology and desirability approach were used to select the best composition. More than 40-times solubility improvement was achieved with the optimized self-nanoemulsifying formulation correlated to solubility of baicalin in distilled water. At this stage, a new sample preparation method was developed for the AFM imaging of reconstituted baicalin-loaded nanodroplets. In phase four the study aimed to highlight how to transform oily preconcentrates with high viscosity to solid carriers, and is it possible to create matrix pellets made of oily components demonstrating acceptable physical characteristics? The results pointed out that the preconcentrate could be effectively adsorbed to MCC and isomalt-based carriers and the low aqueous solubility and dissolution rate of baicalin can be significantly improved by self-nanoemulsifying matrix pellets. The amorphous state of baicalin and the emulsifying agents together are responsible for the enhanced dissolution rate. It can be concluded that despite the challenging pharmaceutical properties of baicalin, its dissolution and solubility can be successfully enhanced with cyclodextrins and self-emulsifying systems. The relationships and data described herein extend beyond baicalin itself, they could be effectively used in case of further molecules.

8. Összegzés

A gyógyszerkutatók egyik legnagyobb kihívása napjainkban az új kémiai entitások rossz vízoldhatóságának és/vagy permeábilitásának, valamint az ebből következő alacsony biohasznosulásának javítása. A bajkalin egy, a *Scutellaria baicalensis* gyökerében található bioaktív flavonoid. Számos farmakológiai hatását leírták (pl. antioxidáns, anxiolítikus), azonban a nem kielégítő biohasznosíthatóság nehezíti orális alkalmazását. A doktori munkámban a bajkalin fiziko-kémiai elemzése, valamint a molekula kihívást jelentő gyógyszerészeti tulajdonságainak az ellensúlyozására alkalmas orális gyógyszerhordozó rendszerek fejlesztése és vizsgálata került bemutatásra. Elsőként a fitofarmakon részletes sav-bázis, bioreleváns oldhatóság, lipofilitás, kristály méret és kristály habitus analízisét végeztem el. Ezt követően hat bajkalin-ciklodextrin zárványkomplexet formuláltam és tanulmányoztam különböző elméleti és experimentális módszerekkel. NMR, termodinamikai számítások és molekulamodellezések alátámasztották, hogy a γ-CD megfelelő a bajkalin komplexálására és szignifikánsan javítja annak oldhatóságát. Munkám harmadik fázisa az ön-nanoemulgeáló rendszerekre fókuszált, ahol a megfelelő összetétel kiválasztása az eredményfelület módszeren és kívánatossági függvényszámításokon alapult. A hatóanyag több mint 40-szeres oldhatóságjavulást mutatott az optimalizált ön-nanoemulgeálódó formuláció esetén a desztillált vízben mért értékhez viszonyítva. Ehhez a részhez kapcsolódott egy új mintaelőkészítési eljárás kidolgozása a rekonstituált bajkalin tartalmú nanocseppek AFM felvételeihez. A negyedik részben célom volt górcső alá venni, hogy miként lehetséges nagy viszkozitású olajos prekoncentrátumok felvitele szilárd hordozókra, és lehetséges-e megfelelő fizikai tulajdonságokkal rendelkező mátrixpelletek előállítása olajos komponensekből? Eredményeim alapján elmondható, hogy a prekoncentrátum sikeresen adszorbeálható MCC és izomalt alapú hordozókra, továbbá a bajkalin alacsony vízoldhatóság és kioldódása javítható ön-nanoemulgeálódó mátrixpelletek alkalmazásával. A kioldódási arány fokozódásáért a molekula amorf állapota és a jelenlévő emulgensek együttesen felelősek. Összegzésként ki szeretném emelni, hogy a bajkalin kihívást jelentő fiziko-kémiai tulajdonságai ellenére a kioldódása és oldhatósága sikeresen növelhető ciklodextrinekkel és önemulgeáló rendszerekkel. A feltárt összefüggések és adatok túlmutatnak a vizsgált hatóanyagon, további felhasználásuk is lehetséges egyéb gyógyszermolekulák esetén.

9. References

1. Ku, M. S. (2008) Use of the Biopharmaceutical Classification System in early drug development. AAPS J. 10: 208–212

2. Marshall, C. (2013) Formulation Development – A Call for Collaboration to Meet the Bioavailability Challenge. Drug Dev. Deliv. 13: 20–25

3. Jakab, G., Bogdán, D., Mazák, K., Deme, R., Mucsi, Z., Mándity, I. M., Noszál, B., Kállai-szabó, N., and Antal, I. (2019) Physicochemical Profiling of Baicalin Along with the Development and Characterization of Cyclodextrin Inclusion Complexes. AAPS PharmSciTech 20: 314

4. Jacob, S. and Nair, A. B. (2018) Cyclodextrin complexes: Perspective from drug delivery and formulation. Drug Dev. Res. 79: 201–217

5. Cid, A. G., Simonazzi, A., Palma, S. D., and Bermudez, J. M. (2019) Solid dispersion technology as a strategy to improve the bioavailability of poorly soluble drugs. Ther. Deliv. 10: 363–382

6. Olusanya, T. O. B., Haj Ahmad, R. R., Ibegbu, D. M., Smith, J. R., and Elkordy, A. A. (2018) Liposomal Drug Delivery Systems and Anticancer Drugs. Molecules 23: 907

7. Kalepu, S., Manthina, M., and Padavala, V. (2013) Oral lipid-based drug delivery systems – an overview. Acta Pharm. Sin. B 3: 361–372

8. Rani, S., Rana, R., Saraogi, G. K., Kumar, V., and Gupta, U. (2019) Self-Emulsifying Oral Lipid Drug Delivery Systems: Advances and Challenges. AAPS PharmSciTech 20: 129

9. Chen, H., Gao, Y., Wu, J., Chen, Y., Chen, B., Hu, J., and Zhou, J. (2014) Exploring therapeutic potentials of baicalin and its aglycone baicalein for hematological malignancies. Cancer Lett. 354: 5–11

10. Zhao, Q. and Cathie, X. C. (2016) Scutellaria baicalensis , the golden herb from the garden of Chinese medicinal plants. Sci. Bull. 34, 1391-1398

11. European Pharmacopoeia 9.0. Scutellariae baicalensis radix 2438 (04/2011) Council of Europe, Strasbourg, 2019: 1262–1263

12. Li-weber, M. (2009) New therapeutic aspects of flavones : The anticancer properties of Scutellaria and its main active constituents Wogonin , Baicalein and Baicalin. Cancer Treat. Rev. 35: 57–68

13. Moore, O. A., Gao, Y., Chen, A. Y., Brittain, R., and Chen, Y. C. (2016) The Extraction, Anticancer Effect, Bioavailability, and Nanotechnology of Baicalin. J. Nutr. Med. diet care 2: 11

14. Olagaray, K. E., Brouk, M. J., Mamedova, L. K., Sivinski, S. E., Liu, H., Robert, F., Dupuis, E., Zachut, M., and Bradford, B. J. (2019) Dietary supplementation of Scutellaria baicalensis extract during early lactation decreases milk somatic cells and increases whole lactation milk yield in dairy cattle. PLoS One 14: e0210744

15. Avdeef, A. and Testa, B. (2002) Physicochemical profiling in drug research: a brief survey of the state-of-the-art of experimental techniques. Cell. Mol. Life Sci. 59: 1681–1689

16. Pinak, P. Preformulation Studies: An Integral Part of Formulation Design. In: Pharmaceutical Formulation Design - Recent Practices (Ahmad, U. and Akhtar, J., eds) IntechOpen, London, 2019, 1-19

17. Mazak, K. and Noszal, B. (2016) Advances in microspeciation of drugs and biomolecules: Species-specific concentrations, acid-base properties and related parameters. J. Pharm. Biomed. Anal. 130: 390–403

18. Takacs-Novak, K., Szoke, V., Volgyi, G., Horvath, P., Ambrus, R., and Szabo-Revesz, P. (2013) Biorelevant solubility of poorly soluble drugs: rivaroxaban, furosemide, papaverine and niflumic acid. J. Pharm. Biomed. Anal. 83: 279–285

19. Liang, R. A. N., Rui-Min, H. A. N., Li-Min, F. U., Xi-Cheng, A. I., Zhang, J. P., and Skibsted, L. H. (2009) Baicalin in radical scavenging and its synergistic effect with β-carotene in antilipoxidation. J. Agric. Food Chem. 57: 7118–7124

20. Mirzahosseini, A., Palla, T., Orgovan, G., Toth, G., and Noszal, B. (2018) Dopamine: Acid-base properties and membrane penetration capacity. J. Pharm. Biomed. Anal. 158: 346–350

21. Sun, H., Chow, E. C., Liu, S., Du, Y., and Pang, K. S. (2008) The Caco-2 cell monolayer: usefulness and limitations. Expert Opin. Drug Metab. Toxicol. 4: 395–411

22. Cai, Y., Li, S., Li, T., Zhou, R., Wai, A. T.-S., and Yan, R. (2016) Oral pharmacokinetics of baicalin, wogonoside, oroxylin A 7-O-beta-d-glucuronide and their aglycones from an aqueous extract of Scutellariae Radix in the rat. J. Chromatogr. B, Anal. Technol. Biomed. life Sci. 1026: 124–133

23. Wang, H., Ma, X., Cheng, Q., Wang, L., and Zhang, L. (2018) Deep Eutectic Solvent-Based Ultrahigh Pressure Extraction of Baicalin from Scutellaria baicalensis Georgi. Molecules 23: 3233

24. Wang, H., Yao, G., and Zhang, H. (2019) Measurement and Correlation of the Solubility of Baicalin in Several Mixed Solvents. J. Chem. Eng. Data 64: 1281–1287

25. Wu, H., Long, X., Yuan, F., Chen, L., Pan, S., Liu, Y., Stowell, Y., and Li, X. (2014) Combined use of phospholipid complexes and self-emulsifying microemulsions for improving the oral absorption of a BCS class IV compound, baicalin. Acta Pharm. Sin. B 4: 217–226

26. Li, B., Wen, M., Li, W., He, M., Yang, X., and Li, S. (2011) Preparation and characterization of baicalin-poly -vinylpyrrolidone coprecipitate. Int. J. Pharm. 408: 91–96

27. Klein, S. (2010) The use of biorelevant dissolution media to forecast the in vivo performance of a drug. AAPS J. 12: 397–406

28. Galia, E., Nicolaides, E., Horter, D., Lobenberg, R., Reppas, C., and Dressman, J. B. (1998) Evaluation of various dissolution media for predicting in vivo performance of class I and II drugs. Pharm. Res. 15: 698–705

29. Yamaguchi Ikeuchi, S., Kambayashi, A., Kojima, H., Oku, N., and Asai, T. (2018) Prediction of the Oral Pharmacokinetics and Food Effects of Gabapentin Enacarbil Extended-Release Tablets Using Biorelevant Dissolution Tests. Biol. Pharm. Bull. 41: 1708–1715

30. Feng, Z., Zhou, J., Shang, X., Kuang, G., Han, J., Lu, L., and Zhang, L. (2017) Comparative research on stability of baicalin and baicalein administrated in monomer and total flavonoid fraction form of Radix scutellariae in biological fluids in vitro. Pharm. Biol. 55: 1177–1184

31. Taiming, L. and Xuehua, J. (2006) Investigation of the absorption mechanisms of baicalin and baicalein in rats. J. Pharm. Sci. 95: 1326–1333

32. Noh, K., Kang, Y., Nepal, M. R., Jeong, K. S., Oh, D. G., Kang, M. J., Lee, S., Kang, W., Jeong, H. G., and Jeong, T. C. (2016) Role of Intestinal Microbiota in Baicalin-Induced Drug Interaction and Its Pharmacokinetics. Molecules 21: 337

33. Kalapos-Kovacs, B., Magda, B., Jani, M., Fekete, Z., Szabo, P. T., Antal, I., Krajcsi, P., and Klebovich, I. (2015) Multiple ABC Transporters Efflux Baicalin. Phytother. Res. 29: 1987–1990

34. Li, M., Shi, A., Pang, H., Xue, W., Li, Y., Cao, G., Yan, B., Dong, F., Li, K., Xiao, W., He, G., Du, G., and Hu, X. (2014) Safety, tolerability, and pharmacokinetics of a single ascending dose of baicalein chewable tablets in healthy subjects. J. Ethnopharmacol. 156: 210–215

35. Kalapos-Kovacs, B., Juhasz, V., Temesszentandrasi-Ambrus, C., Magda, B., Szabo, P. T., Antal, I., Klebovich, I., and Krajcsi, P. (2018) Baicalin is a substrate of OATP2B1 and OATP1B3. Phytother. Res. 32: 1647–1650

36. Tang, Y., Zhu, H., Zhang, Y., and Huang, C. (2006) Determination of human plasma protein binding of baicalin by ultrafiltration and high-performance liquid chromatography. Biomed. Chromatogr. 20: 1116–1119

37. Wei, Y., Pi, C., Yang, G., Xiong, X., Lan, Y., Yang, H., Zhou, Y., Ye, Y., Zou, Y., Zheng, W., and Zhao, L. (2016) LC-UV Determination of Baicalin in Rabbit Plasma and Tissues for Application in Pharmacokinetics and Tissue Distribution Studies of Baicalin after Intravenous Administration of Liposomal and Injectable Formulations. Molecules 21: 444

38. Fong, S. Y. K., Li, C., Ho, Y. C., Li, R., Wang, Q., Wong, Y. C., Xue, H., and Zuo, Z. (2017) Brain Uptake of Bioactive Flavones in Scutellariae Radix and Its Relationship to Anxiolytic Effect in Mice. Mol. Pharm. 14: 2908–2916

39. Zhang, J., Cai, W., Zhou, Y., Liu, Y., Wu, X., Li, Y., Lu, J., and Qiao, Y. (2015) Profiling and identification of the metabolites of baicalin and study on their tissue distribution in rats by ultra-high-performance liquid chromatography with linear ion trap-Orbitrap mass spectrometer. J. Chromatogr. B, Anal. Technol. Biomed. life Sci. 85: 91–102

40. Xing, J., Chen, X., and Zhong, D. (2005) Absorption and enterohepatic circulation of baicalin in rats. Life Sci. 78: 140–146

41. Lai, M.-Y., Hsiu, S.-L., Chen, C.-C., Hou, Y.-C., and Chao, P.-D. L. (2003) Urinary pharmacokinetics of baicalein, wogonin and their glycosides after oral administration of Scutellariae Radix in humans. Biol. Pharm. Bull. 26: 79–83

42. Hang, Y., Qin, X., Ren, T., and Cao, J. (2018) Baicalin reduces blood lipids and inflammation in patients with coronary artery disease and rheumatoid arthritis: a randomized, double-blind, placebo-controlled trial. Lipids Health Dis. 17: 146

43. Zhou, Y.-J., Wang, H., Sui, H.-H., Li, L., Zhou, C.-L., and Huang, J.-J. (2016) Inhibitory effect of baicalin on allergic response in ovalbumin-induced allergic rhinitis guinea pigs and lipopolysaccharide-stimulated human mast cells. Inflamm. Res. 65: 603–612

44. Liu, L., Dong, Y., Shan, X., Li, L., Xia, B., and Wang, H. (2019) Anti-Depressive Effectiveness of Baicalin In Vitro and In Vivo. Molecules 24: 326

45. Peng, L.-Y., Yuan, M., Wu, Z.-M., Song, K., Zhang, C.-L., An, Q., Xia, F., Yu, J.-L., Yi, P.-F., Fu, B.-D., and Shen, H.-Q. (2019) Anti-bacterial activity of baicalin against APEC through inhibition of quorum sensing and inflammatory responses. Sci. Rep. 9: 4063

46. Peng-Fei, L., Fu-Gen, H., Bin-Bin, D., Tian-Sheng, D., Xiang-Lin, H., and Ming-Qin, Z. (2013) Purification and antioxidant activities of baicalin isolated from the root of huangqin (Scutellaria baicalensis gcorsi). J. Food Sci. Technol. 50: 615–619

47. Wu, J., Li, H., and Li, M. (2015) Effects of baicalin cream in two mouse models: 2,4-dinitrofluorobenzene-induced contact hypersensitivity and mouse tail test for psoriasis. Int. J. Clin. Exp. Med. 8: 2128–2137

48. Ding, L., Jia, C., Zhang, Y., Wang, W., Zhu, W., and Chen, Y. (2019) Biomedicine & Pharmacotherapy Baicalin relaxes vascular smooth muscle and lowers blood pressure in spontaneously hypertensive rats. Biomed. Pharmacother. 111: 325–330

49. Xi, Y., Wu, M., Li, H., Dong, S., Luo, E., Gu, M., Shen, X., Jiang, Y., Liu, Y., and Liu, H. (2015) Baicalin Attenuates High Fat Diet-Induced Obesity and Liver Dysfunction: Dose-Response and Potential Role of CaMKKbeta/AMPK/ACC Pathway. Cell. Physiol. Biochem. 35: 2349–2359

50. Guo, C., Chen, X., and Xiong, P. (2014) Baicalin suppresses iron accumulation after substantia nigra injury: relationship between iron concentration and transferrin expression. Neural Regen. Res. 9: 630–636

51. Wang, G., Liang, J., Gao, L., Si, Z., Zhang, X., Liang, G., Yan, Y., Li, K., Cheng, X., Bao, Y., Chuai, M., Chen, L., Lu, D., and Yang, X. (2018) Baicalin administration attenuates hyperglycemia-induced malformation of cardiovascular system. Cell Death Dis. 9: 234

52. Gao, Y., Liu, H., Wang, H., Hu, H., He, H., Gu, N., Han, X., Guo, Q., Liu, D., Cui, S., Shao, H., Jin, C., and Wu, Q. (2018) Baicalin inhibits breast cancer development via inhibiting IkB kinase activation in vitro and in vivo. Int. J. Oncol. 53: 2727–2736

53. Guo, Z., Hu, X., Xing, Z., Xing, R., Lv, R., Cheng, X., Su, J., Zhou, Z., Xu, Z., Nilsson, S., and Liu, Z. (2015) Baicalein inhibits prostate cancer cell growth and metastasis via the caveolin-1/AKT/mTOR pathway. Mol. Cell. Biochem. 406: 111–119

54. Dou, J., Wang, Z., Ma, L., Peng, B., Mao, K., Li, C., Su, M., Zhou, C., and Peng, G. (2018) Baicalein and baicalin inhibit colon cancer using two distinct fashions of apoptosis and senescence. Oncotarget 9: 20089–20102

55. Shu, Y.-J., Bao, R.-F., Wu, X.-S., Weng, H., Ding, Q., Cao, Y., Li, M.-L., Mu, J.-S., Wu, W.-G., Ding, Q.-C., Liu, T.-Y., Jiang, L., Hu, Y.-P., Tan, Z.-J., Wang, P., and Liu, Y.-B. (2014) Baicalin induces apoptosis of gallbladder carcinoma cells in vitro via a mitochondrial-mediated pathway and suppresses tumor growth in vivo. Anticancer. Agents Med. Chem. 14: 1136–1145

56. Yu, Y., Pei, M., and Li, L. (2015) Baicalin induces apoptosis in hepatic cancer cells in vitro and suppresses tumor growth in vivo. Int. J. Clin. Exp. Med. 8, 8958–8967

57. Diao, X., Yang, D., Chen, Y., and Liu, W. (2019) Baicalin suppresses lung cancer growth by targeting PDZ-binding kinase/T-LAK cell-originated protein kinase. Biosci. Rep. 39: BSR20181692

58. Luo, R., Wang, J., Zhao, L., Lu, N., You, Q., Guo, Q., and Li, Z. (2014) Synthesis and biological evaluation of baicalein derivatives as potent antitumor agents. Bioorg. Med. Chem. Lett. 24: 1334–1338

59. Liu, R., Li, X., Wei, J., Liu, S., Chang, Y., Zhang, J., Zhang, J., Zhang, X., Fuhr, U., Taubert, M., and Tian, X. (2019) A Single Dose of Baicalin Has No Clinically Significant Effect on the Pharmacokinetics of Cyclosporine A in Healthy Chinese Volunteers. Front. Pharmacol. 10: 518

60. Fan, L., Zhang, W., Guo, D., Tan, Z.-R., Xu, P., Li, Q., Liu, Y.-Z., Zhang, L., He, T.-Y., Hu, D.-L., Wang, D., and Zhou, H.-H. (2008) The effect of herbal medicine baicalin on pharmacokinetics of rosuvastatin, substrate of organic anion-transporting polypeptide 1B1. Clin. Pharmacol. Ther. 83: 471–476

61. Kalliokoski, A. and Niemi, M. (2009) Impact of OATP transporters on pharmacokinetics. Br. J. Pharmacol. 158: 693–705

62. Noh, K., Nepal, M. R., Jeong, K. S., Kim, S.-A., Um, Y. J., Seo, C. S., Kang, M. J., Park, P.-H., Kang, W., Jeong, H. G., and Jeong, T. C. (2015) Effects of baicalin on oral pharmacokinetics of caffeine in rats. Biomol. Ther. (Seoul). 23: 201–206

63. Gao, N., Zou, D., and Qiao, H.-L. (2013) Concentration-dependent inhibitory effect of Baicalin on the plasma protein binding and metabolism of chlorzoxazone, a CYP2E1 probe substrate, in rats in vitro and in vivo. PLoS One 8: e53038

64. Tian, X., Cheng, Z.-Y., He, J., Jia, L.-J., and Qiao, H.-L. (2013) Concentration-dependent inhibitory effects of baicalin on the metabolism of dextromethorphan, a dual probe of CYP2D and CYP3A, in rats. Chem. Biol. Interact. 203: 522–529

65. Tian, X., Cheng, Z.-Y., Jin, H., Gao, J., and Qiao, H.-L. (2013) Inhibitory Effects of Baicalin on the Expression and Activity of CYP3A Induce the Pharmacokinetic Changes of Midazolam in Rats. Evid. Based. Complement. Alternat. Med. 2013: 179643

66. Cheng, Z.-Y., Tian, X., Gao, J., Li, H.-M., Jia, L.-J., and Qiao, H.-L. (2014) Contribution of baicalin on the plasma protein binding displacement and CYP3A activity inhibition to the pharmacokinetic changes of nifedipine in rats in vivo and in vitro. PLoS One 9: e87234

67. Gao, N., Qi, B., Liu, F., Fang, Y., Zhou, J., Jia, L., and Qiao, H. (2014) Inhibition of baicalin on metabolism of phenacetin, a probe of CYP1A2, in human liver microsomes and in rats. PLoS One 9: e89752

68. Wang, X., He, L.-L., Liu, B., Wang, X., Xu, L., Wang, X.-F., and Sun, T. (2018) Decrease of the affinity of theophylline bind to serum proteins induced by flavonoids and their synergies on protein conformation. Int. J. Biol. Macromol. 107: 1066–1073

69. Gao, N., Fang, Y., Qi, B., Jia, L., Jin, H., and Qiao, H. (2013) Pharmacokinetic changes of unbound theophylline are due to plasma protein binding displacement and CYP1A2 activity inhibition by baicalin in rats. J. Ethnopharmacol. 150: 477–484

70. Wei, Y., Guo, J., Zheng, X., Wu, J., Zhou, Y., Yu, Y., Ye, Y., Zhang, L., and Zhao, L. (2014) Preparation, pharmacokinetics and biodistribution of baicalin-loaded liposomes. Int. J. Nanomedicine 9: 3623–3630

71. Xie, J., Luo, Y., Liu, Y., Ma, Y., Yue, P., and Yang, M. (2019) Novel redispersible nanosuspensions stabilized by co-processed nanocrystalline cellulose-sodium carboxymethyl starch for enhancing dissolution and oral bioavailability of baicalin. Int. J. Nanomedicine 14: 353–369

72. Zhang, S., Wang, J., and Pan, J. (2016) Baicalin-loaded PEGylated lipid nanoparticles: characterization, pharmacokinetics, and protective effects on acute myocardial ischemia in rats. Drug Deliv. 23: 3696–3703

73. Zhao, L., Wei, Y., Huang, Y., He, B., Zhou, Y., and Fu, J. (2013) Nanoemulsion improves the oral bioavailability of baicalin in rats: in vitro and in vivo evaluation. Int. J. Nanomedicine 8: 3769–3779

74. Jakab, G., Fülöp, V., Bozó, T., Balogh, E., Kellermayer, M., and Antal, I. (2018) Optimization of Quality Attributes and Atomic Force Microscopy Imaging of Reconstituted Nanodroplets in Baicalin Loaded Self-Nanoemulsifying Formulations. Pharmaceutics 10: 275

75. Li, B., He, M., Li, W., Luo, Z., Guo, Y., Li, Y., Zang, C., Wang, B., Li, F., Li, S., and Ji, P. (2013) Dissolution and pharmacokinetics of baicalin-polyvinylpyrrolidone coprecipitate. J. Pharm. Pharmacol. 65: 1670–1678

76. Cui, L., Sune, E., Song, J., Wang, J., Jia, X., and Zhang, Z. (2016) Characterization and Bioavailability Study of Baicalin-mesoporous Carbon Nanopowder Solid Dispersion. Pharmacogn. Mag. 12: 326–332

77. Zhang, H., Yang, X., Zhao, L., Jiao, Y., Liu, J., and Zhai, G. (2016) In vitro and in vivo study of Baicalin-loaded mixed micelles for oral delivery. Drug Deliv. 23: 1933–1939

78. Haider, M., Hassan, M. A., Ahmed, I. S., and Shamma, R. (2018) Thermogelling Platform for Baicalin Delivery for Versatile Biomedical Applications. Mol. Pharm. 15: 3478–3488

79. Pouton, C. W. (2000) Lipid formulations for oral administration of drugs: Non-emulsifying, self-emulsifying and "self-microemulsifying" drug delivery systems. Eur. J. Pharm. Sci. 11: 93–98

80. Porter, C. J. H., Pouton, C. W., Cuine, J. F., and Charman, W. N. (2008) Enhancing intestinal drug solubilisation using lipid-based delivery systems. Adv. Drug Deliv. Rev. 60: 673–691

81. Vonderscher, J. and Meinzer, A. (1994) Rationale for the development of Sandimmune Neoral. Transplant. Proc. 26: 2925–2927

82. Pouton, C. W. (2006) Formulation of poorly water-soluble drugs for oral administration: Physicochemical and physiological issues and the lipid formulation classification system. Eur. J. Pharm. Sci. 29: 278–287

83. Valicherla, G. R., Dave, K. M., Syed, A. A., Riyazuddin, M., Gupta, A. P., Singh, A., Wahajuddin, Mitra, K., Datta, D., and Gayen, J. R. (2016) Formulation optimization of Docetaxel loaded self-emulsifying drug delivery system to enhance bioavailability and anti-tumor activity. Sci. Rep. 6: 26895

84. Anton, N. and Vandamme, T. F. (2011) Nano-emulsions and micro-emulsions: clarifications of the critical differences. Pharm. Res. 28: 978–985

85. Hashemnejad, S. M., Badruddoza, A. Z. M., Zarket, B., Ricardo Castaneda, C., and Doyle, P. S. (2019) Thermoresponsive nanoemulsion-based gel synthesized through a low-energy process. Nat. Commun. 10: 2749

86. McClements, D. J. and Rao, J. (2011) Food-grade nanoemulsions: formulation, fabrication, properties, performance, biological fate, and potential toxicity. Crit. Rev. Food Sci. Nutr. 51: 285–330

87. McClements, D. J. (2012) Nanoemulsions versus microemulsions: terminology, differences, and similarities. Soft Matter 8: 1719–1729

88. Anton, N. and Vandamme, T. F. (2009) The universality of low-energy nano-emulsification. Int. J. Pharm. 377: 142–147

89. Anton, N., Benoit, J.-P., and Saulnier, P. (2008) Design and production of nanoparticles formulated from nano-emulsion templates-a review. J. Control. Release 128: 185–199

90. Setya, S., Talegaonkar, S., and Razdan, B. K. (2014) Nanoemulsions:Formulation Methods and Stability Aspects. World J. Pharm. Pharm. Sci. 3: 2214–2228

91. Salem, M. and Ezzat, S. Nanoemulsions in food industry. In: Some New Aspects of Colloidal Systems in Foods (Milani, J. M., ed) IntechOpen, London, 2019, 314-366

92. Wooster, T. J., Golding, M., and Sanguansri, P. (2008) Impact of oil type on nanoemulsion formation and Ostwald ripening stability. Langmuir 24: 12758–12765

93. Acosta, E. J. and Bhakta, A. S. (2009) The HLD-NAC Model for Mixtures of Ionic and Nonionic Surfactants. J. Surfactants Deterg. 12: 7–19

94. Rahman, M. A., Hussain, A., Hussain, M. S., Mirza, M. A., and Iqbal, Z. (2013) Role of excipients in successful development of self-emulsifying/microemulsifying drug delivery system (SEDDS/SMEDDS). Drug Dev. Ind. Pharm. 39: 1–19

95. Yáñez, J. A., Wang, S. W. J., Knemeyer, I. W., Wirth, M. A., and Alton, K. B. (2011) Intestinal lymphatic transport for drug delivery. Adv. Drug Deliv. Rev. 63: 923–942

96. Grove, M., Mullertz, A., Nielsen, J. L., and Pedersen, G. P. (2006) Bioavailability of seocalcitol II: development and characterisation of self-microemulsifying drug delivery systems (SMEDDS) for oral administration containing medium and long chain triglycerides. Eur. J. Pharm. Sci. 28: 233–242

97. Porter, C. J. H., Kaukonen, A. M., Boyd, B. J., Edwards, G. A., and Charman, W. N. (2004) Susceptibility to lipase-mediated digestion reduces the oral bioavailability of danazol after administration as a medium-chain lipid-based microemulsion formulation. Pharm. Res. 21: 1405–1412

98. Williams, H. D., Sassene, P., Kleberg, K., Bakala-N'Goma, J.-C., Calderone, M., Jannin, V., Igonin, A., Partheil, A., Marchaud, D., Jule, E., Vertommen, J., Maio, M., Blundell, R., Benameur, H., Carriere, F., Mullertz, A., Porter, C. J. H., and Pouton, C. W. (2012) Toward the establishment of standardized in vitro tests for lipid-based formulations, part 1: method parameterization and comparison of in vitro digestion profiles across a range of representative formulations. J. Pharm. Sci. 101: 3360–3380

99. O'Rear, E. A. (2015) Review of An Introduction to Surfactants. J. Chem. Educ. 92: 1779–1780

100. Strickley, R. G. (2004) Solubilizing excipients in oral and injectable formulations. Pharm. Res. 21: 201–230

101. Kim, H. J., Yoon, K. A., Hahn, M., Park, E. S., and Chi, S. C. (2000) Preparation and in vitro evaluation of self-microemulsifying drug delivery systems containing idebenone. Drug Dev. Ind. Pharm. 26: 523–529

102. Mahapatra, A. K., Murthy, P. N., Swadeep, B., and Prasad, R. (2014) Self-Emulsifying Drug Delivery Systems (SEDDS): An Update from Formulation Development to Therapeutic Strategies. Int. J. PharmTech Res. 6: 546–568

103. Niczinger, N. A., Kallai-Szabo, N., Dredan, J., Budai, L., and Antal, M. H. and I. (2015) Application of Droplet Size Analysis for the Determination of the Required HLB of Lemon Oil in O/W Emulsion. Curr. Pharm. Anal. 11: 11–15

104. Na, G. C., Yuan, B. O., Stevens Jr., H. J., Weekley, B. S., and Rajagopalan, N. (1999) Cloud point of nonionic surfactants: modulation with pharmaceutical excipients. Pharm Res 16: 562–568

105. Christiansen, A., Backensfeld, T., Denner, K., and Weitschies, W. (2011) Effects of non-ionic surfactants on cytochrome P450-mediated metabolism in vitro. Eur. J. Pharm. Biopharm. 78: 166–172

106. Gurram, A. K., Deshpande, P. B., Kar, S. S., Nayak, U. Y., Udupa, N., and Reddy, M. S. (2015) Role of Components in the Formation of Self-microemulsifying Drug Delivery Systems. Indian J. Pharm. Sci. 77: 249–257

107. Cho, Y.-H., Kim, S., Bae, E. K., Mok, C. K., and Park, J. (2008) Formulation of a cosurfactant-free O/W microemulsion using nonionic surfactant mixtures. J. Food Sci. 73: E115-21

108. Flanagan, J., Kortegaard, K., Neil Pinder, D., Rades, T., and Singh, H. (2006) Solubilisation of soybean oil in microemulsions using various surfactants. Food Hydrocoll. 20: 253–260

109. Mandic, J., Zvonar Pobirk, A., Vrecer, F., and Gasperlin, M. (2017) Overview of solidification techniques for self-emulsifying drug delivery systems from industrial perspective. Int. J. Pharm. 533: 335–345

110. Dokania, S. and Joshi, A. K. (2015) Self-microemulsifying drug delivery system (SMEDDS) – challenges and road ahead. Drug Deliv. 22: 675–690

111. Krstić, M., Medarević, Đ., Đuriš, J., and Ibrić, S. (2018) Self-nanoemulsifying drug delivery systems (SNEDDS) and self-microemulsifying drug delivery systems (SMEDDS) as lipid nanocarriers for improving dissolution rate and bioavailability of poorly soluble drugs. Lipid Nanocarriers Drug Target. 19:473–508

112. Nikolakakis, I. and Partheniadis, I. (2017) Self-Emulsifying Granules and Pellets: Composition and Formation Mechanisms for Instant or Controlled Release. Pharmaceutics 9: 50

113. Sermkaew, N., Ketjinda, W., Boonme, P., Phadoongsombut, N., and Wiwattanapatapee, R. (2013) Liquid and solid self-microemulsifying drug delivery systems for improving the oral bioavailability of andrographolide from a crude extract of Andrographis paniculata. Eur. J. Pharm. Sci. 50: 459–466

114. Liu, M., Zhang, S., Cui, S., Chen, F., Jia, L., Wang, S., Gai, X., Li, P., Yang, F., Pan, W., and Yang, X. (2017) Preparation and evaluation of Vinpocetine self-emulsifying pH gradient release pellets. Drug Deliv. 24: 1598–1604

115. Shahba, A. A.-W., Ahmed, A. R., Alanazi, F. K., Mohsin, K., and Abdel-Rahman, S. I. (2018) Multi-Layer Self-Nanoemulsifying Pellets: an Innovative Drug Delivery System for the Poorly Water-Soluble Drug Cinnarizine. AAPS PharmSciTech 19: 2087–2102

116. Abdalla, A. and Mäder, K. (2007) Preparation and characterization of a self-emulsifying pellet formulation. Eur. J. Pharm. Biopharm. 66: 220–226

117. Matsaridou, I., Barmpalexis, P., Salis, A., and Nikolakakis, I. (2012) The Influence of Surfactant HLB and Oil/Surfactant Ratio on the Formation and Properties of Self-emulsifying Pellets and Microemulsion Reconstitution. AAPS PharmSciTech 13: 1319–1330

118. Miao, Y., Chen, G., Ren, L., and Pingkai, O. (2016) Characterization and evaluation of self-nanoemulsifying sustained-release pellet formulation of ziprasidone with enhanced bioavailability and no food effect. Drug Deliv. 23: 2163–2172

119. Weerapol, Y., Limmatvapirat, S., Jansakul, C., Takeuchi, H., and Sriamornsak, P. (2015) Enhanced dissolution and oral bioavailability of nifedipine by spontaneous emulsifying powders: effect of solid carriers and dietary state. Eur. J. Pharm. Biopharm. 91: 25–34

120. Krupa, A., Szlek, J., Jany, B. R., and Jachowicz, R. (2015) Preformulation studies on solid self-emulsifying systems in powder form containing magnesium aluminometasilicate as porous carrier. AAPS PharmSciTech 16: 623–635

121. Shazly, G. and Mohsin, K. (2015) Dissolution improvement of solid self-emulsifying drug delivery systems of fenofibrate using an inorganic high surface adsorption material. Acta Pharm. 65: 29–42

122. Beg, S., Jena, S. S., Patra, C. N., Rizwan, M., Swain, S., Sruti, J., Rao, M. E. B., and Singh, B. (2013) Development of solid self-nanoemulsifying granules (SSNEGs) of ondansetron hydrochloride with enhanced bioavailability potential. Colloids Surf. B. Biointerfaces 101: 414–423

123. Yeom, D. W., Son, H. Y., Kim, J. H., Kim, S. R., Lee, S. G., Song, S. H., Chae, B. R., and Choi, Y. W. (2016) Development of a solidified self-microemulsifying drug delivery system (S-SMEDDS) for atorvastatin calcium with improved dissolution and bioavailability. Int. J. Pharm. 506: 302–311

124. Weerapol, Y., Limmatvapirat, S., Nunthanid, J., and Sriamornsak, P. (2014) Self-nanoemulsifying drug delivery system of nifedipine: impact of hydrophilic-lipophilic balance and molecular structure of mixed surfactants. AAPS PharmSciTech 15: 456–464

125. Joyce, P., Dening, T. J., Meola, T. R., Schultz, H. B., Holm, R., Thomas, N., and Prestidge, C. A. (2019) Solidification to improve the biopharmaceutical performance of SEDDS: Opportunities and challenges. Adv. Drug Deliv. Rev. 142: 102–117

126. Gumaste, S. G., Dalrymple, D. M., and Serajuddin, A. T. M. (2013) Development of Solid SEDDS, V: Compaction and Drug Release Properties of Tablets Prepared by Adsorbing Lipid-Based Formulations onto Neusilin(R) US2. Pharm. Res. 30: 3186–3199

127. Baek, I., Ha, E.-S., Yoo, J.-W., Jung, Y., and Kim, M.-S. (2015) Design of a gelatin microparticle-containing self-microemulsifying formulation for enhanced oral bioavailability of dutasteride. Drug Des. Devel. Ther. 9: 3231–3238

128. Li, L., Yi, T., and Lam, C. W.-K. (2013) Effects of spray-drying and choice of solid carriers on concentrations of Labrasol(R) and Transcutol(R) in solid self-microemulsifying drug delivery systems (SMEDDS). Molecules 18: 545–560

129. Yi, T., Wan, J., Xu, H., and Yang, X. (2008) Controlled poorly soluble drug release from solid self-microemulsifying formulations with high viscosity hydroxypropylmethylcellulose. Eur. J. Pharm. Sci. 34: 274–280

130. Kim, M.-S., Ha, E.-S., Choo, G.-H., and Baek, I.-H. (2015) Preparation and in vivo evaluation of a dutasteride-loaded solid-supersaturatable self-microemulsifying drug delivery system. Int. J. Mol. Sci. 16: 10821–10833

131. Conceicao, J., Adeoye, O., Cabral-Marques, H. M., and Sousa Lobo, J. M. (2018) Hydroxypropyl-beta-Cyclodextrin and beta-Cyclodextrin as Tablet Fillers for Direct Compression. AAPS PharmSciTech 19: 2710–2718

132. Crini, G. (2014) Review: A History of Cyclodextrins. Chem. Rev. 114: 10940–10975

133. Astray, G., Gonzalez-Barreiro, C., Mejuto, J. C., Rial-Otero, R., and Simal-Gándara, J. (2009) A review on the use of cyclodextrins in foods. Food Hydrocoll. 23: 1631–1640

134. Zhang, X., Liu, J., Hou, W., Tong, J., Ren, L., Sun, G., and Sun, Y. (2016) Preparation and Properties of Pesticide/Cyclodextrin Complex Intercalated into ZnAl-Layered Double Hydroxide. Ind. Eng. Chem. Res. 55: 1550–1558

135. Schardinger, F. (1903) Über thermophile Bakterien aus verschiedenen Speisen und Milch. Zeitschrift für Untersuchung der Nahrungs- und Genußmittel, sowie der Gebrauchsgegenstände 6: 865–880

136. Cramer, F. and Henglein, F. M. (1956) Einschlußverbindungen der Cyclodextrine mit Gasen. Angew. Chemie 68: 649

137. Jansook, P., Ogawa, N., and Loftsson, T. (2018) Cyclodextrins: structure, physicochemical properties and pharmaceutical applications. Int. J. Pharm. 535: 272–284

138. Varadi, J., Hermenean, A., Gesztelyi, R., Jeney, V., Balogh, E., Majoros, L., Malanga, M., Fenyvesi, E., Szente, L., Bacskay, I., Vecsernyes, M., Feher, P., Ujhelyi, Z., Vasvari, G., Arvai, I., Rusznyak, A., Balta, C., Herman, H., and Fenyvesi, F. (2019) Pharmacokinetic Properties of Fluorescently Labelled Hydroxypropyl-Beta-Cyclodextrin. Biomolecules 9: 509

139. di Cagno, M. P. (2016) The Potential of Cyclodextrins as Novel Active Pharmaceutical Ingredients: A Short Overview. Molecules 22: 1

140. Szente and Szejtli. (1999) Highly soluble cyclodextrin derivatives: chemistry, properties, and trends in development. Adv. Drug Deliv. Rev. 36: 17–28

141. Szejtli, J. (1998) Introduction and General Overview of Cyclodextrin Chemistry. Chem. Rev. 98: 1743–1754

142. Rezanka, M. Synthesis of Cyclodextrin Derivatives. In: Cyclodextrin Fundamentals, Reactivity and Analysis (Fourmentin, S., Crini, G., and Lichtfouse, E., eds) Springer International Publishing, Cham, 2018, 57–103

143. European Medicines Agency and Commitee for Human Medicinal Products. Cyclodextrins used as excipients. In: Questions and answers on cyclodextrins used as excipients in medicinal products for human use (EMA/CHMP/333892/2013, ed) London, 2017, 1–16,

144. Saokham, P., Muankaew, C., Jansook, P., and Loftsson, T. (2018) Solubility of Cyclodextrins and Drug/Cyclodextrin Complexes. Molecules 23: 1161

145. Loftsson, T. Formulation of Drug-Cyclodextrin Complexes. In: Percutaneous Penetration Enhancers Chemical Methods in Penetration Enhancement: Drug Manipulation Strategies and Vehicle Effects (Dragicevic, N. and Maibach, H. I., eds) Springer International Publishing, Berlin, 2015, 189–205

146. Gidwani, B. and Vyas, A. (2015) A Comprehensive Review on Cyclodextrin-Based Carriers for Delivery of Chemotherapeutic Cytotoxic Anticancer Drugs. Biomed Res. Int. 2015: 198268

147. Irie, T. and Uekama, K. (1997) Pharmaceutical applications of cyclodextrins. III. Toxicological issues and safety evaluation. J. Pharm. Sci. 86: 147–162

148. Stella, V. J. and He, Q. (2008) Cyclodextrins. Toxicol. Pathol. 36: 30–42

149. Donaubauer, H. H., Fuchs, H., Langer, K. H., and Bar, A. (1998) Subchronic intravenous toxicity studies with gamma-cyclodextrin in rats. Regul. Toxicol. Pharmacol. 27: 189–198

150. Gould, S. and Scott, R. C. (2005) 2-Hydroxypropyl-beta-cyclodextrin (HP-beta-CD): a toxicology review. Food Chem. Toxicol. 43: 1451–1459

151. Loftsson, T. and Brewster, M. E. (2010) Pharmaceutical applications of cyclodextrins: basic science and product development. J. Pharm. Pharmacol. 62: 1607–1621

152. Jug, M. and Mura, P. A. (2018) Grinding as Solvent-Free Green Chemistry Approach for Cyclodextrin Inclusion Complex Preparation in the Solid State. Pharmaceutics 10: 189

153. Loftsson, T., Moya-Ortega, M. D., Alvarez-Lorenzo, C., and Concheiro, A. (2016) Pharmacokinetics of cyclodextrins and drugs after oral and parenteral administration of drug/cyclodextrin complexes. J. Pharm. Pharmacol. 68: 544–555

154. Maestrelli, F., Cirri, M., Mennini, N., Zerrouk, N., and Mura, P. (2011) Improvement of oxaprozin solubility and permeability by the combined use of cyclodextrin, chitosan, and bile components. Eur. J. Pharm. Biopharm. 78: 385–393

155. Jablan, J., Szalontai, G., and Jug, M. (2012) Comparative analysis of zaleplon complexation with cyclodextrins and hydrophilic polymers in solution and in solid state. J. Pharm. Biomed. Anal. 71: 35–44

156. Bragagni, M., Maestrelli, F., and Mura, P. (2010) Physical chemical characterization of binary systems of prilocaine hydrochloride with triacetyl-β-cyclodextrin. J. Incl. Phenom. Macrocycl. Chem. 68: 437–445

157. Jug, M., Becirevic-Lacan, M., and Bengez, S. (2009) Novel cyclodextrin-based film formulation intended for buccal delivery of atenolol. Drug Dev. Ind. Pharm. 35: 796–807

158. Promzeleva, M., Volkova, T., Proshin, A., Siluykov, O., Mazur, A., Tolstoy, P., Ivanov, S., Kamilov, F., and Terekhova, I. (2018) Improved Biopharmaceutical Properties of Oral Formulations of 1,2,4-Thiadiazole Derivative with Cyclodextrins: in Vitro and in Vivo Evaluation. ACS Biomater. Sci. Eng. 4: 491–501

159. Yano, H. and Kleinebudde, P. (2010) Improvement of dissolution behavior for poorly water-soluble drug by application of cyclodextrin in extrusion process: comparison between melt extrusion and wet extrusion. AAPS PharmSciTech 11: 885–893

160. Thiry, J., Krier, F., Ratwatte, S., Thomassin, J.-M., Jerome, C., and Evrard, B. (2017) Hot-melt extrusion as a continuous manufacturing process to form ternary cyclodextrin inclusion complexes. Eur. J. Pharm. Sci. 96: 590–597

161. Medarevic, D., Kachrimanis, K., Djuric, Z., and Ibric, S. (2015) Influence of hydrophilic polymers on the complexation of carbamazepine with hydroxypropyl-beta-cyclodextrin. Eur. J. Pharm. Sci. 78: 273–285

162. He, D., Deng, P., Yang, L., Tan, Q., Liu, J., Yang, M., and Zhang, J. (2013) Molecular encapsulation of rifampicin as an inclusion complex of hydroxypropyl-beta-cyclodextrin: design; characterization and in vitro dissolution. Colloids Surf. B. Biointerfaces 103: 580–585

163. Li, S., Zhai, Y., Yan, J., Wang, L., Xu, K., and Li, H. (2016) Effect of preparation processes and structural insight into the supermolecular system: Bisacodyl and beta-cyclodextrin inclusion complex. Mater. Sci. Eng. C. Mater. Biol. Appl. 58: 224–232

164. Baka, E., Comer, J. E. A., and Tak, K. (2008) Study of equilibrium solubility measurement by saturation shake-flask method using hydrochlorothiazide as model compound. 46: 335–341

165. Orgovan, G. and Noszal, B. (2011) Electrodeless, accurate pH determination in highly basic media using a new set of (1)H NMR pH indicators. J. Pharm. Biomed. Anal. 54: 958–964

166. Mazak, K., Hosztafi, S., Kraszni, M., and Noszal, B. (2017) Physico-chemical profiling of semisynthetic opioids. J. Pharm. Biomed. Anal. 135: 97–105

167. Higuchi, T., Connors, K. A. (1965) Phase solubility studies. Adv. Anal. Chem. Instrum. 4: 117–212

168. Becke, A. D. (1993) Density-functional thermochemistry. III. The role of exact exchange. J. Chem. Phys. 98: 5648–5652

169. Date, A. A. and Nagarsenker, M. S. (2007) Design and evaluation of self-nanoemulsifying drug delivery systems (SNEDDS) for cefpodoxime proxetil. Int. J. Pharm. 329: 166–172

170. Zhou, Z., Dunn, C., Khadra, I., Wilson, C. G., and Halbert, G. W. (2017) Infl uence of Physiological Gastrointestinal Surfactant Ratio on the Equilibrium Solubility of BCS Class II Drugs Investigated Using a Four Component Mixture Design. Mol Pharm. 14: 4132-4144

171. Zhou, Y., Yang, Z.-Y., and Tang, R.-C. (2016) Bioactive and UV protective silk materials containing baicalin - The multifunctional plant extract from Scutellaria baicalensis Georgi. Mater. Sci. Eng. C. Mater. Biol. Appl. 67: 336–344

172. Mazak, K., Doczy, V., Kokosi, J., and Noszal, B. (2009) Proton speciation and microspeciation of serotonin and 5-hydroxytryptophan. Chem. Biodivers. 6: 578–590

173. Szakacs, Z., Beni, S., and Noszal, B. (2008) Resolution of carboxylate protonation microequilibria of NTA, EDTA and related complexones. Talanta 74: 666–674

174. Kiss, T., Sovago, I., and Martin, R. B. (1989) Complexes of 3,4-dihydroxyphenyl derivatives. 9. Aluminum(3+) binding to catecholamines and tiron. J. Am. Chem. Soc. 111: 3611–3614

175. Mazak, K. and Noszal, B. (2014) Drug delivery: a process governed by species-specific lipophilicities. Eur. J. Pharm. Sci. 62: 96–104

176. Banga, S., Chawla, G., Varandani, D., Mehta, B. R., and Bansal, A. K. (2007) Modification of the crystal habit of celecoxib for improved processability. J. Pharm. Pharmacol. 59: 29–39

177. European Medicines Agency. (2000) ICH Guideline Q6A, Specifications: Test Procedures and Acceptance Criteria for New Drug Substances and New Drug Products: Chemical Substances.

178. Shelley, H., Grant, M., Smith, F. T., Abarca, E. M., and Jayachandra Babu, R. (2018) Improved Ocular Delivery of Nepafenac by Cyclodextrin Complexation. AAPS PharmSciTech 19: 2554–2563

179. Wu, S., Sun, A., and Liu, R. (2005) Separation and purification of baicalin and wogonoside from the Chinese medicinal plant Scutellaria baicalensis Georgi by high-speed counter-current chromatography. J. Chromatogr. A 1066: 243–247

180. Yuan, Y., Hou, W., Tang, M., Luo, H., Chen, L.-J., Guan, Y. H., and Sutherland, I. (2008) Separation of Flavonoids from the Leaves of Oroxylum indicum by HSCCC. Chromatographia, 68: 885-892

181. Przybylski, C., Bonnet, V., and Cézard, C. (2015) Probing the common alkali metal affinity of native and variously methylated b-cyclodextrins by combining electrospray-tandem mass spectrometry and molecular modeling. Phys. Chem. Chem. Phys. 17: 19288–19305

182. Solanki, N. (2012) Self Emulsifying Drug Delivery System (Sedds): a Review. Int. J. Pharm. Res. Bio-Science 1: 313–323

183. Neslihan Gursoy, R. and Benita, S. (2004) Self-emulsifying drug delivery systems (SEDDS) for improved oral delivery of lipophilic drugs. Biomed. Pharmacother. 58: 173–182

184. Villar, A. M. S., Naveros, B. C., Campmany, A. C. C., Trenchs, M. A., Rocabert, C. B., and Bellowa, L. H. (2012) Design and optimization of self-nanoemulsifying drug delivery systems (SNEDDS) for enhanced dissolution of gemfibrozil. Int. J. Pharm. 431: 161–175

185. Date, A. A. and Nagarsenker, M. S. (2008) Parenteral microemulsions: An overview. Int. J. Pharm. 355: 19–30

186. Warisnoicharoen, W., Lansley, A. B., and Lawrence, M. J. (2000) Nonionic oil-in-water microemulsions: the effect of oil type on phase behaviour. Int. J. Pharm. 198: 7–27

187. Saritha, D., Subhash, P., Bose, C., and Nagaraju, R. (2014) Formulation and Evaluation of Self Emulsifying Drug Delivery System (Sedds) of Ibuprofen. Int. J. Pharm. Sci. Res. 5: 3511–3519

188. Sood, S., Jain, K., and Gowthamarajan, K. (2014) Optimization of curcumin nanoemulsion for intranasal delivery using design of experiment and its toxicity assessment. Colloids Surfaces B Biointerfaces 113: 330–337

189. Mbah, C. C., Builders, P. F., and Attama, A. A. (2014) Nanovesicular carriers as alternative drug delivery systems: ethosomes in focus. Expert Opin. Drug Deliv. 11: 45–59

190. Tarr, B. D. and Yalkowsky, S. H. (1989) Enhanced intestinal absorption of cyclosporine in rats through the reduction of emulsion droplet size. Pharm. Res. 6: 40–43

191. De Azevedo Ribeiro, R. C., Barreto, S. M. A. G., Ostrosky, E. A., Da Rocha-Filho, P. A., Veríssimo, L. M., and Ferrari, M. (2015) Production and characterization of cosmetic nanoemulsions containing Opuntia ficus-indica (L.) Mill extract as moisturizing agent. Molecules 20: 2492–2509

192. Kassem, A. M., Ibrahim, H. M., and Samy, A. M. (2017) Development and optimisation of atorvastatin calcium loaded self-nanoemulsifying drug delivery system (SNEDDS) for enhancing oral bioavailability: in vitro and in vivo evaluation. J. Microencapsul. 34: 319–333

193. Krogars, K., Heinämäki, J., Vesalahti, J., Marvola, M., Antikainen, O., and Yliruusi, J. (2000) Extrusion–spheronization of pH-sensitive polymeric matrix pellets for possible colonic drug delivery. Int. J. Pharm. 199: 187–194

194. Dukić-Ott, A., Thommes, M., Remon, J. P., Kleinebudde, P., and Vervaet, C. (2009) Production of pellets via extrusion-spheronisation without the incorporation of microcrystalline cellulose: A critical review. Eur. J. Pharm. Biopharm. 71: 38–46

195. Kaushal, A. M., Chakraborti, A. K., and Bansal, A. K. (2008) FTIR studies on differential intermolecular association in crystalline and amorphous states of structurally related non-steroidal anti-inflammatory drugs. Mol. Pharm. 5: 937–945

196. Pachuau, L., Vanlalfakawma, D. C., Tripathi, S. K., and Lalhlenmawia, H. (2014) Muli bamboo (Melocanna baccifera) as a new source of microcrystalline cellulose. J. Appl. Pharm. Sci. 4: 87–94

197. Brdarić, T. P., Marković, Z. S., Milenković, D., and Dimitrić Markovic, J. M. (2012) A joint application of vibrational spectroscopic and quantum mechanical methods in quantitative analysis of baicalein structure. Monatshefte fur Chemie 143: 1369–1378

198. Li, Y., He, Z.-D., Zheng, Q.-E., Hu, C., and Lai, W.-F. (2018) Hydroxypropyl-beta-cyclodextrin for Delivery of Baicalin via Inclusion Complexation by Supercritical Fluid Encapsulation. Molecules 23: 1169

199. Li, J., Chen, Q., Zhang, S., Jiang, Q., Shang, J., Zhou, L., Li, Q., Li, S., Shi, S., Li, Y., and Li, W. (2019) Maltosyl-β-cyclodextrin mediated SupramolecularHost-Guest inclusion complex used for enhancing baicalin antioxidant activity and bioavailability. J. Drug Deliv. Sci. Technol. 54: 101346

10. Publications

10.1. Publications pertaining to the doctoral thesis

I. **Géza Jakab**, Dóra Bogdán, Károly Mazák, Ruth Deme, Zoltán Mucsi, István M. Mándity, Béla Noszál, Nikolett Kállai-Szabó, István Antal. Physicochemical profiling of baicalin along with the development and characterization of cyclodextrin inclusion complexes. *AAPS PharmSciTech,* 2019;20(8) doi:10.1208/s12249-019-1525-6

II. **Géza Jakab**, Viktor Fülöp, Tamás Bozó, Emese Balogh, Miklós Kellermayer, István Antal. Optimization of quality attributes and atomic force microscopy imaging of reconstituted nanodroplets in baicalin loaded Self-nanoemulsifying formulations. *Pharmaceutics* 2018;10, (275):1-17. doi:10.3390/pharmaceutics10040275

III. **Jakab Géza**, Fülöp Viktor, Sántha Konrád, Szerőczei Debóra, Balogh Emese, Antal István. Önemulgeáló hatóanyag-felszabadító rendszerek, mikroemulziók és nanoemulziók formulálási lehetőségei *Acta Pharmaceutica Hungarica* 2017;87(1):27-34.

10.2. Publications pertaining to different subjects

I. László Forgách, Nikolett Hegedűs, Ildikó Horváth, Bálint Kiss, Noémi Kovács, Zoltán Varga, **Géza Jakab**, Tibor Kovács, Parasuraman Padmanabhan, Krisztián Szigeti, Domokos Máthé Fluorescent, Prussian Blue-Based Biocompatible Nanoparticle System for Multimodal Imaging Contrast, *Nanomaterials,* 2020; 10(9) 1732
doi: 10.3390/nano10091732

II. Viktor Fülöp, **Géza Jakab**, Bence Tóth, Emese Balogh, István Antal. Study on optimization of wet milling process for the development of albendazole containing nanosuspension with improved dissolution. *Periodica Polytechnica Chemical Engineering* 2020;64:(4) 401-420
doi: 10.3311/PPch.15569

III. Viktor Fülöp, **Géza Jakab**, Tamás Bozó, Bence Tóth, Dániel Endrésik, Emese Balogh, Miklós Kellermayer, István Antal. Study on the dissolution improvement of albendazole using reconstitutable dry nanosuspension formulation, *European Journal of Pharmaceutical Sciences* 2018;123:70–78. doi:10.1016/j.ejps.2018.07.027

IV. Fülöp Viktor, Balogh Emese, **Jakab Géza**, Antal István. A nanogyógyszerek és nanotechnológia formulálási vonatkozásai I. Bevezetés, biofarmáciai szempontok *Acta Pharmaceutica Hungarica* 2016;86(2):43-52.

11. Acknowledgement

First of all, I would like to express my deepest thanks to my supervisor Prof. István Antal for giving me the opportunity of continuous scientific development and to complete my doctoral thesis. I am grateful for his trust he placed in me in case of different projects at the University.

My special thanks go to dr. Viktor Fülöp, friend and colleague, for supporting me during my work, introducing me in laboratory life and having constructive coffee breaks together.

I would like to thank for the following colleagues the fruitful cooperation, help and teamwork: Dr. Tamás Bozó, Dr. Dóra Bogdán, Dr. Károly Mazák, Dr. Ruth Deme, Dr. Zoltán Mucsi, Prof. Béla Noszál, Dr. István M. Mándity, Dr. Emese Balogh, Dr. Nikolett Kállai-Szabó, Bence Tóth and Prof. Miklós Kellermayer.

My sincere thanks also go to the hard-working and perceptive students with whom I worked together as supervisor: Dóra Németh, Dávid Mándy, Malte Lynen. Special thanks to Bálint Basa for his skills and knowledge, which gave me the opportunity to get acquainted with 3D printing.

I am grateful to my fellow labmates in the Pilot Plant Laboratory and all members of Department of Pharmaceutics. It is an honour to have met Issameddin Aghrbi, friend and colleague, I always enjoyed his company.

These few words cannot express my enormous gratitude and respect to my father, mother and lovely sister. Without their support and advices, I would have never started my PhD and this doctoral thesis would have never been done.

Csenge, just three words: *ad finem temporis*